



HAL
open science

Modélisation des propriétés photophysiques moléculaires à l'aide de la théorie de la fonctionnelle de la densité

Carmela Morgillo

► **To cite this version:**

Carmela Morgillo. Modélisation des propriétés photophysiques moléculaires à l'aide de la théorie de la fonctionnelle de la densité. Chimie analytique. Université Paris sciences et lettres, 2020. Français. NNT : 2020UPSLC008 . tel-03469450

HAL Id: tel-03469450

<https://pastel.hal.science/tel-03469450v1>

Submitted on 7 Dec 2021

HAL is a multi-disciplinary open access archive for the deposit and dissemination of scientific research documents, whether they are published or not. The documents may come from teaching and research institutions in France or abroad, or from public or private research centers.

L'archive ouverte pluridisciplinaire **HAL**, est destinée au dépôt et à la diffusion de documents scientifiques de niveau recherche, publiés ou non, émanant des établissements d'enseignement et de recherche français ou étrangers, des laboratoires publics ou privés.



THÈSE DE DOCTORAT
DE L'UNIVERSITÉ PSL

Préparée à Chimie ParisTech

**Modélisation des propriétés photophysiques
moléculaires**
à l'aide de la théorie de la fonctionnelle de la densité

Soutenue par

Carmela MORGILLO

Le 10 Novembre 2020

Ecole doctorale n° 388

**Chimie physique et chimie
analytique de Paris Centre**

Spécialité

Chimie physique



ParisTech

Composition du jury :

Christophe MOREL Professeur, <i>Université Claude Bernard Lyon1</i>	<i>Président</i>
Nadia REGA Professeur, <i>Università di Napoli "Federico II"</i>	<i>Rapporteur</i>
Éric BRÉMOND Maitre de Conférences, <i>Université de Paris</i>	<i>Examineur</i>
Aurélien MONCOMBLE Maitre de Conférences, <i>Université de Lille</i>	<i>Examineur</i>
Carlo ADAMO Professeur, <i>École Nationale Supérieure de Chimie de Paris</i>	<i>Examineur</i>
Ilaria CIOFINI Directrice de recherche, <i>École Nationale Supérieure de Chimie de Paris</i>	<i>Directeur de thèse</i>

Résumé

Au cours de ces travaux de thèse nous avons étudié, de façon théorique, des propriétés photophysiques de systèmes moléculaires en utilisant, pour leur description, la théorie fonctionnelle de la densité. Les processus photoinduits, comme leur nom l'indique, résultent de l'interaction lumière/matière et correspondent à la réponse du matériau suite à cette interaction. Les sciences qui s'intéressent à ces processus sont la photophysique et la photochimie. La première s'intéresse à la réponse du matériau en terme de processus physique parmi lesquels on retrouve entre autres les différents phénomènes d'émission que sont la fluorescence et la phosphorescence. La seconde s'intéresse elle aux transformations chimiques subies par le matériau suite à l'interaction avec la lumière et on pourra notamment mentionner l'exemple de la création/rupture de liaison induite par la lumière.

Comment appliquer DFT et TD-DFT pour étudier un phénomène photophysique?

Comme indiqué précédemment, le thème principal de ce travail est l'interaction lumière-matière ; il s'agit d'un domaine de recherche et d'applications très large avec par exemple la production et le stockage d'énergie avec des panneaux photovoltaïques, en médecine et chirurgie avec la thérapie photodynamique, mais aussi au quotidien avec les lunettes photochromiques ou les routes luminescentes, certainement la plus belle façon d'observer ce genre de phénomène (Figure 1).

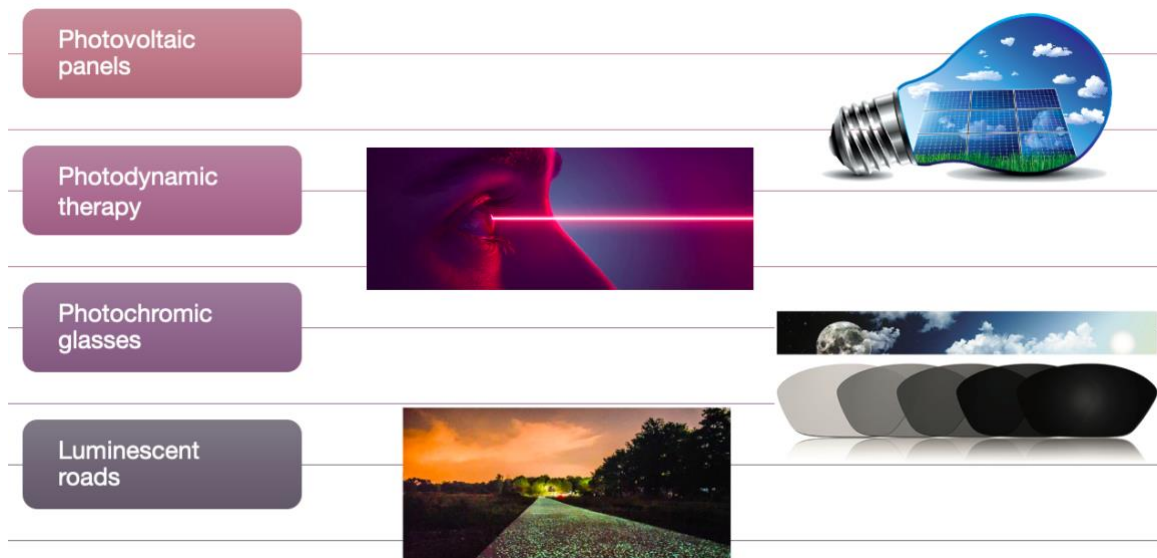


Figure 1. Processus photo-induits : applications

Pour représenter l'interaction de la lumière avec une molécule, il est possible d'utiliser le diagramme de Jablonski où il est possible d'observer les différents processus impliqués dans ce phénomène (Figure 2).

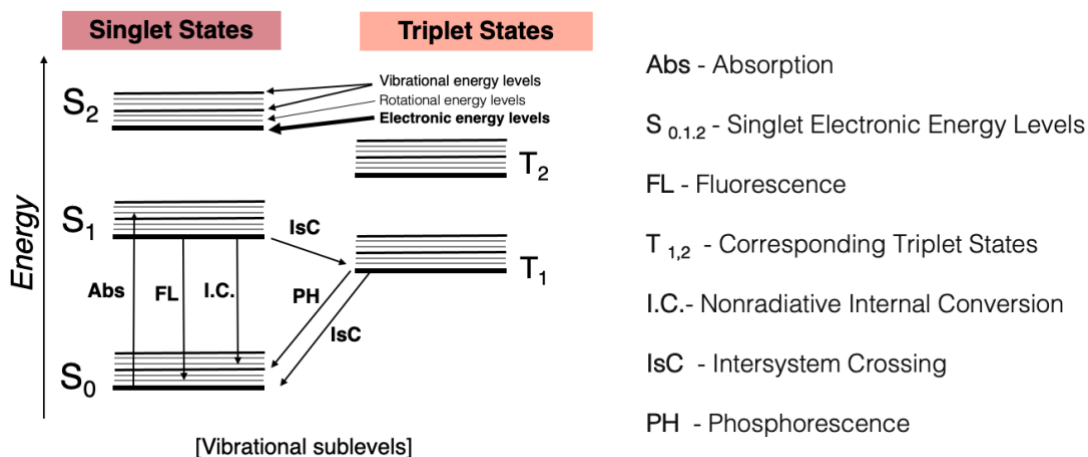


Figure 2. Le diagramme de Jablonski représente les différents processus impliqués lorsque la lumière interagit avec une molécule

D'après la Figure 2, il est possible de comprendre qu'au départ il y a l'absorption de la lumière qui correspond à l'excitation d'un électron du niveau S₀ au niveau S₁ ; alors l'électron peut rayonner par fluorescence, ou passer à un état électronique différent puis rayonner par phosphorescence, ou simplement convertir l'énergie stockée en canaux vibrationnels ou rotationnels sans réémission. On peut dire que chaque jour, il y a des phénomènes photophysiques que l'on peut observer, et la plupart d'entre eux, peuvent être représentés photochimiquement avec ce genre de diagramme. À partir de cette brève introduction, il est

possible de présenter l'âme de notre travail, qui a été d'étudier ces phénomènes photophysiques par ordinateur. En effet, pour l'étude computationnelle de ces processus, nous avons utilisé la DFT et la DFT dépendant du temps (TDDFT). En particulier :

- dans la première partie de ce travail, nous utilisons la DFT et la TD-DFT pour décrire les transferts de charges électroniques ;
- dans la deuxième partie, nous avons combiné la TDDFT avec une méthode graphique pour analyser les caractéristiques spectrales ;
- dans la troisième et dernière partie, nous utilisons la DFT et la TDDFT pour proposer une hypothèse robuste sur les propriétés optiques dans le domaine de la thérapie photodynamique des sondes sensibles au pH.

Pour étudier ces phénomènes photo-induits, il nous fallait décrire les structures moléculaires et leurs états électroniques, puis pour décrire la transition entre ces états et enfin les traduire en termes de propriétés optiques pour les comparer à l'expérience.

L'outil d'élection pour décrire mécaniquement ce type de phénomène, comme nous l'avons déjà dit, est la théorie de la fonctionnelle de la densité. La flexibilité de ce cadre permet d'intégrer différents types de fonctionnalités pour décrire les effets de solvant, les perturbations dépendant du temps et même d'étendre le calcul à des systèmes de grande taille. A partir de ces prémisses, il est désormais possible d'illustrer mon travail en détail :

- lors de la première partie de ce travail, nous avons testé les performances de fonctionnelles doubles hybrides par benchmarking, afin d'étudier avec précision le transfert de charge électronique présent dans les différents ensembles moléculaires analysés
- dans la deuxième partie, notre travail a été de combiner la théorie DFT avec de nouveaux outils pour analyser la nature des transitions électroniques calculées
- et enfin, à partir de données expérimentales, nous avons analysé les propriétés optiques d'éventuelles molécules candidates pour la thérapie photodynamique, confirmant comment l'utilisation de la TD-DFT est capable d'expliquer, et parfois de prédire, des propriétés importantes comme par exemple la dépendance des propriétés optiques du pH.

I- Double Hybrids & TD-DFT

Dans cette partie, nous illustrons avec l'utilisation de la théorie fonctionnelle de la densité, la performance des fonctionnelles doubles hybrides pour étudier le transfert de charge d'électrons dans différents ensembles moléculaires. La théorie de la fonctionnelle de la densité est une méthode quantique qui permet d'étudier la structure électronique des systèmes moléculaires. L'énergie et les propriétés d'un système à N électrons sont exprimé grâce à une fonctionnelle de la densité électronique et, dans la formulation de Kohn-Sham, l'énergie électronique du système est exprimée comme:

$$E^{HK-KS}[\rho(r)] = T_s[\rho(r)] + V_{Ne}[\rho(r)] + J[\rho(r)] + \epsilon_{xc}[\rho(r)]$$

Comportant des contributions due à l'énergie cinétique des électrons, à l'interaction avec un potentiel extérieur généré par les noyaux, à la répulsion coulombienne entre les électrons et aux interaction non classiques -d'échange et de corrélation- entre les électrons.

Malheureusement, la forme fonctionnelle exacte du dernier terme (partie d'échange et corrélation), n'est pas connue donc différentes approximations existent dans la littérature. Ces types d'approximation sont appelés fonctionnelles. Il a été proposé par Perdew de classer les différents fonctionnelles dans l'«échelle de Jacob» connue qui amène de «l'enfer» du monde de Hartree au «paradis» de la précision chimique. En augmentant la précision et le coût de calcul, on rencontre :

- l'approximation de densité locale LDA,
- l'approximation générale du gradient GGA,
- la méta-GGA,
- les fonctionnelles hybrides (GH) et à séparation de portée
- les fonctionnelles doubles hybrides

Au cours de cette première partie, nous nous sommes concentrés en particulier sur l'utilisation des doubles fonctionnelles hybrides, placées dans la plus haute marche de l'échelle de Jacob. Pour les fonctionnelles doubles hybrides, la partie de corrélation d'une fonctionnelle hybride (GH) est corrigée par une correction de type Moller-Plesset :

$$E_{xc}^{DH}[\rho] = a_x E_x^{HF} + (1-a_x) E_x^{DFA}[\rho] + (1-a_c) E_c^{DFA}[\rho] + a_c E_c^{MP2}$$

Lorsque nous voulons calculer des états excités à l'aide des fonctionnelles DFT-DH en utilisant une approche de type Time Dependent DFT il faudra donc aussi tenir en compte des corrections à l'énergie apportées par la présence de la partie MP2 à l'état fondamental

L'énergie de transition est donc corrigée par une contribution dite CIS(D). L'ajout de cette dernière contribution à l'expression d'énergie DFT augmente le coût de calcul à $O(N^5)$

Pour tester les performances des fonctionnelles doubles hybrides pour les états excités, nous avons effectué un benchmark de deux familles de fonctionnelles appelées à la simplicité des familles PBE et BLYP.

Ces deux familles ont été choisies comme représentantes des fonctionnelles non paramétrées (comme PBE, PBE0, LC-PBE, PBE0DH et PBEQIDH), et des fonctionnelles « empiriques » comme BLYP, B3LYP, CAM-B3LYP et B2PLYP.

Le benchmark est réalisé sur trois classes de systèmes moléculaires : le premier ensemble, l'ensemble Thiel, contient 28 molécules, divisées en 4 groupes, les hydrocarbures insaturés (7 molécules); les hydrocarbures aromatiques et hétérocycles (11 molécules); les aldéhydes, cétones et amides (6 molécules), et les nucléobases (4 molécules)

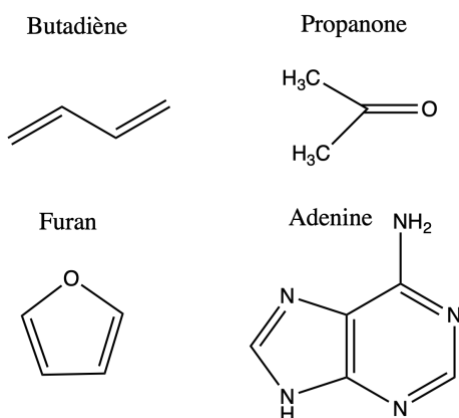


Figure 3. Exemples de molécules de l'ensemble de Thiel:

Le deuxième ensemble de référence, l'ensemble Rlex80-EX7-0, a été récemment développé spécifiquement pour permettre l'évaluation rapide des performances des fonctionnelles d'échange-corrélation pour les états excités à transfert de Charge intramoléculaire. Ici aussi nous avons choisi 2 molécules pour représenter cette ensemble (Figure 4).

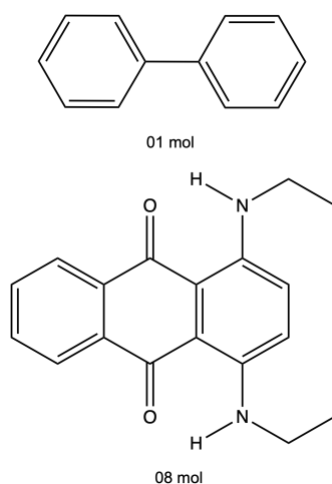


Figure 4. Exemple des molécules de l'ensemble RLex80_EX-7-0 :

Le troisième ensemble, l'ensemble de Baer, contient des dimères composés par une molécule aromatique (benzène, toluène, o-xylène, naphthalène et anthracène substitué) agissant en tant que donneur, et le tétracyanoéthylène (TCNE) agissant comme un accepteur comme indiqué dans la Figure 5 pour les systèmes basés sur le benzène et l'anthracène.

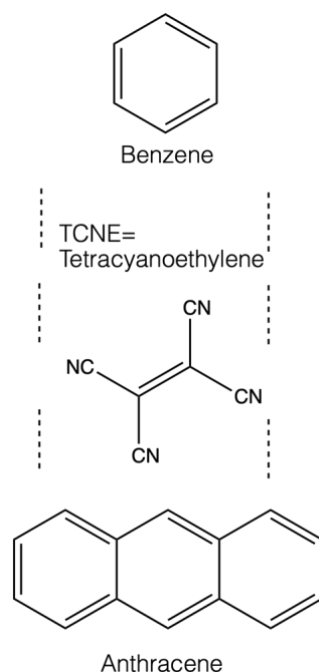


Figure 5. Ensemble de Baer : transfert de charge intramoléculaire.

Nous avons utilisé l'ensemble de Baer pour tester les performances des fonctionnelles DH dans la prédiction des excitations CT intermoléculaire. Dans tous ces ensembles, on peut distinguer des excitations dites locales (ex. ensemble de Thiel et Rlex80-EX7-0.) pour lesquelles la densité électronique reste sur la même partie du système, et des excitations à transfert de charge

lorsque la densité se déplace d'une partie à l'autre de la même molécule (ex. Rlex80-EX7-0), ou à un autre molécule (ensemble Baer). Pour chaque molécule de chaque ensemble, nous avons calculé les énergies de transition et nous les avons comparées avec celles obtenues à un niveau de théorie supérieur : CASPT2 pour l'ensemble de Thiel, Coupled Cluster pour du set Rlex80-EX7-0 et avec l'expérience dans le cas de l'ensemble de Baer.

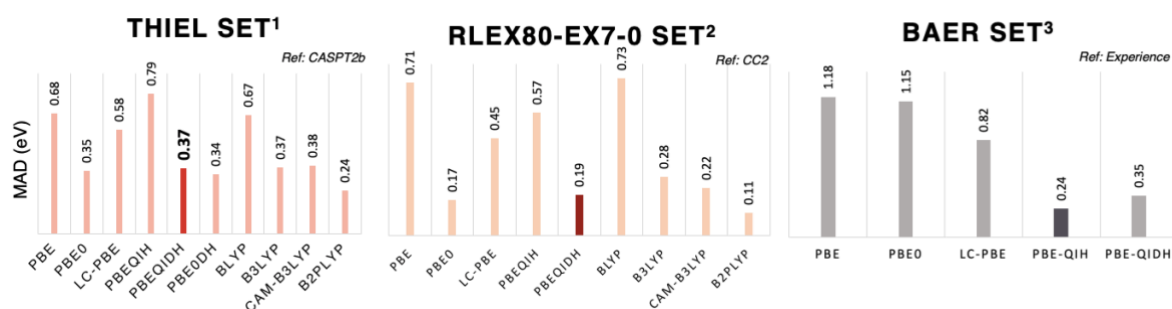


Figure 6. Calcul des énergies d'excitation verticale et comparaison avec une référence pour différents schémas de calcul: écart absolu moyen (EAM)

D'après les graphiques en Figure 6, il est évident que les DHs avec la correction CIS (D) (en rouge, rouge foncé et en gris foncé) donnent une meilleure description. En comparant les deux familles de fonctionnelles (BLYP et PBE0), on observe la même tendance générale : introduire de l'échange exact dans les fonctionnelles B3LYP et PBE0, améliore les performances vis-à-vis des GGA parents (BLYP et PBE). Cette amélioration systématique des performances n'est pas observée en passant de ces hybrides globaux (B3LYP et PBE0) aux hybrides à séparation de portée correspondantes (CAM-B3LYP et LC-PBE), pour lesquels la concordance avec les données de référence est généralement plus mauvaise à l'exception représenté par la performance CAM-B3LYP. En effet, dans le cas de la famille PBE, LC-PBE montre une MAD total plus important par rapport à l'hybride global PBE0 correspondant (0,58 eV par rapport à 0,35 eV). En revanche, toutes les fonctionnelles doubles hybrides représentent au mieux qu'une légère amélioration par rapport à l'hybride global avec un MAD total passant de 0,35 eV à 0,24eV (de B3LYP à B2PLYP). Il convient de noter que dans le cas de la famille PBE, les performances du PBE-QIDH et du PBE0-DH sont pratiquement les mêmes (0,40 eV) que celles du PBE0 (0,30 eV). En observant la fonctionnelle PBE-QIDH, on peut voir directement l'étendue des corrections CISD. Clairement en raison du pourcentage élevé d'échange HF, la fonctionnelle PBE-QIH surestime les énergies de transition fournissant de très grands MAD. En fait, dans ce cas, les corrections sont très importantes (0,79 contre 0,37 eV) soulignant ainsi l'importance du traitement correct des contributions perturbatives dans les fonctionnelles DH. Comparé à l'ensemble Thiel, le RLex80-EX7-0 comprend également des transitions avec un

caractère de transfert de charge intramoléculaire important. Dans l'ensemble, les mêmes tendances déjà observées pour l'ensemble Thiel peuvent être notées. En effet, si les hybrides globaux (B3LYP et PBE0) représentent toujours le meilleur compromis coût / précision, les doubles hybrides, et en particulier B2PLYP, sont extrêmement performants avec un MAD total allant de 0,11eV (B2PLYP) à 0,19 eV pour PBE-QIDH, respectivement. Il est à noter que toutes les fonctions DH fonctionnent très bien pour les molécules qui présentent des transitions de caractère CT partiel. En fait, dans un tel cas, l'inclusion d'un plus grand pourcentage d'échange HF dans le PBE-QIH ne suffit pas à récupérer l'énergie de transition correcte. Néanmoins, si les deux B3LYP et PBE0 fournissent des énergies d'excitation CT intramoléculaire très précises, il est bien connu que ces fonctionnelles hybrides globales ne parviennent pas à se reproduire par des excitations CT spatiales ; pour tous les dimères de l'ensemble de Baer, la première transition correspond à celle observable comme attendu d'après les données expérimentales. Les plus petites erreurs sont obtenues en utilisant la fonction PBE-QIDH tandis que les erreurs extrêmement grandes sont calculées au niveau GGA (PBE) ou hybride global (PBE0). Les DH sont également plus performantes en ce qui concerne les hybrides séparés par plage (LC-PBE). Pour obtenir un cadre complet et confirmer davantage ces résultats, l'ensemble des dimères anthracène-TCNE substitués par Baer a également été considéré comme un exemple le dimère Anthracène 9 méthyl Tetraciano éthylène. Cette transition est une excitation HOMO-LUMO, avec l'HOMO centrée sur le donneur aryle et la LUMO sur l'accepteur TCNE. Comme le montre la Figure 7 :

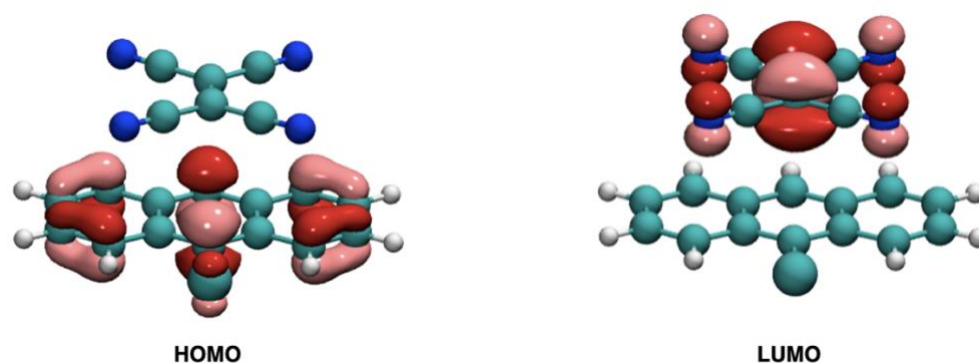


Figure 7. Orbitales moléculaires du Anthracène 9-méthyl TCNE

Il convient de noter l'accord avec les données expérimentales de la Figure 8.

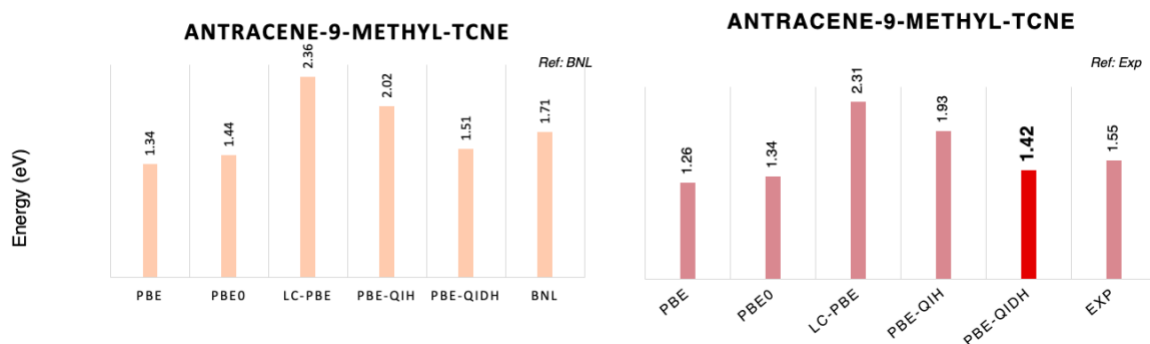


Figure 8. Calcul des énergies d'excitation verticale en phase gazeuse et solution du Anthracène 9-méthyl TCNE

Ceci est essentiellement dû à l'annulation d'erreur puisque les énergies de transition sont fondamentalement sous-estimées à tous les niveaux de la théorie car c'est l'effet du solvant, qui décale également expérimentalement les énergies de transition vers le rouge. Dans ces données, il y a une sous-estimation des énergies de transition fournies par le PBE et PBE0 et une surestimation de l'énergie de transition fournie par le LC-PBE. Dans l'ensemble, à partir de l'analyse de nos données, nous pouvons conclure que les DH représentent une bonne alternative aux hybrides pour le traitement des excitations de transfert de charge intramoléculaire.

Pour conclure cette première partie, on peut dire que les fonctionnelles DHs peuvent être considérées comme efficaces dans le cadre de la TD-DFT pour prédire les énergies des états excités, en particulier de composés moléculaires relativement grands et avec un caractère de transfert de charge marqué, ce qui est connu être très problématique à décrire avec les fonctionnelles couramment utilisées tels que les hybrides globaux. De plus, l'algorithme décrit et implémenté se caractérise par le même coût de calcul que celle de l'algorithme à l'état fondamental utilisé pour MP2, bien qu'une augmentation linéaire des coûts soit observée en fonction du nombre d'états excités considérés.

II - GLOBAL TRANSITION CONTRIBUTIONS GRIDS

Dans la deuxième partie de ce travail, nous avons développé et appliqué une méthode permettant une description globale et graphique des états excités d'un système moléculaire que nous avons appelé **GLOBAL TRANSITION CONTRIBUTIONS GRIDS** (GTCCG). Nous avons appliqué cette méthode à une série d'hydrocarbures aromatiques polycycliques (HAP). Figure 9.

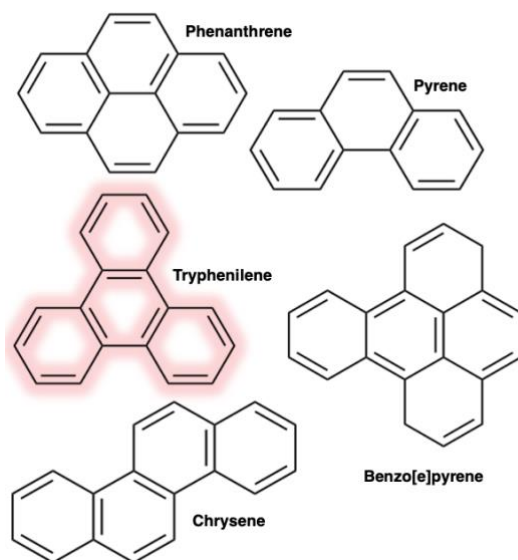


Figure 9. Hydrocarbures aromatiques polycycliques (HAP)

Ces systèmes ont été choisis car ils présentent des transitions de type π - π^* , qui se distinguent par leur caractère de transfert de charge (1La) ou d'excitation locale. (1Lb). Notre objectif était d'utiliser l'analyse GTCCG pour voir si ce type d'analyse est capable de repérer la différence entre deux classes différentes de fonctionnelles (type BLYP et type PBE) dans la description des états excités de ces molécules. Ce type d'analyse a été entièrement réalisé pour la molécule de triphénylène (en rouge sur la Figure 9) utilisée comme cas de test. L'analyse standard des excitations électroniques est basée sur l'analyse des paires électron-trou impliquées dans chaque transition. Ceci est fait en analysant les orbitales moléculaires impliqués dans chaque transition. Récemment, la méthode TCM a été introduite et utilisée dans le cas des nanoparticules d'or pour repérer les orbitales impliquées dans les transitions. De la même manière, dans notre analyse, à partir des calculs TD-DFT, nous construisons les grilles sommant pour chaque paire d'orbitales vides occupées leur contribution à la transition électronique calculée. Une valeur élevée dans la grille signifie donc que soit cette paire d'orbitales est fortement impliquée dans une seule transition, soit est impliquée dans plusieurs de plus faible intensité. Les deux types d'analyse sont présentées dans la Figure 10.

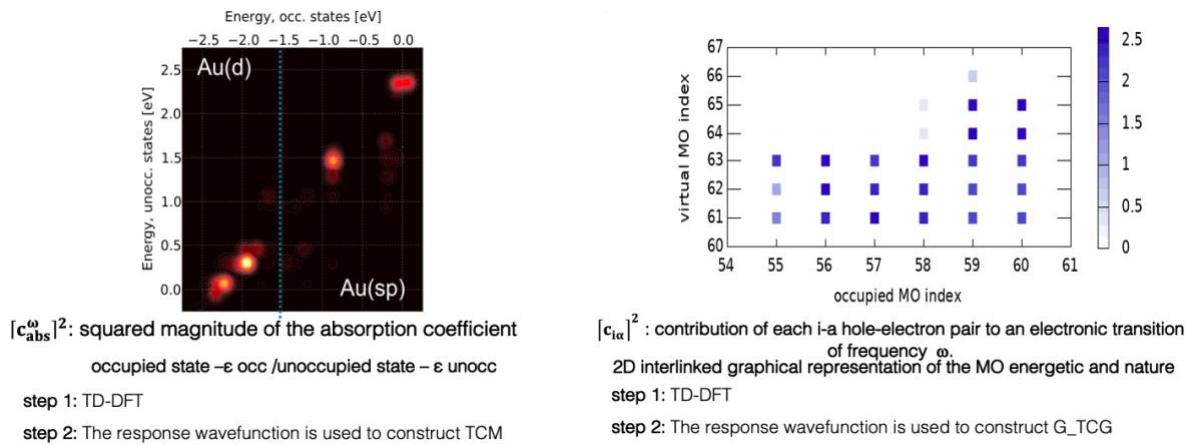


Figure 10. Transition Contribution Map (TCM) (à gauche) ; Global Transition Contribution Grid (G_TCG)(à droite)

A côté de ces types de cartes, les coefficients peuvent être pondérés par l'énergie ou par la force de l'oscillateur permettant dans ce dernier cas de voir quelle paire d'orbitales contribuent aux transitions visibles. Les fonctionnelles analysés pour le calcul des énergies d'absorption, comme dit précédemment, sont les deux familles BLYP et PBE, qui ont donné des tendances similaires comme on peut le voir sur la Figure 11.

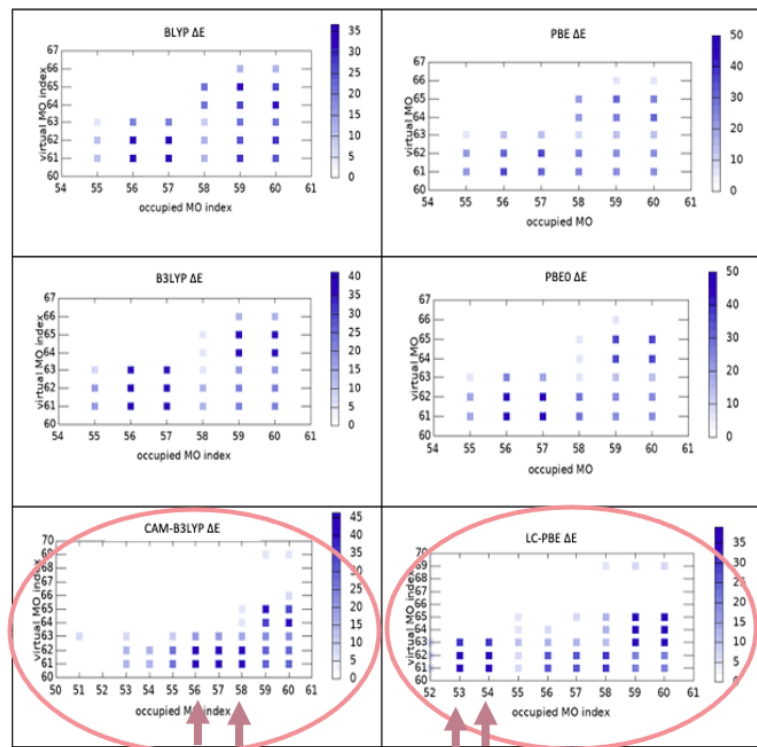


Figure 11. G_TCG_E pour les familles des fonctionnels BLYP et PBE

Par exemple, dans les deux cas pour le maillage G_TCG_E (où E est pour l'énergie), les résultats obtenus avec le GGA et les fonctionnelles hybrides ne montrent pas de différences d'analyse significatives. D'autre part, des modèles différents importants ont été détectés avec

l'utilisation de fonctionnelles hybrides à séparation de portée telles que CAM-B3LYP et LC-PBE, car ils ont montré des contributions orbitales différentes. En particulier, les GGA et les Global Hybrids présentes des contribution similaires où les orbitales proches de l' HOMO-LUMO et sont les plus impliqués, mais CAM_B3LYP et LC-PBE ont montré une différence importante mettant en évidence des contributions plus importantes des orbitales internes. Pour donner un autre exemple, nous rapportons dans la Figure 12 la grille de contribution à la transition globale où les coefficients sont pondérés par la valeur de la distance de transfert de charge ou D_{CT} (G_{TCG_D}):

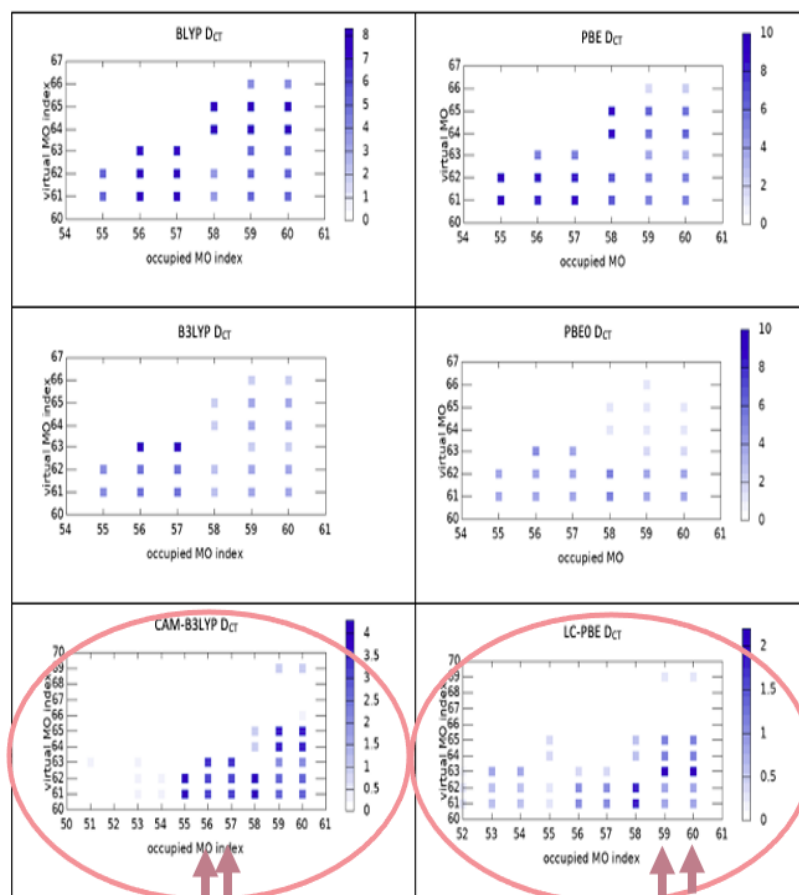


Figure 12. G_{TCG_D} pour les familles des fonctionnels BLYP et PBE

Fait intéressant, les graphiques obtenus pour les différentes fonctionnelles montrent des différences importantes. En particulier, on peut noter que si GGA et les hybrides globaux indépendamment sur la famille montrent des tendances et des valeurs très similaires, les deux hybrides à séparation de portée montrent un comportement global différent et, plus important

encore, une valeur globale plus locale comme on peut le déduire du fait que l'échelle de l'axe z est réduite d'un facteur 2.

En conclusion, affirmer que :

- L'approche G_TCG pourrait aider à l'analyse de systèmes possédant des structures électroniques complexes et une variété d'orbitales moléculaires denses proches des orbitales frontières telles que les nanoparticules ou les grands systèmes π -conjugués.
- Cette méthode peut être utilisée pour repérer qualitativement les différences dans le comportement de différentes familles de fonctionnelles dans l'estimation de l'énergétique et de la nature des transitions calculées de manière condensée et qualitative.

Comme perspective sur ce deuxième travail, nous pouvons dire qu'il sera envisageable de construire des grilles globales non pas à un nombre fixe d'Etat Excités mais pour les états excités présents dans une fenêtre spectrale d'intérêt. Un autre type d'analyse pourrait être fourni en se concentrant exclusivement sur la contribution de paires orbitales spécifiques occupées - i- inoccupées -a-.

III- Photodynamic Therapy et Amino-OPEs

Dans la dernière partie de nos travaux, nous nous sommes intéressés à l'étude des propriétés optiques d'une classe de molécules récemment synthétisées comme possibles candidats comme photosensibilisateurs pour la thérapie photo-dynamique (PDT). Ce travail a été mené en collaboration avec l'équipe du professeur Fausto Puntoriero de l'Université de Messine. La thérapie photo-dynamique est une technique largement utilisée en médecine et en chirurgie au cours de la dernière décennie. Cette technologie repose sur l'utilisation combinée de 3 éléments : la matière, la lumière et le photosensibilisateur (PS) comme le montre la Figure 13.

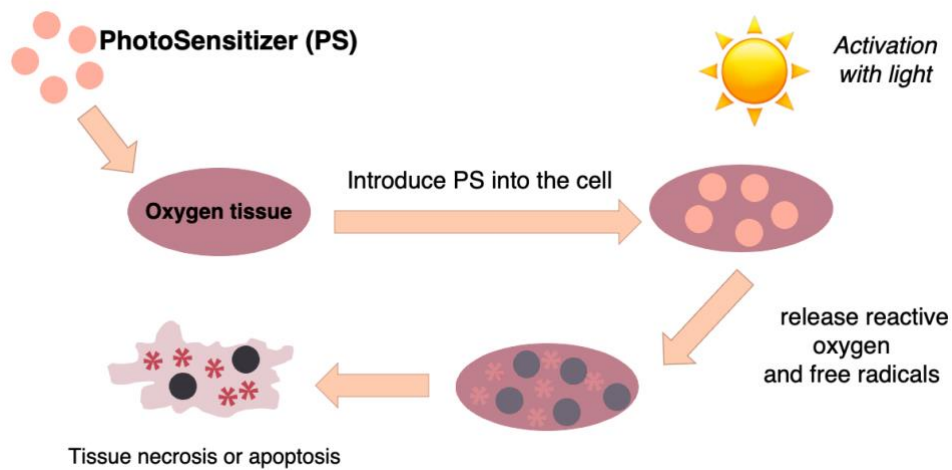


Figure 13. Processus de thérapie photodynamique

Le PS entre dans le corps au contact de tissus où il y a de l'oxygène ; une fois que le PS est en contact avec ces cellules, il est irradié par une source lumineuse et soumis à une réaction photochimique en présence de l'oxygène qui produit de l'oxygène singulet. Enfin l'Oxygène, au contact des tissus cancéreux, provoque l'apoptose et la mort de la cellule cancéreuse. Cette réaction est représentée photochimiquement sur la Figure 14.

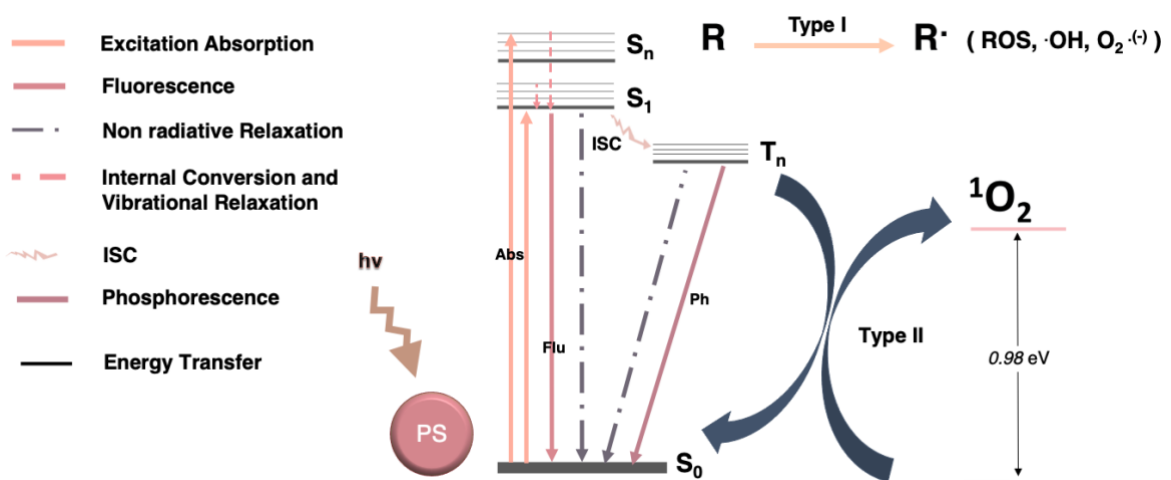


Figure 14. Mécanisme photochimique impliqué dans la PDT

Après une excitation électronique due à l'absorption lumineuse, il est possible de peupler les états excités de la molécule (états S_n sur la Figure) ; deux mécanismes peuvent ensuite être suivis :

- le premier, dans lequel un complexe ROS, ou un radical est produit ;
- le second, où après la population d'un état excité triplet de la molécule, l'oxygène singulet est produit.

Les radicaux et l'oxygène singulet ont le même rôle qui provoque la mort des cellules.

Dans le cadre de cette thèse, nous nous sommes concentrés sur les molécules d'Oligo Phénylène Ethynylène (OPE) et en particulier sur les trois molécules ici représentées (Figure 15).

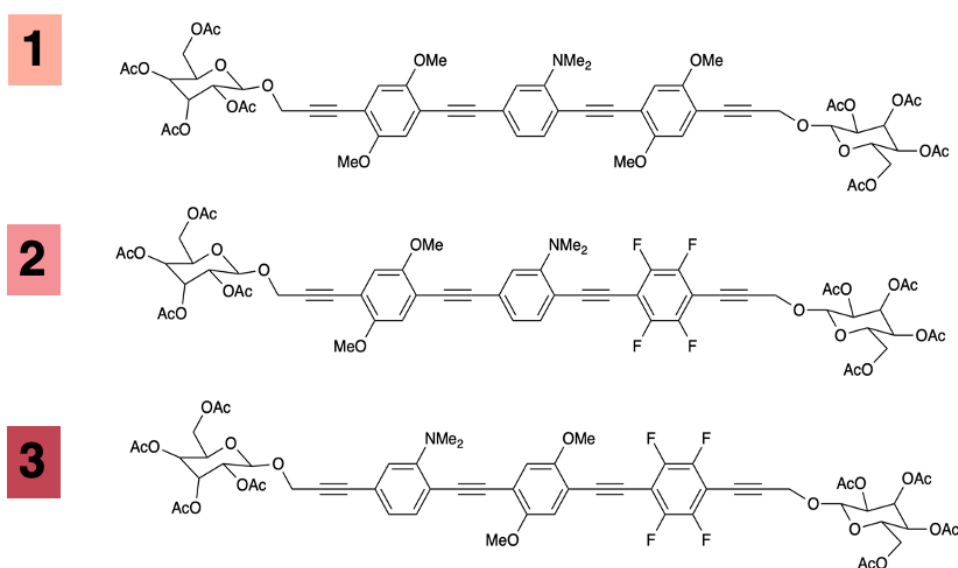


Figure 15. Amino oligo phénylène éthynylène - OPE

Ces molécules présentent certaines caractéristiques communes : elles présentent un noyau hydrophobe fonctionnalisé avec des groupements hydrophiles. Ils sont utilisés à la fois pour faciliter la perméation de la membrane cellulaire et des processus glycolytiques avancés (ce que l'on appelle l'effet Warburg) en raison de la présence des fragments glucose. Apparemment, ces PS devraient également absorber la lumière et, pour cette raison, le noyau central conjugué a été fonctionnalisé avec des groupes donneurs et accepteurs à des positions différentes, afin de produire des molécules avec des états excités qui absorbent intensément ou sont émissifs avec un caractère de CT. Le but de notre recherche théorique était donc de comprendre par analyse de l'état excité calculé vertical l'effet des groupes donneur et accepteur sur les propriétés optiques des 3 OPE. Nous avons voulu étudier l'effet de ces groupes à la fois en absorption et en émission. Enfin, les amines étant protonables, nous avons effectué plusieurs calculs pour vérifier si ces molécules pourraient être utilisées comme sondes de pH. En effet,

s'elle présentaient une différence marquée soit en absorption, soit en émission entre les espèces de la forme neutre et protonée, ces molécules pourraient être utilisées pour sonder le pH de la solution, car la molécule changera de couleur en fonction du pH. Dans un premier temps, nous avons étudié la structure moléculaire de ces systèmes en utilisant la DFT. Toutes les propriétés optiques ont ensuite été calculées en utilisant différentes fonctionnelles l'hybride global PBE0 et l'hybride à séparation de portée CAM-B3LYP. Le solvant a été inclus en utilisant un modèle de continuum polarisable (CPCM) et le dichlorométhane a été considéré comme solvant comme dans les expériences. Les états excités verticaux pour les spectres d'absorption ou les états excités relaxés pour l'émission ont été calculés au niveau TD-DFT. Les résultats obtenus pour l'absorption en utilisant les deux fonctionnelles sont représentés en Figure 16 :

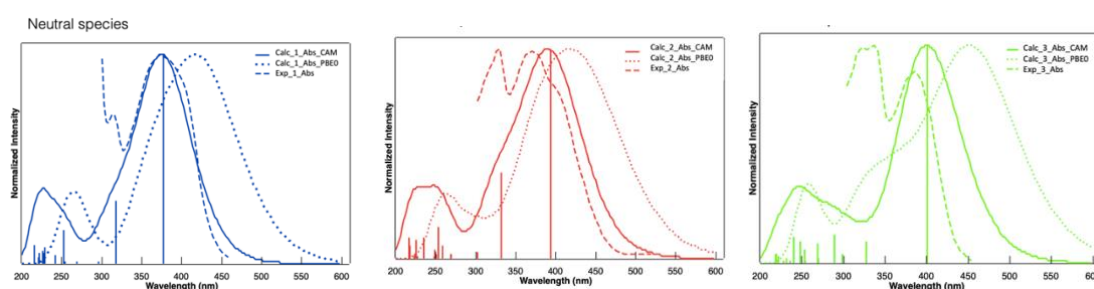


Figure 16. Spectre d'absorption des molécules 1 (bleu), 2 (rouge) et 3 (vert) comparé à PBE0 (petites lignes en pointillés) et CAM-B3LYP (lignes pleines) fonctionnelles avec les données expérimentales (lignes en pointillés).

Les spectres expérimentaux (ligne pointillée) ainsi que les spectres calculés au niveau PBE0 (ligne pointillée) et CAM-B3LYP (ligne complète) sont représentés dans le cas des molécules 1, 2 et 3. Bien que la fonctionnelle PBE0 donne déjà d'assez bons résultats, la fonctionnelle CAMB3LYP s'est avérée être plus adaptée à l'étude de ces systèmes avec un très bon accord avec les données expérimentales. Dans l'ensemble, les deux fonctionnelles PBE0 et CAM-B3LYP sont capables de reproduire correctement la tendance globale allant de 1 à 3 mais la fonctionnelle CAM-B3LYP est en meilleur accord avec l'expérience. En effet, ces résultats sont cohérents avec la nature des transitions calculées. Indépendamment de la fonctionnelle utilisée, le pic le plus intense des spectres provient d'une seule transition montrant un caractère HOMO-LUMO prédominant. D'un point de vue orbitalaire, le LUMO est très délocalisé sur les trois noyaux phényle mais dans le cas de la molécule 3 une localisation sur le cycle contenant l'accepteur de fluor F peut être notée. Néanmoins, cette localisation est de loin moins forte que la localisation de l'HOMO sur le donneur aminé (Figure 17).

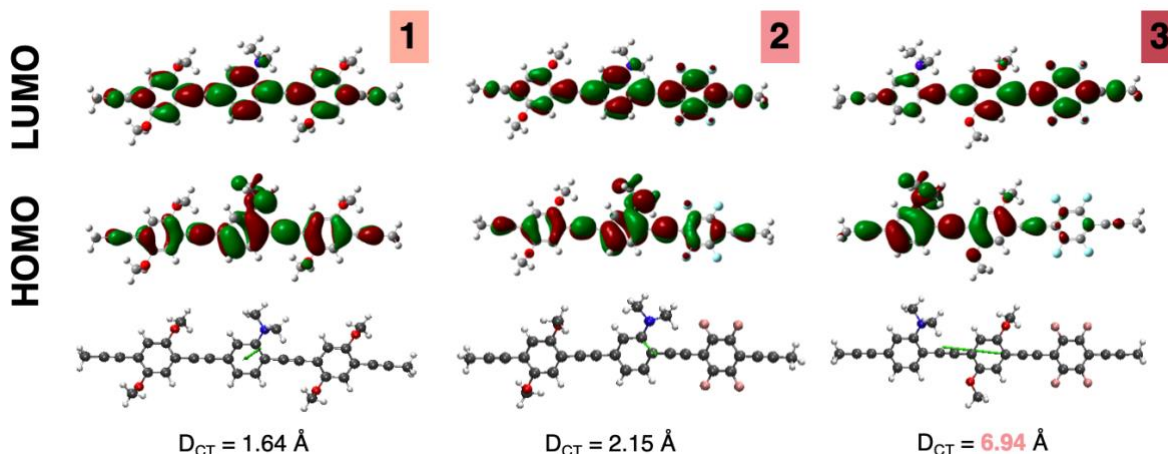


Figure 17. Orbitales moléculaires (MO) de 1, 2, 3 (absorption) calculées au niveau CPCM (CH₂Cl₂) -CAM-B3LYP (isodensité = 0,025 au).

Ceci est également clairement démontré par l'analyse proposée par le D_{CT} , comme le montre également la Figure 17 ci-dessus. Alors que pour la molécule 1, il n'y avait pratiquement pas de transfert de charge, avec un D_{CT} de seulement 1,64 Å ; la molécule 2 a montré un D_{CT} plus grand en raison de la localisation de l'HOMO sur le groupe amino et finalement le meilleur effet CT est obtenu avec la molécule 3 montrant la plus grande distance entre le cycle accepteur et le donneur d'amino ($D_{CT} = 6,94$ Å). D'un point de vue chimique, nos résultats montrent que le groupe amino est un meilleur donneur que le groupe OMe et que le groupe fluor n'est probablement pas encore un accepteur suffisamment bon en raison de la faible polarisation que ces atomes induisent sur le LUMO. Par conséquent, pour déplacer l'absorption vers une plus grande longueur d'onde (énergies plus petites) et pour augmenter le caractère CT, un meilleur groupe accepteur doit être utilisé. En ce qui concerne les émissions, le même protocole utilisé pour calculer l'absorption a été utilisé et les spectres simulés correspondants sont ici représentés sur la Figure 18 :

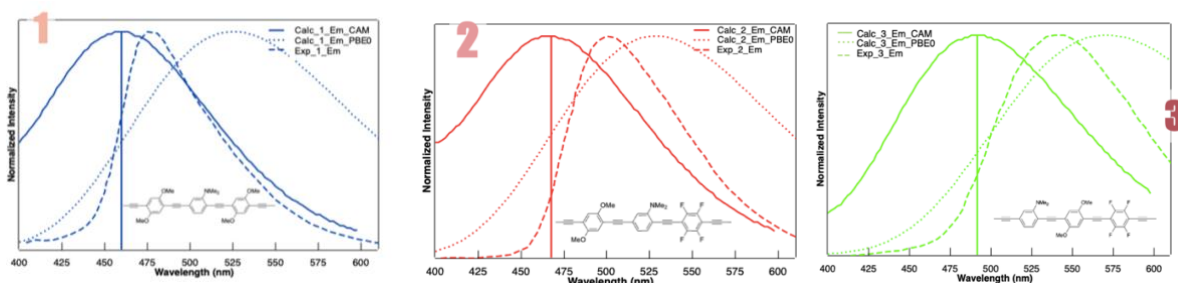


Figure 18. Spectre d'émission des molécules 1 (bleu), 2 (rouge) et 3 (vert) calculé avec les fonctionnelles PBE0 (petits tirets) et CAM-B3LYP (traits pleins) ainsi que des données expérimentales (traits tiretés).

D'un point de vue méthodologique, nous pouvons voir que l'énergie maximale d'émission est sous-estimée à PBE0 et légèrement surestimée au niveau CAM-B3LYP. Néanmoins, l'erreur

au niveau de CAM-B3LYP est généralement inférieure à celle du PBE0. La plus grande erreur est observée pour la molécule 3 à PBE0. Ceci n'est pas surprenant puisque comme nous l'avons vu précédemment, la molécule 3 présente le plus grand CT et donc on s'attend à ce que la sous-estimation de l'énergie CT déjà observée en absorption soit amplifiée par relaxation dans l'émission. L'analyse de la nature de l'orbitale impliquée dans la transition électronique responsable de l'émission que sont en réalité les HOMO et les LUMO de chaque système montre clairement le caractère CT amélioré de la molécule 3. En effet, pour cette molécule le CT est augmenté par rapport à celui calculé à l'absorption verticale (d'environ 6 Å à 7 Å) (Figure 19)

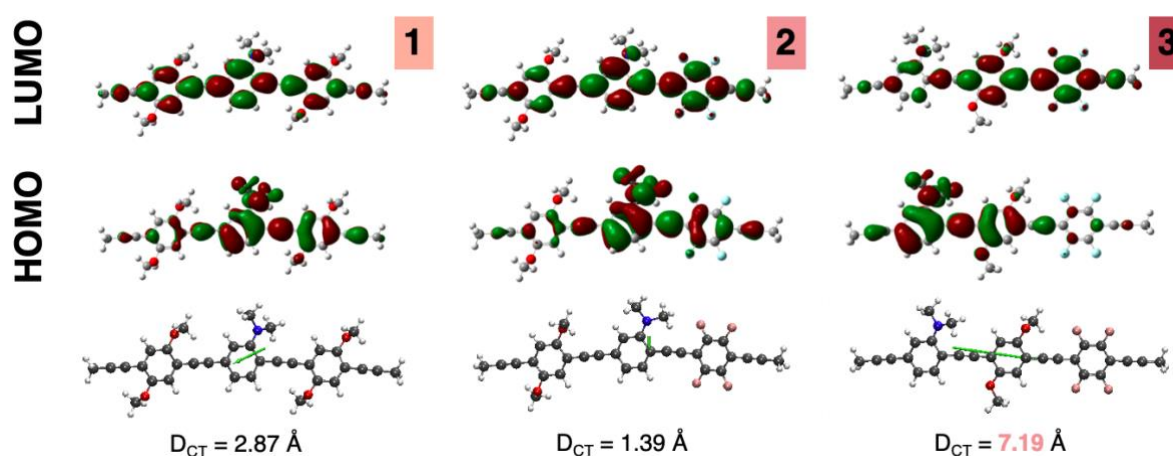


Figure 19. Orbitales moléculaires (MO) de 1, 2, 3 (émission) calculées au niveau CPCM (CH_2Cl_2) -CAM-B3LYP (isodensité = 0,025 au).

Pour le système neutre, nous concluons qu'à partir de l'analyse des résultats obtenus à la fois pour l'absorption et l'émission, les observations générales suivantes peuvent être tirées :

- d'un point de vue méthodologique, la fonctionnelle CAM-B3LYP est capable de reproduire correctement les spectres d'absorption et d'émission des trois systèmes ;
- la transition d'absorption la plus intense et responsable également d'émission est une excitation HOMO-LUMO dont le caractère CT dépend de la localisation de ces deux orbitales sur le groupe donneur et accepteur, respectivement ;
- le groupement amino est un bon donneur permettant de localiser le trou, et d'autre part l'accepteur utilisé (les atomes de fluor) ne localise pas fortement le LUMO réduisant ainsi le caractère push-pull de ces systèmes.

Dans l'ensemble, un bon CT est obtenu uniquement dans le cas de la molécule 3. Par conséquent, pour augmenter le caractère CT et donc potentiellement aussi l'absorption vers le décalage maximum d'émission, un accepteur plus fort doit être utilisé.

Nous nous sommes ensuite concentrés sur l'analyse de molécule dans leur forme protonée. Les calculs d'émission sont capables de reproduire l'émission relative uniquement de manière qualitative (Figure 20).

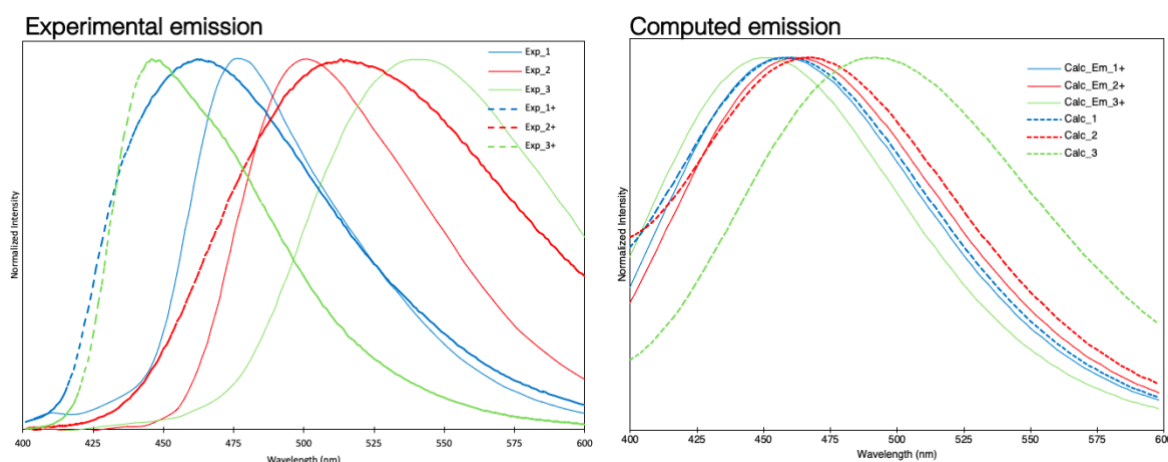


Figure 20. Spectres d'émission des molécules 1, 2, 3 et 1, 2, 3 à partir de données expérimentales (à gauche) et calculés avec la fonctionnelle CAM-B3LYP (à droite)

Néanmoins, la quantité importante à reproduire n'est pas l'absorption ou l'émission absolue mais le déplacement d'absorption ou d'émission allant de l'espèce neutre vers l'espèce protonée. Expérimentalement, le décalage le plus important est observé pour la molécule 3 en vert pour laquelle un fort déplacement vers une énergie plus élevée est observé. Ce décalage est reproduit qualitativement par notre calcul confirmant encore le fait que la molécule 3 pourrait être utilisée comme senseur de pH. En guise de conclusions générales, en appliquant le TD-DFT à cet ensemble de photosensibilisateurs tout d'abord d'un point de vue méthodologique, nous avons montré que CAM-B3LYP permet la description quantitative de l'absorption et de l'émission de ces systèmes et une description qualitative des protonés. D'un point de vue chimique, nous avons pu montrer que les spectres d'absorption et d'émission sont dominés par la présence d'une transition HOMO-LUMO intense dont le caractère CT dépend de la nature et de la position des groupements donneur et accepteur. En particulier, nous avons montré que le groupe amino est un bon groupe donneur permettant la localisation de l' HOMO mais que le groupe fluor n'est pas suffisamment fort pour localiser la LUMO et renforcer le caractère CT de ces systèmes. En revanche, la protonation affectant le groupe donneur amino, joue comme prévu un très grand rôle pour la molécule 3 qui est la seule à montrer un décalage suffisamment important entre les formes neutre et protonée en émission.

Pour donner des conclusions globales sur l'ensemble du travail discuté précédemment, il est possible de dire que l'utilisation de la théorie fonctionnelle de la densité nous a permis d'étudier différents systèmes et sujets.

Les fonctionnelles DH de la TDDFT se sont avérées être des méthodes valides pour la description des systèmes moléculaires montrant aussi des excitations à transfert de charge.

L'analyse basée sur les GLOBAL TRANSITION CONTRIBUTIONS GRIDS (G_TCG) est une méthode alternative valide d'analyse des caractéristiques spectrales.

-La théorie de la fonctionnelle de la densité est capable de reproduire, confirmer et prédire le rôle du système moléculaire utilisé dans le domaine PDT, et également de décrire les propriétés optiques en accord les données expérimentales.

En tant que perspectives, outre une validation plus solide de GTC_G, l'utilisation des NTO et la restriction du sous-ensemble pertinent de paires orbitales seront testées comme des moyens de fournir un outil efficace d'analyse globale. Un lien quantitatif vers d'autres descripteurs à côté de l'indice D_{CT} est également prévu pour ce qui concerne la deuxième partie. Pour la dernière partie de ce travail, et comme perspective, nous pouvons supposer que la désacétylation des terminaisons glucose sera fondamentale pour étudier les propriétés photophysiques en solution aqueuse des dérivés des OPE.

TABLE OF CONTENTS

GENERAL INTRODUCTION	1
THEORETICAL BACKGROUND	7
1.1 THEORETICAL METHODS	7
<i>The polyelectronic wavefunction</i>	<i>10</i>
1.2 DENSITY FUNCTIONAL THEORY	11
<i>The Kohn-Sham method</i>	<i>13</i>
<i>The atomic basis set</i>	<i>15</i>
<i>The exchange correlation functional</i>	<i>19</i>
<i>Local density approximation</i>	<i>21</i>
<i>Generalized gradient approximation and kinetic energy density</i>	<i>22</i>
<i>Hybrid functionals and adiabatic connection</i>	<i>24</i>
<i>Range-separated hybrid functionals</i>	<i>26</i>
<i>Double hybrid functional overview</i>	<i>27</i>
1.3 TIME-DEPENDENT DENSITY FUNCTIONAL THEORY	28
1.4 SOLVENT MODELS	31
<i>Explicit model</i>	<i>31</i>
<i>Implicit model</i>	<i>32</i>
REFERENCES	35
DOUBLE HYBRIDS AND TIME-DEPENDENT DENSITY FUNCTIONAL THEORY: IMPLEMENTATION AND BENCHMARK ON CHARGE TRANSFER EXCITED STATES	AN 39
2.1 CONTEXT	39
<i>Double hybrid density functional approximations</i>	<i>40</i>
<i>Introduction to the double hybrids functionals</i>	<i>41</i>
2.2 TIME DEPENDENT DENSITY FUNCTIONAL THEORY AND DOUBLE HYBRID (DH) DENSITY FUNCTIONAL APPROXIMATIONS (DFAS)	43
2.3 COMPUTATIONAL DETAILS	49
2.4 RESULTS AND DISCUSSION	50
2.5 CONCLUSIONS	60
REFERENCES	61
A GLOBAL VIEW OF EXCITED STATES USING <i>GLOBAL TRANSITION CONTRIBUTIONS</i> GRIDS: THE TRIPHENYLENE MOLECULE AS TEST CASE	65
3.1 INTRODUCTION	65

3.2 COMPUTATIONAL DETAILS	68
<i>The transition contribution map (TCM) and global transition contribution grid (G_TCG) analysis</i>	<i>68</i>
3.3 RESULTS AND DISCUSSION	70
3.4 CONCLUSIONS AND PERSPECTIVES	77
REFERENCES	78
AMINO-OLIGO PHENYLENE ETHYNYLENES (AMINO-OPES) AS BIOCOMPATIBLE PHOTOSENSITIZERS IN PDT:A THEORETICAL INVESTIGATION OF OPTICAL PROPERTIES	81
4.1 INTRODUCTION	81
<i>Required components for PDT.....</i>	<i>87</i>
<i>Amino-OPEs: a new class of third generation photosensitizers?</i>	<i>91</i>
4.2 COMPUTATIONAL DETAILS	93
<i>Validation of the model</i>	<i>94</i>
4.3 RESULTS AND DISCUSSION	96
<i>Ground state: structural features.....</i>	<i>96</i>
<i>Ground state : absorption properties</i>	<i>97</i>
<i>Excited state: structural features and emission energies.....</i>	<i>100</i>
<i>Protonated species: structures and optical properties.....</i>	<i>102</i>
4.4 CONCLUSIONS AND PERSPECTIVES	107
REFERENCES	108
GENERAL CONCLUSIONS AND PERSPECTIVES.....	111
5.1 OUTLINE.....	111
5.2 PERSPECTIVES	114
APPENDICES	119
APPENDIX A	119
APPENDIX B	137

General Introduction

Schopenhauer once said:

"Only the light that one turns on to oneself shines later on for others too"

On 19 January 2015 the International year of Light and Light-based Technologies was celebrated in Paris, the United Nations thus recognized the great role of light in technological innovations, scientific discoveries and life.

Can be cited many examples of photochemical and photophysical processes with light, or better, to control matter with light:

- Molecular motors: they are made of molecules that have possible rotational degrees of freedom around single or double bond. In general, molecular motors involving rotation around simple bonds are chemically activated¹ but the ones involving rotations around a double bond needs light to be activated².
- Molecular photoswitch: a photoswitch consists in a molecule that can be reversibly shifted between two (or more) stable states by light^{3,4}.

Concerning the emission process, one has to notice that the control of light emission (color and/or intensity) can be the target but light can also be part of the experimental conditions and can allow for example the excitation of a molecule at a particular wavelength and the opening/closure of a particular photochemical and/or photophysical channel. Photochemical and photophysical sciences study all the physico-chemical processes induced by light (from UV to near IR including visible light). These processes concern the excited states of the atoms, molecules or systems under study. Photophysics concerns all the physical processes induced by light while photochemical sciences are interested in photoinduced chemical transformation. As the boundary between those two domains is not always perfectly clear, they can be considered complementary. If one is interested in photophysical processes one needs to consider the chemical transformations that may be induced (photochemistry) while if one is interested in photochemical processes, one has to take into account the photophysical processes that are also involved. Both photophysical and photochemical processes are present in nature but also in high- technology applications. For the first one, one can cite for example photosynthesis or mechanism of the vision.

Indeed, one has to notice that the most readily available light source is the Sun. For the second one, the source of light can be the Sun but also lamps or laser beams for which it is possible to control both the intensity and the type of light (wavelength). One of the most popular application is photography developed in 1816, but we can also mention photo dynamic therapy (PDT) as an alternative to chemotherapy to cure cancer.

During my PhD I have been focused in the study of photophysical processes using theoretical methods.

Light-induced processes

The so-called 'photoactive' materials are those interacting with light; this interaction will lead to an observable response.

From the interaction of light with matter, various phenomena can emerge such as refraction, reflection, diffraction or absorption. The last, is the ability and possibility of systems to absorb the energy of electromagnetic radiation.

In quantum mechanics, the energy of the constituent particles of matter is quantized, that is to say that it can only assume particular discrete values. The characteristic phenomena for each system are induced by the difference between energy levels of atoms. A characteristic distribution of energy levels is associated with each molecular system. The absorption of a certain wavelength is peculiar to each system and gives rise to a characteristic absorption spectrum. Absorption therefore depends on both the nature of the system and the frequency of the radiation. It is for this reason that absorption is used to investigate the nature of the system itself. To bring an electron from the ground state to an excited state, it is necessary to supply it with a sufficient amount of energy, equal to or greater than the quantum leap between the two levels. In this case the jump is caused by the absorption of a photon.

Under certain conditions, following the absorption phenomenon, the so-called emission phenomenon can be observed. Electrons, when at their stationary energy levels, do not radiate energy. Radiative or nonradiative decay processes occur only when an electron is in an excited state, from which it spontaneously tends to return to the ground state. The leap from a higher to a lower level is accompanied sometimes by the emission of a photon (radiative).

A light-induced process can be studied in terms of electron density redistribution in response to a light-induced perturbation, in order to investigate the electronic properties of a wide range of molecules.

Theoretical chemistry has now reached high levels of accuracy that makes possible to characterize the extent of a deformation or the reactivity. For excited state it is possible describe a reactive process following its path, along the reaction coordinate, from the absorption of energy to its different possible evolutions using different strategies and computational tools. One of the most used theoretical methods, the same that we have used for all system I have analyzed, is time-dependent density functional theory (TD-DFT). Although there are many possible approaches to the study of photochemical processes, they can be divided into two categories: the first is to study the time evolution of a wave packet through the resolution of the time-dependent Schroedinger equation; the second approach is to sequence the course of a light-induced reaction through the characterization of minima on the potential energy surfaces along which the reaction develops, thus identifying passages in the photochemical iter that connects the Franck-Condon region, when the system absorbs when it returns to the ground state. For this thesis work, the second approach mentioned above has been followed.

Electron density is the fundamental observable parameter used for understanding and studying the properties of the molecular excited state. It is well known that photophysical properties of a given molecular system can be strongly influenced, and are defined by the presence of particular structural features, for example a strong electron donor and electron acceptor groups that direct the charge transfer in the excited state. In this context, thanks to many studies conducted in recent years, a good number of strategies have been devised to characterize the photoinduced charge transfer and to modulate the processes of excited states.

In this work we will try to give a complete picture of the photo-induced processes studied, as an effect of the synergy between density and energy and of all the resulting information. In fact, while energy allows us to characterize the local properties of potential surfaces, electron density (or rather the study of its distribution) gives us the possibility to add the necessary element for a more complete and efficient description.

The study of the optical properties of materials has made tremendous progress in the last decades thanks to the advancements of computational chemistry and chemistry in general.

Computational studies in combination with experimental approaches have allowed great progress in the understanding and study of photophysical and photochemical phenomena that have led to the description of complex molecular systems previously unknown.

The general objective of this project is to develop new computational approaches allowing the design of new single-molecule architectures with emphasis on the exploitation of reversible conformational changes induced by light in the excited state.

Within the framework of this project we will also develop tools of analysis, for the investigation of excited state processes and properties of molecular systems of increasing complexity.

These subjects have been exposed as it follows:

- In the first chapter an introduction of theoretical methods, a review of some existing tools developed in the last decades. The discussion is centered in particular on the DFT and TD-DFT.

- In the second chapter, we present a computational study that allowing to observe electronic excited states using a particular recent class of functionals, the co-called double hybrids.

The aim was to verify if these were suitable, for the study of different molecular systems focusing on inter-molecular charge transfer.

- In the third chapter, we propose a new graphical approach to map orbital energies of a chosen molecular system to its excited state descriptors in the case of a TD-DFT calculations.

- In the last chapter, DFT and TD-DFT methods were applied to a family of photosensitizers that are possible candidates as drug in photodynamic therapy. Their optical properties were elucidated and rationalized. This work was done in collaboration with the experimental laboratory of the University of Messina of Prof. Fausto Puntoriero.

References

- 1) Kelly, T. R.; De Silva, H.; Silva, R. A. *Nature*, **1999**, 401(6749):150–152.
- 2) Koumura, N.; Zijlstra, R. W. J.; van Delden, R. A.; Harada, N.; Feringa, B. L. *Nature*, **1999**, 401(6749):152–155.
- 3) Feringa, B. L.; van Delden, R. A.; Koumura, N.; Geertsema, E. M. *Chem. Rev.*, **2000**, 100(5):1789–1816.
- 4) Knipe, P. C.; Thompson, S.; Hamilton, A. D. *Chem. Sci.*, **2015**, 6:1630–1639.

Theoretical background

1.1 Theoretical methods

Theoretical and Computational Chemistry provides an interface between chemistry, physics, mathematics and computational sciences. The growing of this field has been supported by the advancement in the computational technology as well as by the methodological developments. The solution of the so called *many-body problem* that arises from *Schrödinger equation* for more than two particles, requires very large computational efforts. The equation for many particle systems cannot be solved exactly by analytical mathematical methods. Computational methods can, however, provide approximated solutions to the many body problem (which in principle may be refined to any desired degree of accuracy), based on the wave function methods such as Hartree Fock (HF) and post HF methods (e.g. perturbation theory MPn n=2, 3...), configuration interaction (CI), and coupled cluster (CC). An alternative way is given by density functional theory (DFT) originally developed for electron-gas systems by Thomas and Fermi in 1927⁴. The DFT overcomes the main problem in the wave function methods, i.e. the wave function complexities with the increasing of electrons, since DFT depends exclusively on three spatial coordinates. The computational cost is lower than post HF methods and comparable to the HF one. DFT was developed by Hohenberg and Kohn who proved the one to one correspondence between the electron density of a system and the energy, therefore the ground state electronic energy is determined completely by the electron density. The main problem concerns the functional connecting electron density and state energy that is unknown, although it has been proven that each different density yields a different ground state energy. Indeed, a lot of functionals have been proposed.

The Schrödinger equation

Quantum mechanical methods aims to solve the Schrödinger equation¹, which allows us to describe the electronic structure of atoms and molecules. The time-dependent Schrödinger equation is expressed as follows ^(1*):

$$H\Psi(r, t) = i \frac{\partial \Psi(r, t)}{\partial t} \quad 1.1$$

where $\Psi(r, t)$ is the time-dependent wavefunction and H is the polyelectronic Hamiltonian. For a stationary system, Eq. 1.1 becomes the time independent Schrödinger equation:

$$H\Psi(r) = E\Psi(r) \quad 1.2$$

Where E is the energy of the stationary system and $\Psi(r)$ the corresponding wavefunction, depending only on the spatial coordinates r of the N electrons and M nuclei.

The Hamiltonian is made up of a nuclear Hamiltonian (H_N) and an electronic Hamiltonian H_e :

$$H = H_e + H_N \quad 1.3$$

The Hamiltonian, H , can be written as a sum of kinetic and potential operators of the electrons (e) and the nuclei (N):

$$H = T_e + T_N + V_{Ne} + V_{NN} + V_{ee} \quad 1.4$$

For a system containing N electrons and M nuclei, T_e and T_N can be expressed as:

$$T_e = -\frac{1}{2} \sum_{i=1}^N \nabla_i^2 \quad ; \quad T_N = -\frac{1}{2} \sum_{A=1}^M \frac{\nabla_A^2}{M_A} \quad 1.5$$

^(1*) All the equations will be expressed using the atomic units.

Where M_A is the mass of the nuclei A and ∇^2 is the Laplacian operator. V_{Ne} , V_{NN} and V_{ee} are the potential energy operators of the nuclei-electron electrostatic interaction, the electronic repulsion and the nuclear repulsion respectively and can be expressed as:

$$V_{Ne} = -\sum_{i=1}^N \sum_A^M \frac{Z_A}{r_{iA}} \quad ; \quad V_{ee} = \sum_{i=1}^N \sum_{j>i}^N \frac{1}{r_{ij}} \quad ; \quad V_{NN} = \sum_A^M \sum_{A>B}^M \frac{Z_A Z_B}{r_{AB}} \quad 1.6$$

with r_{iA} , r_{ij} and r_{AB} are the electron i - nuclei A , electron i - electron j and nuclei A - nuclei B distances respectively. Z_A and Z_B are the nuclear charge of the nuclei A and B . If the system interacts with an external field, such as an electric or magnetic field, Eq.1.4 will contain a new term, V_{ext} , that describes the interaction of the electrons/nuclei with this external perturbation. Obtaining the exact solution of the Schrödinger equation (1.2) is possible only for hydrogenic atoms or for the H_2^+ systems while in the case of poly-electronic systems approximations are necessary. One of these is the so-called Born-Oppenheimer approximation². This simplification is based on the consideration that the mass of the nuclei is much larger than that of the electrons (around 1836 times for the lightest nucleus) and, for this reason, the electrons will move faster than the nuclei. Therefore, the electrons will instantaneously feel the field generated by a fixed distribution of charges represented by the nuclei. We can therefore decouple the movement of the atoms and that of the electrons and the Eq.1.4 can thus be simplified as T_N will be equal zero and V_{NN} will be constant. The electronic Hamiltonian will then be expressed as:

$$H_e = T_e + V_{Ne} + V_{ee} \quad 1.7$$

Therefore, solving the Schrodinger equation will be equivalent to solve the following equation, for a fixed position of the nuclei:

$$H_e \Psi_e = E_e \Psi_e \quad 1.8$$

where E_e is the electronic energy. The total energy will be obtained summing to the electronic energy the constant contribution coming from the fixed nuclei-nuclei repulsion V_{NN} . For simplicity, the multi-electronic wavefunction $\Psi_e(x_1, \dots, x_N)$ will be noted as $\Psi(x_1, \dots, x_N)$ where x_i are the coordinates of the electron i .

Over the years, different methods have been developed to solve Schrodinger's electronic equation, referring to different types of approximations.

These methods can be divided into two categories: methods based on Hartree-Fock³ and methods following the density functional theory (DFT). The studies presented in this thesis have been conducted using methods rooted on the DFT.

The polyelectronic wavefunction

The polyelectronic wavefunction (WF) of a system has to respect the Pauli principle that imposes to the WF to be anti-symmetric. When two electrons are inverted, the sign of the WF should change.

$$\Psi(x_1, x_2, \dots, x_i, \dots, x_j, \dots, x_N) = -\Psi(x_1, x_2, \dots, x_j, \dots, x_i, \dots, x_N) \quad 1.9$$

In 1929, Slater proposed a simple wavefunction that fulfills this condition⁴. The polyelectronic wavefunction is expressed as a determinant composed of mono-electronic wavefunctions, $\phi(x)$:

$$\Psi(x_1, x_2, \dots, x_N) = \frac{1}{\sqrt{N!}} \begin{bmatrix} \phi_1(x_1) & \cdots & \phi_N(x_1) \\ \vdots & \ddots & \vdots \\ \phi_1(x_N) & \cdots & \phi_N(x_1) \end{bmatrix} \quad 1.10$$

The mono-electronic functions expressed in Eq. 1.10 are called spin-orbitals.

$$\phi_i(x) = \phi_i(r)\sigma(s) \quad 1.11$$

Each spin-orbital depends on the spatial and spin coordinates of one electron. $\phi(r)$ and $\sigma(s)$ are respectively the spatial orbital and the function that describe the spin, that can assume only two values (alpha or beta). It is possible also to consider that a wavefunction is composed of a linear combination of several Slater determinants but for the methods presented hereafter, that are all single-reference methods, the wavefunction of the ground state will be described by only one Slater determinant.

1.2 Density functional theory

Density functional theory is a quantum method which allows to study the electronic structure of molecular systems. In this theory, contrary to wavefunction methods, the energy and the properties of any N electron system are described using the electronic density as main variable. This method allows to get rid of the wave function dependent on 3N Cartesian coordinates for a system of N electrons; the wave function can be replaced by the electronic density $\rho(r)$, which depends only on 3 coordinates. The electronic density and the wave function are linked by the following relationship:

$$\rho(r) = N \int d^3 r_2 \int d^3 r_3 \dots \int d^3 r_N \Psi^*(r, r_2, \dots, r_N) \Psi(r, r_2, \dots, r_N) \quad 1.12$$

Historically, the principle on which DFT is based can be traced back to the Thomas-Fermi model⁵ developed in 1927. The Thomas-Fermi model was then improved by Dirac, who added an exchange energy also dependent only on the electronic density of the system. However, it is only in 1964 that Hohenberg and Kohn⁶ formulated the fact that electron density can be used to describe a N electron system. Two theorems were proposed and are described hereafter.

- Existence of the theorem

The external potential $v_{ext}(r)$, and hence the total energy, is a unique functional of the electron density $\rho(r)$.

According to this theorem, all the observables of a system in its ground state, and in particular its energy, can be expressed as a function of the electronic density. A functional, is a function of a function. The electronic energy of a chemical system can be written in this form:

$$E[\rho(r)] = T_e[\rho(r)] + V_{ee}[\rho(r)] + T_{Ne}[\rho(r)] \quad 1.13$$

The potential generated by the nuclei can be considered as a particular case of the external potential, v_{ext} , which the electrons are affected by. It is therefore possible to generalize the equation 1.14 in the form of the equation:

$$E[\rho(r)] = F_{HK}[\rho(r)] + \int v_{ext}(r)\rho(r)dr \quad 1.14$$

The F_{HK} function groups the kinetic energy of electrons and their interactions. This last functional is called universal functional, which does not depend on the external potential and therefore not even on the system under examination.

The energy of a system is *a priori* exact thanks to the knowledge of F_{HK} and of the electronic density only.

- The variational principle

The groundstate energy can be obtained variationally: the density that minimises the total energy is the exact groundstate density.

This second theorem applies the variational principle of quantum mechanics to the particular case of DFT. The energy of a system obtained using a trial electron density approach will always be higher than the exact energy obtained using the exact density.

$$F_{HK}[\rho(r)] + \int v_{ext}(r)\rho(r)dr = E[\rho(r)] \geq E_{exact}[\rho_{exact}(r)] \quad 1.15$$

The variational principle allows to select the electronic density which is the closest to the real value of the real density, chosen in a set of test densities, such as the one that minimizes the total energy of the system. These two theorems show that only the electronic density of a system defines both its Hamiltonian and the value of the observables which derive from it. The original Hohenberg-Kohn analysis involved a minimization over all v -representable densities, but this definition has been somehow overcome by looking at the problem from an alternative view, known as Levy's constrained search formalism⁷. The constrained search starts from the definition that the ground state energy E_0 , corresponding to the Hamiltonian in Eq. 1.7 can be mathematically expressed as:

$$E[\rho(r)] = \min_{\Psi} \langle \Psi | T + V_{ee} + V_{Ne} | \Psi \rangle \quad 1.16$$

The result of this search is the wave function $\Psi[\rho]$ that yields the minimum energy. But one can reach an identical result by splitting the constrained search in two steps. The first search is performed over all wavefunctions that return a given density; the second one over all densities, to select the one that returns the overall lowest energy, called the ground state density $\rho_0(r)$. The constrained search demonstrates that we only need to consider N -representable densities, those associated with an antisymmetric N -electron wavefunction Ψ .

The Kohn-Sham method

In 1965 Walter Kohn and Lu Jeu Sham proposed an exact method to express the exact energy of a N electron system⁸. This method, called Kohn-Sham method, is based on the fact that the kinetic energy of a non-interacting electron gas of a given density, called Ts, can be exactly expressed analytically, contrary to the kinetic energy functional of an interacting electron gas which is not known. In particular Ts can be expressed as:

$$T_s = \frac{1}{2} \sum_i^{el} \langle \psi_i | \nabla_i^2 | \psi_i \rangle \quad 1.17$$

The molecular orbitals, introduced to apply the analytical formula of Ts, are used to construct the multi-electronic wave function of the system, which takes the form of a Slater determinant. Recall that Slater's determinant is a simple mathematical way of approximating the multi-electronic wave function of a system that respects the principle of symmetry of the wave function for fermions, imposed by the indistinguishability of particles in quantum mechanics.

$$\Psi_{Slater}(r_1, r_2, \dots, r_N) = \frac{1}{\sqrt{N!}} \begin{bmatrix} \psi_1(r_1) & \dots & \psi_N(r_1) \\ \vdots & \ddots & \vdots \\ \psi_1(r_N) & \dots & \psi_N(r_N) \end{bmatrix} \quad 1.18$$

The introduction of molecular orbitals and the use of the kinetic energy of a gas of free electrons leads to a system of N coupled monoelectronic equations whose solutions make it possible to calculate the wave function and, consequently, the electronic density. (Eq1.19,1.20 ,1.21). In summary, this method allows to calculate the electronic structure of an electronic gas, in the absence of interactions and subjected to an effective potential, v_{eff} , which has the same electronic density as the real system.

$$H_{KS} \psi_i = \varepsilon_i \psi_i \quad 1.19$$

$$H_{KS} = -\frac{1}{2} \nabla^2 + \int \frac{\rho(r)\rho(r')}{|r-r'|} dr' + v_{ext}(r) + v_{xc}[\rho(r)] = \frac{1}{2} \nabla^2 + v_{eff}[\rho(r)] \quad 1.20$$

$$v_{xc}[\rho(r)] = \frac{\delta E_{xc}}{\delta \rho} \quad 1.21$$

The first term of the Hamiltonian is a term of kinetic energy, the second represents the coulomb interaction between the electrons, the third is the external potential (due to the nuclei), and the last, v_{xc} , represents the potential of exchange and correlation. The last term of energy can be written according to the following form:

$$E_{xc} = (T_{real} - T_s) + \left(V_{ee} - \int \frac{\rho(r)\rho(r')}{|r-r'|} dr' \right) \quad 1.22$$

This relation makes it possible to correct the replacement of the real kinetic energy by the kinetic energy of a system of electrons without interaction and makes it possible to take into account non-classical interactions between electrons. DFT can thus be considered as an exact theory as long as the XC functional is exactly defined. Therefore, the HK-KS energy of a molecular system, E^{HK-KS} , can be expressed as the sum of four terms:

$$E^{HK-KS}[\rho(r)] = T_s[\rho(r)] + V_{Ne}[\rho(r)] + J[\rho(r)] + \epsilon_{XC}[\rho(r)] \quad 1.23$$

where T_s is the kinetic energy of non-interacting electrons, V_{Ne} is the potential representing the electron/nuclei interaction, J corresponds to the classical Coulomb repulsion between electrons and ϵ_{XC} stands for the exchange-correlation functional (XCF). In this way, Kohn and Sham, have created a method for calculating the energy of a system in its ground state. This method will yield the exact energy of a system only if the exchange and correlation potential is known, otherwise it cannot be applied. Since the exact exchange correlation functional expression is not known different approximation were developed to estimate it.

The atomic basis set

In order to solve the Kohn-Sham equations for molecules it is necessary to define the space where the molecular wavefunction extends. This is done by introducing a set of variable functions (ref), called basis sets. The molecular orbitals, which are defined using a linear combination of bases functions (or atomic orbitals χ_i) centered on each atom, it is important to point out that a basis set should be chosen enough large to get a good description of molecular wavefunctions. In real calculations, molecular orbitals are expressed as a linear combination of bases functions: in the case of a system composed by several atoms, molecular orbitals (MO) can be described as linear combination of one electron function (or atomic orbitals χ_i) centered on each atom. The spatial part of each MO, $\phi(r)$, is built as a Linear Combinations of Atomic Orbitals (LCAO):

$$\phi_i(r) = \sum_{\mu} c_{\mu i} \chi_{\mu}(r) \quad 1.24$$

where $c_{\mu i}$ is the coefficient representing the weight of the atomic orbital $\chi_{\mu}(r)$ in the MO. The set of $\chi_{\mu}(r)$ atomic orbitals constitutes the atomic basis set. As a result, the electronic Schrödinger equation assumes a matrix representation, and can be solved by linear-algebraic matrix techniques. Generally, quantum chemical calculations are performed using either Slater-type orbitals (STO) or Gaussian-type orbitals (GTO). The former has an exponential form:

$$\chi^{STO} = \frac{[2\zeta]^{n+\frac{1}{2}}}{[(2n)!]^{\frac{1}{2}}} r^{n-2} e^{-\zeta r} Y_l^m(\Theta, \Pi) \quad 1.25$$

with n , l and m as principal, angular and spin quantum numbers, $Y_l^m(\Theta, \Pi)$, spherical harmonics as a function of radial coordinates and ζ as the exponent of the function which controls its overall spread out away from nuclear center. STOs have the advantage that they closely mimic the orbital shape of the hydrogen atom. The calculation of their integrals is cumbersome. Therefore, the common approach is to use a linear combination of GTOs to reproduce as close as possible the overall form of a given STO. The general for of GTO is:

$$\chi^{GTO} = \left(\frac{2\alpha}{\pi}\right)^{3/4} \left[\frac{[8\alpha]^{i+j+k} i!j!k!}{(2i)!(2j)!(2k)!}\right] x^i y^j z^k e^{-\alpha r} \quad 1.26$$

Gaussian functions are less similar to the 1s hydrogen functions for two reasons: they are not peaked at the nuclear center, and they decay more rapidly. To account for this limitation, contracted Gaussian functions (CGTO) are constructed as linear combination of so-called primitive Gaussian functions according to the expression:

$$\chi^{GTO} = \sum_{\mu} d_{\mu r} \chi_{\mu}^{GTO} \quad 1.27$$

where $d_{\mu r}$ are the contraction coefficients, allowing to control the overall shape of the CGTO. Each primitive function in the linear combination presents the same character (i, j and k are identical) and they differ in the exponent α . In addition, for a given contraction, the standard procedure is to hold the coefficients constant and control the weight of each contraction by an external coefficient. As a consequence, one minimizes the number of coefficients to be determined during the optimization of the overall wave function, reducing the calculation cost. The choice of the atomic basis set is particularly important; the more the basis set is extended, the more accurately the system is described, but the longer the computational time is. Therefore, selecting a basis set is solving a dilemma by taking into account the accuracy/effort balance. The basis sets can be divided in:

- Minimal basis sets: they often give inaccurate results, while they are helpful in understanding qualitatively and quickly thanks to low computational costs (e.g. ST0-2G, ST0-3G).
- Split-valence basis sets: A typical example are Pople type basis set⁹. In this basis set, core electrons are treated with one contracted basis function containing in n-Gaussian primitives, whereas the valence orbitals are treated with two (double- ζ) or three (triple- ζ) basis functions, each with a, b, c Gaussian primitives. The nomenclature for Pople basis sets is n-abcG with n=3 or 6, a=2 or 3, b=1 and c=0 or 1. Two special types of bases functions are usually added to complement the basis: polarization and diffuse functions. The formers are added in order to give flexibility by providing functions with higher angular momentum. The nomenclature for including polarization functions is, for the case of 6-311G for example, 6-311G(d,p). The d indicates that an extra set of d function is added on “heavy” atoms like carbon and nitrogen, whereas the p indicates that polarization functions are added on the hydrogen atoms as well. The latter, diffuse functions, can be added to describe phenomena occurring far from the nuclei (H-bonds, delocalized electrons, excited states. . .). They possess the same angular quantum number as the valence basis functions but decay more slowly when going away from the nucleus.

The nomenclature for adding diffuse functions to the 6-311G basis set is 6-311++G, where the first “+” indicates that extra functions are added to heavy atoms whereas the second “+” is dedicated to hydrogen atoms.

- Other typical functions are Dunning type basis sets¹⁰. Double, triple and quadruple zeta basis sets are multiple basis function corresponding to each atomic orbital, including both valence and core orbitals or just the valence orbitals (e.g. cc-pVDZ, cc-pVTZ, cc-pVQZ). This basis sets, are designed for converging Post-Hartree–Fock calculations systematically to the complete basis set limit using empirical extrapolation techniques. For first- and second-row atoms, the basis sets are cc-pVNZ where N=D, T, Q, 5, 6, ... (D=double, T=triples, etc.). The 'cc-p', stands for 'correlation-consistent polarized' and the 'V' indicates they are valence-only basis sets. They include successively larger shells of polarization (correlating) functions (d, f, g, etc.). More recently these 'correlation-consistent polarized' basis sets have become widely used and are the current state of the art for correlated or post-Hartree–Fock calculations.

Other examples of these are:

cc-pVDZ - Double-zeta

cc-pVTZ - Triple-zeta

cc-pVQZ - Quadruple-zeta

cc-pV5Z - Quintuple-zeta, etc.

aug-cc-pVDZ, etc. - Augmented versions of the preceding basis sets with added diffuse functions.

cc-pCVDZ - Double-zeta with core correlation

While the usual Dunning basis sets are for valence-only calculations, the sets can be augmented with further functions that describe core electron correlation. These core-valence sets (cc-pCVXZ) can be used to approach the exact solution to the all-electron problem, and they are necessary for accurate geometric and nuclear property calculations.

Diffuse functions can also be added for describing anions and long-range interactions such as Van der Waals forces, or to perform electronic excited-state calculations, electric field property calculations. A recipe for constructing additional augmented functions exists; as many as five augmented functions have been used in second hyperpolarizability calculations in the literature. Because of the rigorous construction of these basis sets, extrapolation can be done for almost any energetic property. However, care must be taken when extrapolating energy differences as the individual energy components converge at different rates: the Hartree–Fock energy converges exponentially, whereas the correlation energy converges only polynomially.

To understand how to get the number of functions take the cc-pVDZ basis set for H: There are two s ($L = 0$) orbitals and one p ($L = 1$) orbital that has 3 components along the z-axis ($m_L = -1, 0, 1$) corresponding to p_x , p_y and p_z . Thus, five spatial orbitals in total. Note that each orbital can hold two electrons of opposite spin.

In this thesis we have considered Pople basis sets and Correlation-consistent basis sets.

The exchange correlation functional

General criteria

The major challenge in DFT is finding the appropriate form of the exchange correlation energy, $E_{xc}[p]$, and the resulting $V_x [p]$. Currently, although we do not know the exact form of this functional, there are a number of approximate forms that are fairly good. These approximate models can roughly be divided into three classes:

i) Methods that use a local density approximation (LDA). LDA is based on assumption that the electron density varies very slowly and locally with position and can thus be treated as a homogeneous electron gas. This is not the case for molecules, where the electron density is not uniform. Although LDA gives surprisingly accurate predictions for solid state physics, it is not a useful model for chemistry due to its severe overestimation of chemical bond energies and underestimation of activation barriers.

ii) Methods that combine the electron density calculations with a gradient correction factor, namely Generalized Gradient Approximation (GGA). In order to account for the non-homogeneity of the real electron density, the information about the gradient of the charge density $\nabla P(R)$ was introduced. Although the GGA functionals have showed to give more accurate predictions for thermochemistry than the LDA ones, they still underestimate the activation barriers.

iii) Hybrid methods that are combination of HF exchange and DFT exchange correlation. They are more accurate than both GGA and LDA. A hybrid exchange correlation functional is usually constructed from a linear combination of HF exact exchange, and DFT exchange correlation obtained via either GGA or LDA. To approximate the XCF part, we usually split this term into two parts. The first one (ϵ_x) aims to represent the exchange contribution and accounts for the interaction between electrons with the same spin (from Pauli principle) and the second part (ϵ_c) aims estimating the correlation effects not included in the first term.

$$\epsilon_{xc}[\rho(r)] = \epsilon_x[\rho(r)] + \epsilon_c[\rho(r)] \quad 1.28$$

The inclusion of exact HF exchange often improves calculated results, although the optimum fraction to include the HF exchange depends on the specific property of interest.

New functionals improved by including a suitable fraction of the exact exchange is nowadays a standard feature. At least, part of the improvement may arise from reducing the self-interaction error, since HF theory is completely self-interaction free. A typical approach is proposed for a magic combination of exchange and correlation functionals by a few adjustable scaling parameters and a choice of basis set in order to reproduce a selected set of experimental data. This procedure is not theoretically justified and should be merely considered as data fitting without much physical relevance. Therefore, this procedure can be taken as an experimental fitting to functions that can be useful to predict specific properties for a series of compounds. One may furthermore differentiate the functionals based on their use or lack of experimental data for the parameterization in the functional forms. The non-empirical ones, such as PBE functionals, use the free parameters to fulfill many requirements. Empirical ones, such as the BLYP or B3LYP, were attempted to improve the performance by fitting the free parameters to give a good agreement with experimental data. The main difference between the hybrid functionals is due to the different portion of the HF exact exchange functional E_x^{HF} . Hereafter are presented different families of XCF. They can be classified regarding their accuracy on a scale, the so-called Jacob's Ladder (Figure 1). Functionals vary from very simple to very complex. On Jacob's ladder of approximations¹¹ each rung represents a different level of approximation that should recover the results of lower rungs in the appropriate limits, but add more capabilities.

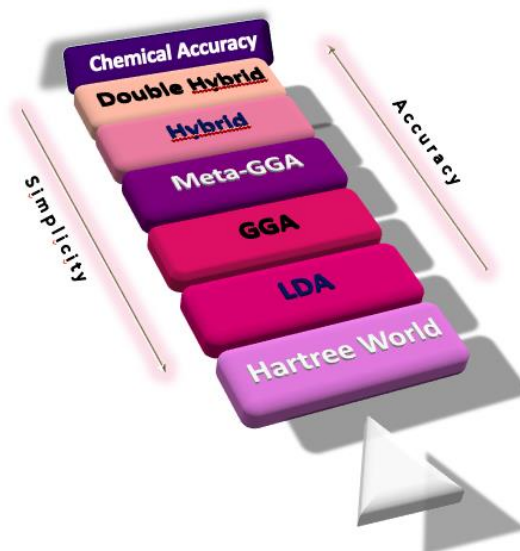


Figure 1. Illustration of the Jacob's ladder adapted from Perdew's work¹².

Local density approximation

The lowest rung is the local density approximation (LDA), in which the XC energy density depends only on the density at a point and is that of the uniform electron gas of that density. This is the simplest density functional. It was used for a generation in materials science, but is insufficiently accurate for most chemical purposes. LDA typically overbinds molecules by about 30 kcal/mol, an unacceptable error for chemical applications. We will start to describe the shape of various functionals, which constitute a fundamental part for the advancement in the DFT field. All these formulations differ by the functional dependence of E_{xc} on the electron density. E_{xc} is expressed as the integral of the product between the electron density and a so-called energy density ϵ_{xc} that depends from the electron density:

$$E_{XC}[\rho(r)] = \int dr \rho(r) \epsilon_{XC}[\rho(r)] \quad 1.29$$

In this equation, the energy density is a sum of individual exchange and correlation contributions. The Local Density Approximation¹³ takes into account the energy density at each position r , computed using the value of ρ at the same position- therefore the functional is local.

$$E_{XC}^{LDA}[\rho(r)] = \int dr \rho(r) \epsilon_{XC}[\rho^*(r)] dr_{\rho^*=\rho} \quad 1.30$$

The functionals LDA approximation is still used for large systems where the electronic density is uniform, indeed for each given point the exchange-correlation energy, indeed is computed as the energy of a uniform gas of the same local density.

Generalized gradient approximation and kinetic energy density

The second level of the Jacob's ladder corresponds to the Generalized Gradient Approximation (GGA)¹⁴. The electronic density of a molecule is not uniform leading to a limitation in the use of LDA approximation. A way to get over a part of these limitations is to build exchange correlation functionals which depend not only on the local value of the density but also on its gradient. Usually, gradient corrected functionals are obtained by adding a correction term to LDA functional:

$$E_{XC}^{GGA}[\rho(r)] = \epsilon_{xc}^{LDA}[\rho(r)] + \Delta\epsilon_{xc} \left[\frac{|\nabla\rho(r)|}{\rho^{\frac{4}{3}}(r)} \right] \quad 1.31$$

where the correction depends on the dimensionless reduced gradient $\frac{|\nabla\rho(r)|}{\rho^{\frac{4}{3}}(r)}$.

The new XCF is thus the XCF of the LDA approximation with a correction taking into account the inhomogeneity of the density. One has to notice that the XCF, as for LDA approximation, still depends on the density and its gradient at a given point inducing a "local" character for this approximation also.

$$\epsilon_{XC}^{GGA}[\rho(r), \nabla\rho(r)] = \epsilon_{XC}^{LDA}[\rho(r)] + \Delta\epsilon_{XC} \left[\frac{|\nabla\rho|}{\rho^{\frac{4}{3}}} \right] \quad 1.32$$

GGA can be improved by considering also the second derivative of the electron density also known as the kinetic energy density, ∇^2 . Those functionals are known as meta-GGA functionals¹⁵ and are built using the second order derivative.

$$E_{XC}^{meta-GGA}[\rho(r)] = \int \rho \epsilon_{XC}[\rho, \nabla\rho, \nabla^2\rho] dr \quad 1.33$$

GGA functional is more accurate than LDA. Most importantly, they greatly reduce the bond dissociation energy error, and generally improve transition-state barriers. But, unlike LDA, there is no single universal form. Popular GGAs include PBE¹⁶ and BLYP^{17,18} functionals.

PBE

The PBE functional belongs to the class of generalized gradient approximation (GGA) functionals for the exchange-correlation energy E_{xc} . PBE is a parameter-free GGA functional and is the one developed by Perdew, Burke and Ernzerhof. In this GGA functional there is the inclusion of gradient correction without introducing experimentally fitted parameters which makes them valid for a wide range of systems. It is known for its general applicability and gives rather accurate results for a wide range of systems.

BLYP

The frequently used among those parameterized BLYP functional combines Becke's 1988 exchange functional with the correlation functional by Lee, Yang, and Parr. This functional, containing only one parameter, fits the exact Hartree-Fock exchange energies of a wide variety of atomic systems with remarkable accuracy, surpassing the performance of previous functionals containing two parameters or more.

Hybrid functionals and adiabatic connection

Higher on the Jacob's ladder one can find the hybrid functionals. According to Kohn-Sham scheme, the E_{xc} functional is defined assuming a fully non-interacting reference system of particles. Instead one could imagine to follow-up the extent of the electron-electron interaction with extra parameter. This last consideration is the idea which underlies the adiabatic connection formalism¹⁹, which make it possible to establish the relationship between the real and the non-interacting system. The adiabatic connection follows directly from the Hellmann-Feynman theorem, which relates the derivative of the Hamiltonian with respect to that same parameter. As a result, the exchange-correlation energy can be expressed as:

$$E_{xc} = \int_0^1 \langle \Psi(\lambda) | V_{xc}(\lambda) | \Psi(\lambda) \rangle \quad 1.34$$

where the parameter λ controls the amount of electron-electron interaction. When $\lambda=1$ the total interaction energy ($E_{xc}-E_h$) is equal in value to the exact exchange energy E_{xc}^{HF} . The parameter λ allows to go smoothly from the fully non-interacting to the interacting system (at a fixed density value ρ_0). The exchange correlation energy is the average of the exchange correlation hole E_h :

$$E_{xc} = \int_0^1 \langle \Psi(\lambda) | V_{ee}(\lambda) | \Psi(\lambda) \rangle - J[\rho] = E_h[\rho] \quad 1.35$$

As exchange correlation energy arises from electron-electron interaction, a logical improvement to the GGA approach is to construct the exchange correlation functional in a systematic way, by mixing a fraction of exact exchange, derived from HF theory²⁰ with a standard LDA or GGA. As a result, the E_{xc} can be expressed as:

$$E_{xc} = (1 - a)E_{xc}^{DFT} + aE_x^{HF} + E_c^{GGA} \quad 1.36$$

Drawing this connection between the interacting and non-interacting systems form the basis for what are known as hybrid density functionals. Using the adiabatic connection formalism, one can express the exchange-correlation potential as a function of λ . This results in a polynomial function of degree $n-1$ and depends on the parameter λ , which controls the mixing of both the exchange and correlation from DFT, and the HF exchange.

The integer n then controls the speed with which the correction brought to DFT is cancelled when λ tends toward the unit:

$$U_{XC}^\lambda[\rho(r)] = E_{XC}^{DFT}[\rho(r)] + (E_X^{HF}[\rho(r)] + E_X^{DFT}[\rho(r)])(1 - \lambda)^{n-1} \quad 1.37$$

Integration of the equation 1.31 over the interval $\lambda \in [0,1]$ gives:

$$E_{XC}[\rho] = \int_0^1 d\lambda U_{XC}^\lambda[\rho(r)] = E_{XC}^{DFT}[\rho(r)] + \frac{1}{n}(E_X^{HF}[\rho(r)] + E_X^{DFT}[\rho(r)]) \quad 1.38$$

PBE0

The PBE0 functional was proposed by Carlo Adamo et al. in 1999²¹. This functional was built starting from the functional PBE²², which is part of the GGA family and does not contain any empirical parameters. In PBE0, 25% of the exchange is replaced with 25% of Hartree-Fock exchange. Recall the replacement with the Hartree-Fock exchange was proposed by Perdew on purely theoretical considerations that allow to say that PBE0 is an hybrid functional (so called for the Hartree-Fock exchange part) without adjusted parameter.

$$E_{XC}^{PBE0}[\rho(r)] = E_{XC}^{PBE}[\rho(r)] + \frac{1}{4}(E_X^{HF} - E_X^{PBE}[\rho(r)]) \quad 1.39$$

B3LYP

The B3LYP²³ is the most used hybrid functional parametrized and one of the most successful functional in term of overall performance. B3LYP incorporates a portion of 20 % of exact exchange functional from HF theory with exchange and correlation functional from other references (ab-initio or semi-empirical methods). More precisely, this functional combines GGA (B88²⁴ and LYP²⁵) and LDA (VWN²⁶) functionals and HF exchange.

$$E_{XC}^{B3LYP}[\rho(r)] = E_{XC}^{LDA}[\rho(r)] + a_0(E_X^{HF} - E_X^{LDA}[\rho(r)]) + a_x(E_X^{GGA}[\rho(r)] - E_X^{LDA}[\rho(r)]) + a_c(E_C^{GGA}[\rho(r)] - E_C^{LDA}[\rho(r)]) \quad 1.40$$

where $a_0=0.20$, $a_x=0.72$ and $a_c=0.81$. One can see that the last two terms are used to correct both exchange and correlation GGA energies by subtracting the LDA energy.

Range-separated hybrid functionals

Savin stated that at short distances, the dominant interaction is the dynamic correlation whereas at large distances, the non-Coulombic interaction (from the exchange part, nicely described within HF approach) is dominant²⁷ (1996). Therefore, depending on the considered interaction (at short or long distance), the ratio of HF exchange should not be constant. New XCF has been developed taking into account the possibility for the ratio of HF exchange to change upon variation of the inter-electronic distance. They are known as range-separated hybrids (RSH). The percentage of HF exchange is thus varying if one considers short range (SR) or long range (LR) interaction. This is taken into account by splitting the electron-repulsion operator into two parts:

$$\frac{1}{r_{12}} = \frac{1 - [a + b \operatorname{erf}(\gamma r_{12})]}{r_{12}} + \frac{a + b \operatorname{erf}(\gamma r_{12})}{r_{12}} \quad 1.41$$

where r_{12} is the inter-electronic distance and a and b are parameters and γ is an attenuation factor. A better asymptotic behavior is thus found when the inter-electronic distance is increasing. Benchmark studies have shown that RSH functionals provide accurate excitations energies for excitations presenting a charge transfer character^{28,29}.

LC-PBE

This functional³⁰ works particularly well in combination with the short-range variant of the Perdew-Burke-Ernzerhof (PBE) exchange functional and in addition, the prefix LC- may be added to apply the long correction of Hirao and coworkers³¹. Considering a decomposition by splitting of the Coulomb operator into short-range (SR) and long-range (LR) parts, a long-range corrected (LC) hybrid of a Density Functional Approximation (DFA) is defined as:

$$E_{XC}^{LC-DFA} = E_X^{SR-DFA}(\omega) + E_X^{LR-HF}(\omega) + E_C^{DFA}(\omega) \quad 1.42$$

This long-range-corrected hybrid is remarkably accurate for a broad range of molecular properties, such as thermochemistry, barrier heights of chemical reactions, bond length. The description of the processes involving long-range charge transfer because for the most part, non-Coulomb part of exchange functionals becomes very inaccurate at large distances, making them unsuitable for modeling processes such as electron excitations to high orbitals.

CAM-B3LYP

CAM-B3LYP is a range-separated hybrid functional. This functional is based on the Coulomb-attenuating method (CAM) along with the global hybrid B3LYP. It also considers a larger percentage of exact HF exchange for long-range (0.65) than for short-range (0.19) inter-electronic interactions. This functional is thus qualified of long range corrected functional. The parameters of the electronic-repulsion operator (Eq. 1.30) that are γ , a and b are set to 0.33, 0.19 and 0.46 respectively.

Double hybrid functional overview

At the highest level of the scale we find the double hybrid functionals, used in this work and which we will discuss in the next chapter.

During this PhD, Generalized Gradient Approximation (GGA), Hybrid and Double Hybrid functionals were used as investigative tools.

1.3 Time-Dependent Density Functional Theory

The previously mentioned works of Hohenberg, Kohn and Sham have permitted to study the ground states of the systems. However, it is not possible to use those formalisms when the system is being perturbed by an external potential that is time-dependent as this is the case for the light-matter interaction. The Time-Dependent version of DFT, TD-DFT, allows the description of such phenomenon. It has been proposed by Runge and Gross in 1984³². According to TD-DFT formalism, when a polyelectronic system is perturbed by an external time-dependent potential, all the properties are determined thanks to the value of the time-dependent density at a time t , $\rho(r,t)$. The Runge Gross theorems are the equivalent of the Hohenberg and Kohn's ones excluding the fact that this time the external potential is time-dependent. It ensures a unique relationship between the external time-dependent potential $v_{ext}(r,t)$ and the time-dependent-density, $\rho(r,t)$.

Analogously to the KS equations, one can write time-dependent equations to solve the time-dependent Schrödinger equation to retrieve the desired properties, i.e the excited state electronic density:

$$H_{RG}\Psi_i(r,t) = i\hbar \frac{\partial}{\partial t}\Psi_i(r,t) \quad 1.43$$

with:

$$H_{RG} = T_s[\rho(r)] + \int \frac{\rho(r,t)\rho(r',t)}{r-r'} dr' + v_{ext}(r,t) + v_{XC}[\rho(r)](r,t) \quad 1.44$$

and

$$v_{XC}[\rho(r)](r,t) = \frac{\partial A_{XC}[\rho(r)]}{\partial \rho(r,t)} \quad 1.45$$

As in DFT, the A_{XC} functional is not analytically known. An approximation, called adiabatic approximation, allows us to write the functional as follows:

$$A_{XC}[\rho(r)] = \int E_{XC}[\rho_t(r), t] dt \quad 1.46$$

E_{XC} represents the exchange-correlation energy introduced in the KS formalism and $\rho_t(r)$ is the electronic density at a time t . This approximation is available only if the external potential is slowly varying with time.

The exchange-correlation potential is calculated only for the density considered at the time t . It can thus be considered as a local approximation with respect to the time. The exchange-correlation potential is finally written as:

$$v_{XC}[\rho(r)](r, t) = \frac{\partial A_{XC}[\rho(r)]}{\partial \rho(r, t)} \approx \frac{\partial E_{XC}[\rho(r)]}{\partial \rho_t(r)} = v_{XC}[\rho_t(r)](r) \quad 1.47$$

By applying the adiabatic approximation, the exchange-correlation potential that will be used is the one of time-independent DFT. However, one needs also to solve the equations proposed by Runge and Gross for a time-dependent (at any time) external potential. Within the Linear Response (LR) theory, one can write the time-dependent external potential as the sum of a time-independent and time-dependent term:

$$v_{ext}(r, t) = v_{ext}^0(r) + v_{ext}^1(r, t) \quad 1.48$$

Based on the same approach, one can rewrite the electronic density:

$$\rho_{ext}(r, t) = \rho_{ext}^0(r) + \rho_{ext}^1(r) + .. \quad 1.49$$

The first-order corrected density can be calculated using the linear response function:

$$\rho_{ext}^{(1)}(r, t) = \iint \chi(r, r', t - t') v_{ext}^{(1)}(r', t') dr dt' \quad 1.50$$

If the external perturbation is an oscillating electromagnetic field (as this is the case for light for example), with a pulsation ω , the pulsations for which the LR function is diverging (known as the poles of the function) correspond to the electronic transitions of the system, that is to say the absorption values. In the case of a system containing non-interacting electrons, the LR function, χ , is a sum of fractional terms with at the denominator, the pulsation difference and the energetic gap between occupied and virtual orbitals. In this, the transitions are occurring at energies that correspond to the energetic gap between occupied and virtual orbitals.

$$\chi_s(r, r', \omega) = \sum_i^{occ} \sum_j^{virt} \frac{\Psi_i^*(r) \Psi_j(r) \Psi_i^*(r') \Psi_j(r')}{\omega - \epsilon_j + \epsilon_i + i\eta} \quad 1.51$$

where terms with i and j indices correspond to properties related to occupied and virtual orbitals respectively. However, in real systems, the electrons are in interaction and the LR function has a more general expression:

$$\chi(r, r', \omega) = \chi_s(r, r', \omega) + \iint \chi_s(r, r_1, \omega) k(r_1, r_2, \omega) \chi_s(r_2, r', \omega) dr_1 dr_2 \quad 1.52$$

The function $\kappa(r_1, r_2, \omega)$, the kernel, allows to take into account the electron-electron interactions. The transition energies are no longer the energetic differences between occupied and virtual orbitals. Casida, based on the general formulation of the LR and the kernel, proposed an eigenfunction whose eigenvalues are the excitation energies^{33,34}. The oscillator strengths of the transition, representing the intensity of this transition, between two electronic states, Ψ_0 and Ψ_1 characterized by the energy E_1 and E_0 , are obtained as follows:

$$f = \frac{2}{3} (E_1 - E_0) |\langle \Psi_1 | \vec{R} | \Psi_0 \rangle|^2 \quad 1.53$$

When studying a fluorescence phenomenon (return of a system from the excited state to the ground state with the emission of a photon), this oscillator strength becomes the Einstein coefficient for spontaneous emission, A which allows to evaluate the lifetime of the excited state t :

$$A = \frac{(E_1 - E_0)^2}{2\varepsilon_0 \pi \hbar^4 c^3} f \quad ; \quad \tau = \frac{1}{A} \quad 1.54$$

This method allows to calculate the absorption and emission spectrum of molecular systems with great precision and with calculation times shorter than some post-HF methods.

1.4 Solvent Models

Taking into account the environment in which the molecules are is of major importance for the calculation of the molecular properties. When molecules are solvated, one needs to consider the solvent effect in the calculation. Two different approaches are possible to mimic the effects of the environment, the solvent can be treated implicitly or explicitly.

Explicit model

The solvent molecules can be treated explicitly that is to say that the molecules are atomically described. It allows the description of specific solute-solvent interactions (hydrogen bonds for example). Because the solvent molecules have to be explicitly positioned, the polarity around the solute is more realistic. A dynamic study can be necessary to consider a reliable configuration of the solvent molecules around the solute. One can thus consider specific interaction explicitly and still have a reasonable calculation cost by playing on the level of theory used for each system.

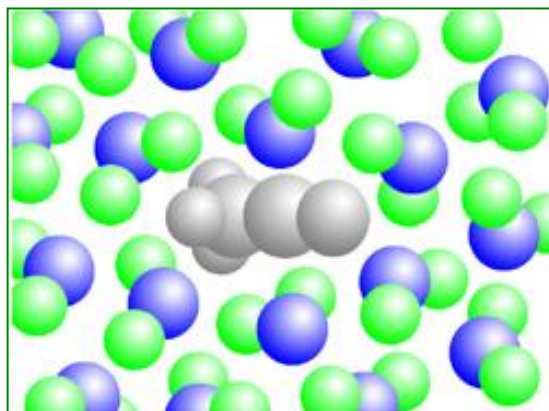


Figure 2. Explicit solvent model: considering the molecular details of each solvent molecules.

Implicit model

Within the implicit model, the solvent is described as a homogeneous medium, characterized by a dielectric constant. This constant is defined for all the usual solvents. In our case the solvent was the Methylene chloride ($\epsilon=9.1$). Solvent molecules are thus not explicitly described in this approach.

We present here the Polarizable Continuum Model (PCM) that has been used during our studies³⁵. The solvation free energy, ΔG equivalent to all the average solute/solvent interactions, can be written as follows:

$$\Delta G = \Delta G_{el} + \Delta G_{cav} + \Delta G_{dr} \quad 1.55$$

where:

- ΔG_{el} is the electrostatic contribution. It corresponds to the interaction between the charges of the solute and the charges of the solvent, created by the continuum at the solute-solvent interface.
- ΔG_{cav} the cavitation energy. This is the energy that is necessary to create the cavity of the solute in the continuum.
- ΔG_{dr} the dispersion-repulsion energy. It represents the interaction between molecules that have instantaneous polarization.

Within the PCM method both nuclear and electronic degrees of freedom of the solute in its ground state are in equilibrium with the solvent (this is the equilibrium limit)³⁶. When a system is interacting with an external field, as this is the case upon UV-Vis irradiation, the polarization of the interacting system is modified accordingly to the frequency of the applied field. When the frequency is low (slow process), the solvent molecules have time to orient themselves in the direction of the applied field. When the frequency is increasing (fast process), only the electrons are reactive enough to adapt themselves to the external field. Considering an electronic transition from a ground state (GS) to an excited state (ES), two different approaches for the solute-solvent interaction can be used:

- The equilibrium (eq) limit. In this case, the solvent has time to adapt itself to the new electronic configuration of the solute (the ES).

- The non-equilibrium (neq) limit. Here, only the electrons of the solvent have time to adapt to the electronic configuration of the ES.

Within the Franck-Condon approximation, a transition between two electronic states is so fast that it is considered as vertical. Therefore, it should be computed within the “neq” limit.

For absorption, the solvent is in equilibrium with the GS but in non-equilibrium with the ES. For emission, the solvent is in equilibrium with the ES but in non-equilibrium with the GS.

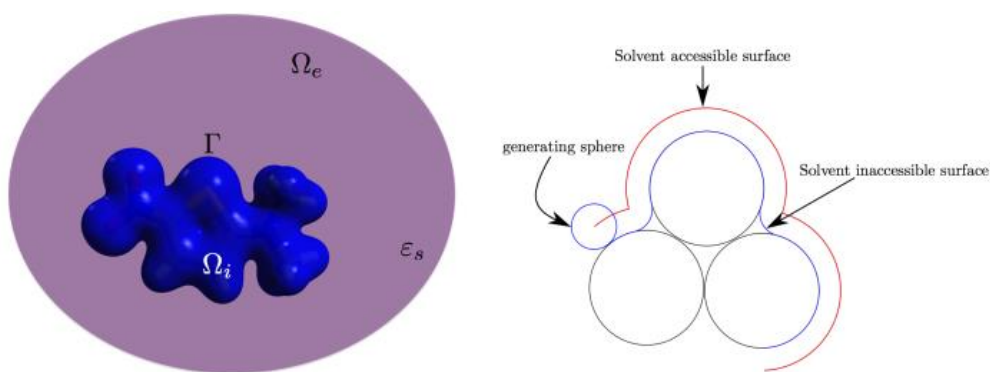


Figure 3. PCM model: treating the solvent as a continuous medium.

In addition, different levels of refinement exist to simulate how the PCM cavity is polarized in the excited state:

- The Linear-Response (LR) model^{36,37} this is the most straightforward scheme, in which the change in the PCM charges is calculated in terms of the transition densities.

- The State-Specific (SS) approaches. One can cite for example the corrected LR (cLR) scheme³⁸ that rely on the change of total dipole moment upon transition to model the solvent response to the change of state or the approach due to Roberto Improta, Vincenzo Barone, Giovanni Scalmani and Mike J.Frisch(IBSF)³⁹.

The LR formulation is generally well-suited for strongly dipole-allowed transitions characterized by a small change of the electron density, i.e., for local ES, whereas the SS is more suited for charge transfer cases, in which the oscillator strength is small but the change of dipole is large^{35,40}.

References

- 1) Schrödinger, E. *Phys. Rev.*, **1926**, 28:1049–1070.
- 2) Born, M.; Oppenheimer, R. *Ann. Phys. (Berlin)*, **1927**, 389(20):457–484.
- 3) Hartree, D. R. *Math. Proc. Camb. Philos. Soc.*, **1928**
- 4) Slater, J. C. *Phys. Rev.*, **1929**, 34:1293–1322.
- 5) Thomas, L. H. *Proc. Cambridge Phil. Soc.* 23,542, **1927**
- 6) Hohenberg, P. Kohn W.; *Phys. Rev.*, **1964**, 136B864–B871.
- 7) Levy, M. *Phys. Rev.* vol.26 1200-1208, Jan **1982**
- 8) Kohn, W.; Sham, L. J. *Phys. Rev.*, **1965**, 140A1133–A1138.
- 9) Ditchfield, R.; Hehre, W. J.; Pople, J. A. *J. Chem. Phys.*, **1971**, 54:724–728.
- 10) Dunning, T. H. *J. Chem. Phys.*, **1989**, 90 (2): 1007–1023.
- 11) Perdew, J. P.; Schmidt, K. *AIP Conf. Proc.* **2001**, 577,1–20.
- 12) Perdew, J. P.; Ruzsinszky, A.; Constantin, L. A.; Sun, J.; Csonka, G. I. *J. Chem. Theory Comput.*, **2009**, 5(4):902–908.
- 13) Khon, W.; Sham, L.J. *Phys. Rev.*, **1965**, vol 140 1133-1138.
- 14) Perdew, J.P.; Burke, K.; Ernzerhof, M. *Phys. Rev.Lett.* **1997** vol.78 1396.
- 15) Tao, J et al. *arXiv.org*, **2003**, 146401.
- 16) Perdew, J. P.; Burke, K.; Ernzerhof, M. *Phys. Rev. Lett.* **1997**, 78, 1396 (E).
- 17) Becke, A. D. *Phys. Rev.A*, **1988**, 38, 3098–3100.
- 18) Lee, C.; Yang, W.; Parr, R. G. *Phys. Rev. B*, **1988**, 37, 785–789.
- 19) Becke, A.D. *The Journal of Chemical Physics*, **1993**, vol.98, 5648-5652.

- 20) Szabo, A.; Ostlund, N. *Dover Publication Inc.*, **1982**, NYC.
- 21) Adamo, C.; Barone, V. *The Journal of Chemical Physics*. **1999**, 110 (13): 6158–6170.
- 22) Perdew, J. P.; Burke, K.; Ernzerhof, M. *Phys. Rev. Lett.*, **1997**, 78:1396–1396.
- 23) Becke, D. *J. Chem. Phys.*, **1993**, 98, 5648–5652.
- 24) Becke, D. *Phys. Rev. A*, **1988**, 38:3098–3100.
- 25) Lee, C.; Yang, W.; Parr, R. G. *Phys. Rev. B*, **1988**, 37,785–789.
- 26) Vosko, S. H.; Wilk, L.; Nusair, M. *Can. J. Phys.*, **1980**, 58(8)-1200–1211.
- 27) Savin, A. *Theoretical and Computational Chemistry*, **1996**, vol.4, 327 – 357. Elsevier.
- 28) Jacquemin, D.; Perpète, E. A.; Scuseria, G. E.; Ciofini, I.; Adamo, C. *J. Chem. Theory Comput.*, **2008**, 4(1)-123–135.
- 29) Jacquemin, D.; Planchat, A.; Adamo, C.; Mennucci, B. *J. Chem. Theory Comput.*, **2012**, 8, 2359–2372.
- 30) Vydrov, O.A.; Scuseria, G.E. *J. Chem. Phys.* **2006**, 125, 234109.
- 31) Song, J-W.; Hirose, T.; Tsuneda, T.; Hirao, K. *J. Chem. Phys.*, **2007**, 126, 154105.
- 32) Runge, E.; Gross, E. K. U. *Phys. Rev. Lett.*, **1984**, 52 (12): 997–1000.
- 33) Casida, M. *World Scientific.*, **1995**.
- 34) Casida, M.; Huix-Rotllant, M. *Annu. Rev. Phys. Chem.*, **2012**, 63(1)-287–323.
- 35) Mennucci, B. *Wiley Interdisciplinary Reviews: Computational Molecular Science*, **2012**, 2, 386–404.
- 36) Cammi, R.; Mennucci, B. *J. Chem. Phys.*, **1999**, 110 (20)-9877–9886.
- 37) Cossi, M.; Barone, V. *J. Chem. Phys.*, **2001**, 115 (10)-4708–4717.

38) Caricato, M.; Mennucci, B et al. *J. Chem. Phys.*, **2006**, 124, 124520.

39) Improta, R., Barone, V.; Scalmani, G.; Frisch, M. J. *J. Chem. Phys.*, **2006**, 125(5)-054103.

40) Guido, C. A.; Jacquemin, D.; Adamo, C.; Mennucci, B. *J. Chem. Theory Comput.*, **2015**, 11(12)-5782–5790.

Double Hybrids and Time-Dependent Density Functional Theory: An Implementation and Benchmark on Charge Transfer Excited States

2.1 Context

In this chapter, we studied the implementation of a formalism allowing the use of Double Hybrid (DH) Density Functional Approximations (DFAs) with Time Dependent Density Functional Theory. In particular, we focused on the analysis of their performance for the description of through space charge-transfer (CT) excitations which are well known to be very problematic to be described with commonly used functionals, such as global hybrids.

For this study, two different families of DFAs were compared, each of them containing pure, hybrid (global and range separated hybrids) and double-hybrid functionals. The results obtained show that very good performance for the description of CT excitations can be obtained using DHs. In particular, these functionals provide results with an accuracy comparable to that of adjusted range separated functionals, with the relevant difference that for DHs no parameter is tuned on a specific class of compounds to reproduce its excited state properties thus making them more appealing for a general use. Furthermore, the algorithm described and implemented is characterized by the same computational cost scaling as that of the ground state algorithm employed for MP2 and double hybrid DFAs.

Double hybrid density functional approximations

Double hybrids functionals were developed from 1996 with Ernzerhof's¹. His work has led to significant progress in the field of density functional theory applied to double-hybrid (DH) approximations. Then the B2PLYP approach developed by Grimme² introduces in the approximation a fraction of the second order Møller-Plesset (MP2) correlation in a global hybrid (GH) exchange and correlation expression:

$$E_{xc}^{DH}[\rho] = a_x E_x^{HF} + (1-a_x) E_x^{DFA}[\rho] + (1-a_c) E_c^{DFA}[\rho] + a_c E_c^{MP2} \quad 2.1$$

where E^{HF} denotes the Hartree-Fock like exchange, and E^{DFA} is the semilocal exchange and correlation density-functional approximation (DFA). Like for a global-hybrid, the first three terms are computed following a self-consistent pathway. The last term is added at the end and evaluated from the optimized GH Kohn-Sham (KS) orbitals, even if orbital-optimized approaches already exist³. Following Eq.(1) most of DHs in the literature are based on the generalized-gradient approximation (GGA) or meta-GGA, another scale spin components of the MP2 part, some others are built with a perturbative term computed from B3LYP^{4,5} or PBE0^{6,7}. All these DHs have the same features: two empirical parameters a_x and a_c , adapted on different datasets in agreement with the property of the systems under consideration. Toulouse et al. derived a family of one-parameter DHs^{8,9,10} starting from the formalism of the adiabatic connection (CA). Again, Fromager generalizes these studies to a two-parameter DH formalism with a fraction of exact parts of exchange and perturbation¹¹. This theory, however, does not define specific values for the parameters, essential for the development of the double hybrid functional. Afterwards, more accurate studies have shown that an average on the adiabatic connection, a cubic relationship between a_x and a_c and the PBE density function led to an excellent candidate without parameters: the double hybrid PBE0-DH^{12,13}. Recently, Brémond and collaborators have created a new double-hybrid model functional from the exchange of adiabatic connection and the integration of correlation, defining that the amount of correlation calculated by the perturbation is fixed at 1/3 and the exact exchange ratio can vary between 2/3 and 1¹⁴. This quadratic integrand double-hybrid (QIDH) is coupled with PBE and TPSS semilocal functionals, and the amount of exact exchange is set to decrease the SIE of many-electron systems. The overall performances of PBEQIDH are close to that of PBE0-DH but improve the SIE treatment.

As previously mentioned, to test the robustness of the method, a benchmark was made using two families of functionals starting from the simplest ones, to the most accurate double hybrids. The DHs used were PBE0-DH, PBEQIDH and B2PLYP.

PBE0-DH

In this functional the ratio of the Hartree-Fock, Kohn-Sham, and perturbation terms (MP2) is determined on the basis of physical considerations. PBE0-DH contains a small MP2 contribution (12.5%). From the obtained results, PBE0-DH seems to represent a significant improvement with respect to the PBE0 functional, a parameter free hybrid; its performances are comparable to the ones found using other parameterized double hybrids.

PBEQIDH

This functional is based on a quadratic form that models the integrand of the coupling parameter, whose components are chosen to satisfy several well-known limiting conditions. Its integration leads to DHs containing a single parameter controlling the amount of exact exchange, which is determined by requiring it to depend on the weight of the MP2 correlation contribution. Two new parameter-free DHs functionals are derived in this way, by incorporating the non-empirical PBE and TPSS functionals in the underlying expression.

$$E_{xc}^{QIDH} = \frac{\lambda_x+2}{3} E_x^{HF} + \frac{1-\lambda_x}{3} E_x^{DFA}[\rho] + \frac{1}{3} E_c^{MP2} + E_c^{DFA}[\rho] \quad 2.2$$

Introduction to the double hybrids functionals

Approaches rooted in DFT nowadays provide valuable insights for the understanding of a wide variety of chemical problems as witnessed by their widespread use in the last two decades¹⁵⁻¹⁷. Their success mainly relies on a very favorable cost to accuracy ratio enabling the description of ground state properties of relatively large molecular systems. Nonetheless the accuracy reached using DFT approaches strongly depends on the nature of the density functional approximation (DFA) used and, in particular, on the expression of the contribution to exchange and correlation energies^{15,16}. For the time being, one of the most sophisticated and accurate DFAs for ground state properties are represented by the so called Double Hybrid functionals (DH) casting in the DFA expression both Hartree-Fock (HF) exchange and a second order perturbative contribution computed with Kohn-Sham orbitals to the correlation¹⁸⁻²⁰.

These functionals thus introduce an explicit dependence of the energy expression on both occupied and virtual orbitals. Several papers in literature, following the seminal works of Truhlar²¹ and Grimme²⁰, have demonstrated their rigorous theoretical foundation¹⁸⁻²⁶.

If these functionals have proven to be extremely performant for many ground state properties (such as thermochemistry or the description of weak interacting systems²⁷⁻²⁸) nonetheless their largest limitation is the computational cost associated to the evaluation of their non-local correlation contribution. Indeed, even if scaling techniques may reduce the computational effort without altering their accuracy, DHs, with a formal scaling of $\mathcal{O}(N^4)$ at best, still remain expensive when compared to ‘standard’ global or range separated hybrids DFAs.

This situation is even more involved when considering the use of DHs for the treatment of excited state. Grimme and Neese proposed in 2007²⁹ a Time Dependent formulation in the context of the Tamm-Dancoff approximation for DHs resting on a standard linear response formulation corrected by a second-order perturbative term derived from the Head-Gordon’s CIS(D) approach³⁰ (hereafter TD(A)-DHFT). This correction to excitation energy is scaled by the weight of the second order (MP2) correlation term in the ground state energy expression. Using this formalism several authors have applied DHs to compute vertical excitation energies of organic molecules up to medium size³¹⁻³⁴. Recently, scaling techniques^{35, 36} have been applied to both increase the TD(A)-DHFT accuracy and reduce associated computational cost (for instance by neglecting spin opposite terms)^{32,37}.

Since the results obtained are extremely encouraging in term of accuracy, in the present work we describe the implementation and benchmarking of TD(A)-DFT approaches focusing on the analysis of their performance for the description of through space charge-transfer (CT) excitations which are well known to be very problematic to be described using standard global hybrid approaches³⁸⁻⁴³.

Two different families of functionals will be compared: those derived imposing the fulfillment of some theoretical constraints, and those based on a more empirical fitting approach. For each of these families the performance of pure (GGA), hybrid (global and range separated hybrids) or double-hybrid functionals will be firstly assessed on standard benchmark and next analyzed using a set of charge transfer dimers, recently investigated by Baer and collaborators, as test case⁴².

2.2 Time Dependent Density Functional Theory and Double Hybrid (DH) Density Functional Approximations (DFAs)

The description of electronic excited states can be approached in several different ways. Conceptually the easiest approach is based on the Configuration Interaction method truncated to include only singly excited determinants (CIS)⁴⁴. In this case the excited states are found by diagonalizing the Hamiltonian matrix that spans only the subspace generated by singly excited determinants. In its extreme simplicity CIS method lacks an explicit treatment of the electronic correlation of the ground (reference) determinant. This is often recovered, at a much greater computational cost, by including higher order excited determinants, such as in the case of the CIS(D) method where doubly excited determinants are included. The CIS method can thus be considered the entry level approach for the treatment of excited states, just as the HF method is the basic model to study the ground state electronic structure. Following this line of development, the same considerations that lead to the use of second order Møller–Plesset perturbation theory (MP2), to include correlation effects at the HF ground state level, can be applied to the CIS method. Indeed, an MP2 correction of CIS states was firstly proposed by Foresman *et al.*⁴⁵.

According to the resulting CIS-MP2 method, the excited state energies depend on two kind of perturbations applied on the ground state: the static electron-electron correlation operators T_n (where n classifies the number of electrons considered in the excitation) and the time dependent ones U_n . Each one of the U_n -s should be considered as the first order developing term of the related static operator T_n . For example, at the second order in perturbation theory these operators assume the form:

$$T_2\Phi_0 = \frac{-1}{4} \sum_{ijab} \Phi a_{ij}^{ab} \Phi_{ij}^{ab} = \frac{-1}{4} \sum_{ijab} \frac{\langle \Phi_{ij}^{ab} | V | \Phi_0 \rangle}{\Delta_{ij}^{ab}} \Phi_{ij}^{ab} = \frac{-1}{4} \sum_{ijab} \Phi \frac{\langle ij | ab \rangle}{\Delta_{ij}^{ab}} \Phi_{ij}^{ab} \quad 2.3$$

$$U_2\Phi_0 = \frac{-1}{4} \sum_{ijab} b_{ij}^{ab} \Phi_{ij}^{ab} = \frac{-1}{4} \sum_{ijab} \frac{\langle \Phi_{ij}^{ab} | V | U_1 \Phi_0 \rangle}{\Delta_{ij}^{ab} - \omega} \Phi_{ij}^{ab} \quad 2.4$$

where V is the perturbation potential due to the electron correlation, a and b are the amplitudes relative to T and U operators respectively, Δ is an energy difference between HF orbital energies and, as usual, the i, j indicate occupied orbitals whereas a, b stand for virtual ones.

In its first formulation the excited energy E^{CIS} with the $MP2$ correction is then written as:

$$E^{CIS-MP2} = \langle \Phi_{CIS} | V | U_2 \Phi_0 \rangle + \langle \Phi_{CIS} | V | U_3 \Phi_0 \rangle = \frac{-1}{4} \sum_{ijab} \frac{(u_{ij}^{ab})^2}{\Delta_{ij}^{ab} - \omega} - \frac{1}{36} \sum_{ijkabc} \frac{(u_{ijk}^{abc})^2}{\Delta_{ijk}^{abc} - \omega} \quad 2.5$$

where the Φ_{CIS} excited state mixes with states that came from the spaces of the double ($U_2\Phi_0$) and triple ($U_3\Phi_0$) excitations through the perturbation to rise the direct and indirect terms, respectively. The indirect terms indeed describe triple excitation determinantal states that are created by the MP2 perturbation (a double excitation) of a single excited state. These are the terms responsible for the lack of *self-consistency* and the main computational burden, with an algorithmic complexity of $O(N^6)$.

An appealing approximation of the indirect terms in Eq. 2.5, based on the comparison of CISD and CCSD expansion, involves replacing the U_3 operator with the product T_2U_1 , i.e. assuming that the MP2 amplitudes of pairs of electrons not involved in the excitations remain unchanged. The resulting CIS(D) method³⁰ and has the following total energy expression:

$$E^{CIS(D)} = E^{MP2} - \frac{1}{4} \frac{\sum_{ijab} (u_{ij}^{ab})^2}{\Delta_{ij}^{ab} - \omega} + \sum_{ia} b_i^a v_i^a \quad 2.6$$

then the (D)-corrected transition energy $\omega^{CIS(D)}$ has to be computed with respect to the MP2 energy of the ground state as $\omega^{CIS(D)} = E^{CIS(D)} - E^{MP2}$. In Eq. 2.7 and Eq. 2.8 the quantities u_{ij}^{ab} and v_i^a are defined as

$$u_{ij}^{ab} = \sum_c (\langle ab || cj \rangle b_i^c) - (\langle ab || ci \rangle b_j^c) + \sum_k (\langle ka || ij \rangle b_k^b) - (\langle kb || ij \rangle b_k^a) \quad 2.7$$

$$v_i^a = \frac{1}{2} \sum_{jkb} \langle jk || bc \rangle (b_i^b a_{jk}^{ca} + b_j^a a_{ik}^{cb} + 2b_j^b a_{ik}^{ac}) \quad 2.8$$

The computational complexity of the CIS(D) method is reduced to $O(N^5)$ with respect to CIS-MP2, but more importantly *size-consistency* is recovered.

During the 25 years since the introduction of the CIS(D) method in 1994, time-dependent Density Functional Theory (TD-DFT) has emerged as the method of choice for the study of excited states, by providing a convenient compromise between accuracy and computational cost. In its full form, TD-DFT is a method related to the random phase approximation (RPA), and as such it involves both single excitations and deexcitations. However, following the Tamm-Dancoff approximation, TD(A)-DFT is equivalent to perform a CIS calculation starting from the Kohn-Sham ground state determinant, involving only single excitations.

On the other hand, while TD(A)-DFT was being recognized as the method of choice for the study of excited states, Grimme²⁰ proposed an approach to apply the usual MP2 perturbative correction to a Kohn-Sham ground state determinant. This idea led to a new class of density functional approximations (DFA) termed double hybrids, which are characterized by the energy expression

$$E_{xc}^{DH}(\rho) = a_x E_x^{HF} + (1 - a_x) E_x^{DFA}(\rho) + (1 - a_c) E_c^{DFA}(\rho) + a_c E_c^{MP2} \quad 2.9$$

where the x and the c subscripts indicate exchange and correlation contributions, respectively, while E^{HF} is the usual Hartree-Fock exchange energy and E_c^{MP2} is the correlation energy correction according to the MP2 approach. The addition of this last contribution to the DFT energy expression increases the computational cost to $O(N^5)$ but allows for an enhanced accuracy of the description of the electronic ground state, especially in those cases known to be problematic for standard DFAs^{27, 28}. The combination of double hybrid DFA and a second order perturbative correction equivalent to CIS(D) can be readily achieved in the context of TD(A)-DFT, while for TD-DFT the most practical approach still involves just the use of the excitation single amplitudes in the (D) correction²³. This can be done essentially introducing the correction to the contribution stemming from the DFA part Ω_{TDA-GH} in Eq. 2.10 for the same amount the MP2 is involved in the ground state energy of Eq. 2.9 end obtaining that:

$$\Omega_{TDA-DH} = \Omega_{TDA-GH} + a_c \omega^{CIS(D)} \quad 2.10$$

Also in this context the computational scaling and the performance of double hybrids can be improved if a separate scaling for the same-spin (SS) and the opposite-spin (OS) contributions to the E_c^{MP2} corrections is applied^{37,46}. Similarly, different scaling factors for the SS and SO terms has also been proposed and used to tune excited state calculations using the CIS(D) correction⁴⁶. Moreover, an additional parameter λ can be introduced, which scales the TD(A)-DFT transition energy in the denominator of the second term on the right-hand side of equation 2.5³⁷. Here, any scaling of the U_1 and the T_2 terms or λ values other than one, were employed only for purpose of validating our implementation against results published in the literature. To the best of the authors' understanding the (D) correction to TD(A)-DFT calculations using double-hybrid DFAs, has been until now implemented only in codes that make systematic use of the resolution-of-the-identity (RI) approximation⁴⁷ such as ORCA⁴⁸, and Q-Chem⁴⁹.

Despite the nonnegligible saving in computational cost, the use of the RI approximation relies on the assumption that the auxiliary expansion basis set being used is complete. However, “there is no guarantee that the approximation becomes uniformly better as the [...] completeness of the basis increases or that error in the approximation is known a priori”⁴⁷.

The novelty of this work consists in our choice to evaluate the (D) correction within the code that implements the MP2 semi-direct algorithm, which is used in most practical cases by the Gaussian program⁵⁰ to compute E^{MP2} . Such algorithm, originally described in reference 51, does not rely in the RI approximation. One important feature of our implementation is the ability to compute the (D) correction to a list of N states at a cost of about $(N+1)$ MP2 calculation. All required quantities are assembled from AO two electron integrals which are generated *on the-fly* in a direct fashion. In the first pass, the ground state DH-DFA energy is computed and at the same time we can also evaluate the contribution to the last term on the right hand side of Eq.(4) arising from the whole v_i^a terms that contribute to the (D) correction for all the N states under consideration. This can be explained rewriting this last term inserting Eq.2.8 in Eq.2.6 and recognizing the similarity with Eq.2.13, 2.14 and 2.15 in reference 52 in the following manner:

$$\sum_{ia} b_i^a v_i^a = \frac{1}{2} \sum_{iab} b_i^a (S2)_{ab} b_i^b + \frac{1}{2} \sum_{ija} b_i^a (S1)_{ij} b_j^a + \frac{1}{2} \sum_{ikac} b_i^a a_{ik}^{ac} F_{kc} \quad 2.11$$

where the quantities $(S1)_{ij}$ and $(S2)_{ab}$ are defined as

$$(S1)_{ij} = \sum_{kbc} \langle jk || bc \rangle a_{ik}^{cb} \quad ; \quad (S2)_{ab} = \sum_{jkc} \langle jk || bc \rangle a_{jk}^{cb} \quad 2.12$$

and they are evaluated using the existing MP2 gradient code³⁸. This allows to save a lot of computations because, for example we do not need to form the two-electron integrals with three virtual indexes during the evaluation of $(S2)_{ab}$. To continue, the last term in Eq. 2.11 involves a Fock matrix including Coulomb and (full) exchange contributions only,

$$F_{kc} = \sum_{jb} \langle jk || bc \rangle b_j^b \quad 2.13$$

which is produced in a direct fashion from the single amplitudes transformed to the AO basis.

This same term is evaluated for all the N states as the ground state E^{MP2} is computed as usual by multiplying the a_{ij}^{ab} double amplitudes with the fully transformed $\langle ab||ij \rangle$ integrals in the MO basis.

Following this first pass, N more MP2-like energy calculations are performed to compute instead the second term on the right hand side of Eq. 2.6 for each of the excited state under consideration. In fact, it can be shown that the required u_{ij}^{ab} terms are *double-like* amplitudes and can be written as

$$u_{ij}^{ab} = \langle ab||\tilde{t}j \rangle + \langle ab||i\tilde{j} \rangle - \langle \tilde{a}b||ij \rangle - \langle a\tilde{b}||ij \rangle \quad 2.14$$

where the two-electron integrals in each term, are transformed on three indexes using the regular MO coefficients, while the remaining index, marked with the tilde, is transformed using a second set of MO coefficients pre-contracted with the single amplitudes,

$$C_{\mu\tilde{i}} = \sum_c C_{\mu c} b_i^c \quad C_{\mu\tilde{a}} = \sum_j C_{\mu j} b_j^a \quad 2.15$$

This means that the difference between a regular two-electron integral and the tilded ones in Eq.2.14 resides only in one of the four quarter transformation where, instead of transforming the AO to one of the MO, we are transforming to one of the excitation orbitals usually a combination of occupied and virtual MO. Bearing in mind that an excitation orbital belongs to the same space spanned by the regular MO it is straightforward to employ the same algorithm used to compute the E^{MP2} energy to evaluate the second term on the right hand side of Eq.2.6. It is only necessary to recognize that we form the u_{ij}^{ab} amplitudes instead of the usual a_{ij}^{ab} double amplitudes, and that we have include the TD(A)-DFT transition energy Ω_{TDA-GH} of the excited state in the denominator. The resulting algorithm is then a generalization of the one initially proposed in reference 51. Explicitly, in the first quarter transformation a second kind of partially transformed integrals $\langle \tilde{i}v||\lambda\sigma \rangle$ is produced in addition to the $\langle iv||\lambda\sigma \rangle$, while at the end of the second quarter transformation three kinds of *half-transformed* integrals are made available, namely $\langle \tilde{i}v||\lambda\sigma \rangle$, $\langle i\tilde{a}||\lambda\sigma \rangle$ and $\langle ia||\lambda\sigma \rangle$. The third and fourth quarter transformations is then run two times on $\langle ia||\lambda\sigma \rangle$ to produce two sets of fully transformed integrals $\langle ia||j\tilde{b} \rangle$ and $\langle ia||\lambda\sigma \rangle$. On the other hand the usual second half transformations is applied to $\langle \tilde{i}a||\lambda\sigma \rangle$ and $\langle ia||\lambda\sigma \rangle$ to produce $\langle \tilde{i}a||j\tilde{b} \rangle$ and $\langle i\tilde{a}||j\tilde{b} \rangle$, respectively. At this point, all the basics tilded integrals are available and, as the regular MP2 energy code does, it is possible to build routinely their *anti-symmetrized* combinations appearing in Eq. 2.14, to calculate the u_{ij}^{ab} amplitudes.

These amplitudes are then added up with their relative weight depending on orbital energy difference to form the second term on the right hand side of Eq. 2.6.

The algorithm described above to calculate the (D) correction on one excited state is characterized by the same computational cost scaling as that of the ground state algorithm employed for MP2 and double hybrid DFAs. Then a linear increase in cost is observed as a function of the number of excited states which are considered to be corrected.

2.3 Computational Details

All the calculations were performed with a modified version of the Gaussian development code⁵⁰. Ground state structural optimization were performed at the MP2⁵³ /6-31G(d)^{54,55} level of theory for all molecules belonging to the Thiel⁵⁶ and RLex80-EX7-0^{34,57} subsets. Optimized structures for the Baer set (obtained at the B3LYP⁴⁴ level with cc-pVDZ and aug-cc-pVDZ⁴⁵) were taken from the reference 42.

Vertical singlet excited states were computed at the TD-DFT level using different exchange-correlation functionals namely: BLYP^{60,61}, B3LYP^{58,62}, CAM-B3LYP⁶³, PBE⁶⁴, PBE0^{65,66}, LC-PBE⁶⁷; the B2PLYP²⁰, PBE0-DH²⁶, and PBE-QIDH²⁵ in the case of the Thiel and RLex80-EX7-0 sets. The TZVP basis⁶⁸ was used both for the Thiel and the RLex80-EX7-0 set. For selected molecules of this latter the def2-TZVP triple- ζ basis set⁶⁹ used in the original publication of Bremond *et al.*³⁴ was also tested and the corresponding results are reported in SI.

In the case of the Baer Set, PBE, PBE0, LC-PBE, and PBE-QIDH functionals were considered using the cc-pVDZ and aug-cc-pVDZ basis sets. All calculations involving DH functionals were performed at the TDA level to allow comparison with previous work.

Solvent effects (methylene chloride) included using an implicit solvation model as implemented in the Gaussian code (C-PCM⁷⁰).

2.4 Results and Discussion

In order to validate our implementation, we firstly computed the excitation energies of the molecules belonging to the Thiel set for which DHs results can be found in literature³¹ and more recently ameliorated by the use of scaling techniques of spin-component and spin-opposite (SCS/SOS) of electron-pair contributions to the nonlocal correlation components³⁷. The set contains the 28 molecules, following the original paper of Thiel, in 4 groups: 1) unsaturated hydrocarbons (7 molecules); 2) aromatic hydrocarbons and heterocycles (11 molecules); 3) aldehydes, ketones and amides (6 molecules), and 4) nucleobases (4 molecules) as shown in figure 1:

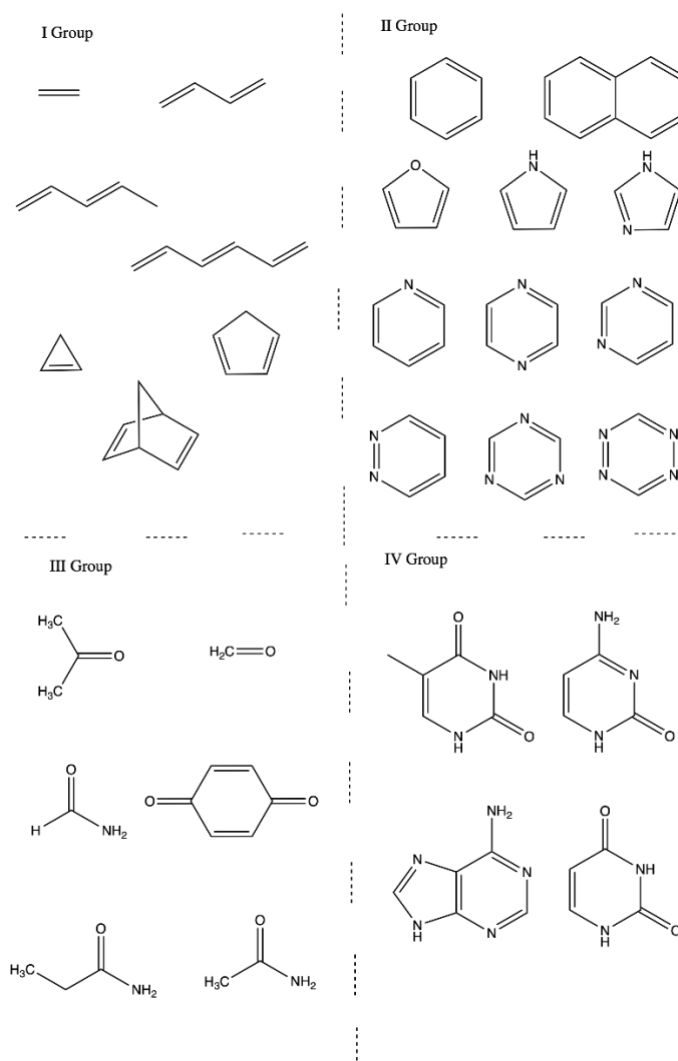


Figure 1. Benchmark set of molecules considered from W. Thiel et al., *J. Chem. Phys.*, 2008, 128, 134110.

Detailed data (that are computed transition energies) for each group can be found in Appendix A while the resulting Mean Absolute Deviations (MADs) are reported in Table 1.

As expected, the obtained results are completely consistent to the previously reported data³¹ for what concerns the B2PLYP functional with a computed MAD of 0.24 eV to be compared with the 0.22 eV result reported in literature, thus validating our current implementation. Comparing the two families of functionals, that are those resting on the Becke exchange and LYP correlation with those mixing PBE exchange and correlation, the same general trend can be observed. Introducing exact exchange (B3LYP and PBE0) enhances the performances with respect to parent GGAs (BLYP and PBE) especially in the case of Group 3 and Group 4 molecules. This systematic improvement of performance is not observed when going from these global hybrids (B3LYP and PBE0) to the corresponding range separated hybrids (CAM-B3LYP and LC-PBE) for which the agreement with the reference data is generally worse with few exceptions being represented by CAM-B3LYP performance for group 1 and group 3 molecules. Indeed, in the case of the PBE family the range separated LC-PBE shows a larger total MAD with respect to the corresponding global hybrid PBE0 (0.63 eV with respect to 0.30 eV). On the other hand, all double hybrid functionals represent at best only a slight improvement with respect to global hybrid with total MAD reducing from 0.35 eV to 0.26 eV (from B3LYP to B2PLYP). Of note in the case of the PBE family both the PBE-QIDH and PBE0-DH performance is slightly worse (0.40 eV) than that of PBE0 (0.30 eV) essentially due to the extremely good agreement with the reference data observed for the PBE0 functional for the molecules belonging to group 2 and group 4 with a MAD of 0.25 eV and 0.18 eV, respectively. All these general trends are in agreement with previously reported investigations^{31,34}. Worth of discussion are indeed the results labelled as ‘‘PBE-QIH’’ in Table 1.

Functional	MAD (eV)				
	Group 1	Group 2	Group 3	Group 4	Total
BLYP	0.72	0.39	0.70	0.86	0.61
B3LYP	0.60	0.24	0.36	0.29	0.31
CAM-B3LYP	0.54	0.29	0.44	0.26	0.35
B2PLYP^a	0.31	0.29	0.21	0.16	0.26
PBE	0.78	0.38	0.68	0.86	0.62
PBE0	0.60	0.25	0.38	0.18	0.30
LC-PBE	0.63	0.52	0.62	0.57	0.63
PBE-QIH^a	0.54	0.84	0.77	1.01	0.88
PBE-QIDH^a	0.39	0.46	0.29	0.34	0.40
PBE0-DH^a	0.25	0.47	0.26	0.33	0.40

Table 1. Computed Mean Absolute Deviation (MAD, in eV) for all functionals for the Thiel benchmark set. For groups definition refer to Figure 1. PBE-QIH results are obtained from PBE-QIDH TD(A)-DFT calculations not including the doubles correction (that is the $\alpha_c\omega^{CIS(D)}$ term in eq. 7). ^{a)} Within the Tamm-Dancoff approximation.

These data correspond to the MADs associated to excitation energies computed at TD(A)-DFT level using the PBE-QIDH functional but not including the doubles corrections. Comparison between the PBE-QIH and PBE-QIDH MADs thus allow to evaluate directly the magnitude of these corrections. Clearly due to the large percentage of HF exchange, the PBE-QIH functional overestimates the transition energies providing very large MAD independently of the group of molecules considered with MADs ranging from 0.84 eV for group 1 to 1.01 eV for group 4. Indeed, in this case the corrections ($a_c \omega^{CIS(D)}$) are very large ranging from 0.15 eV to roughly 0.70 eV, thus highlighting the importance of the correct treatment of perturbative contributions in DH functionals. To further test our implementation the seven molecules belonging to the RLex80-EX7-0 set were also considered. This benchmark set, depicted in Figure 2, was recently specifically developed to enable the fast evaluation of the performance of exchange correlation functionals for excited states.³⁴

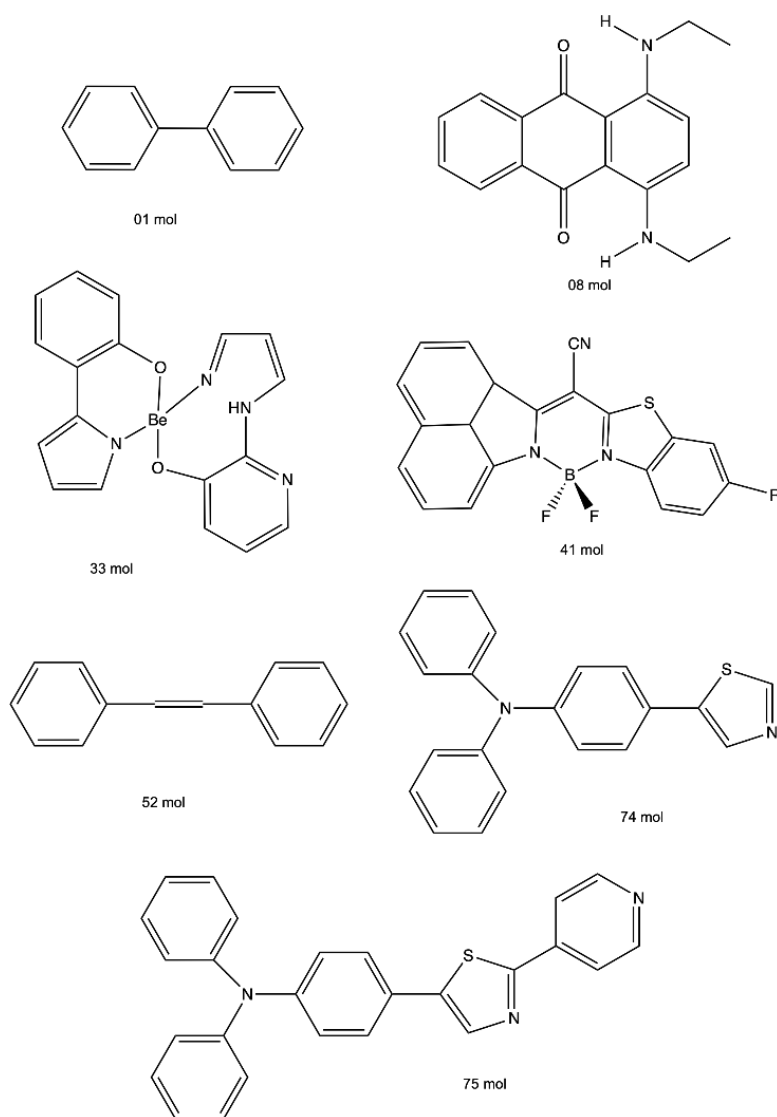


Figure 2. Benchmark set of molecules considered from Brémond, E. et al, *J. Chem. Theory Comput.*, 2017, 13, 5539–555.

In Table 2, there are data obtained using the TVPZ basis set for all functionals but the results and conclusions are comparable to those obtained using the 6-31+G(d) basis set for GGA and hybrids functionals and the def2TZVP basis for DH functionals as suggested in the original paper.

	01 Mol	08 Mol	33 Mol	41 Mol	52 Mol	74 Mol	75 Mol	MAD
BLYP	0.57	0.3	1.06	0.98	0.34	0.72	1.16	0.73
B3LYP	0.15	0.06	0.27	0.71	0.08	0.14	0.52	0.28
CAM-B3LYP	0.00	0.19	0.15	0.42	0.2	0.41	0.2	0.22
B2PLYP^a	0.09	0.04	0.02	0.27	0.01	0.08	0.23	0.11
PBE	0.53	0.3	1.04	0.94	0.33	0.71	1.15	0.71
PBE0	0.05	0.01	0.1	0.62	0.01	0	0.37	0.17
LC-PBE	-0.17	0.43	0.44	0.11	0.5	0.88	0.65	0.45
PBE-QIH^a	-0.32	0.74	0.72	0.1	0.64	1.01	0.49	0.57
PBE-QIDH^a	0.02	0.21	0.29	0.07	0.19	0.45	0.12	0.19
PBE0-DH^a	0.06	0.28	0.25	0.24	0.22	0.35	0.08	0.21
CC2	5.41	2.24	4.06	4.77	2.65	3.71	3.37	

Table 2. Relative and Mean Absolute Deviations (MAD, in eV) computed using the TZVP basis set for the molecules belonging to the RLex80-EX7-0 data set (figure 1). The reference CC2 values, taken from reference 57, are also reported. ^a Within the Tamm-Dancoff approximation.

Data reported in this table are obtained using the TVPZ basis set for all functionals but the results and conclusions are comparable to those obtained using the 6-31+G(d) basis set for GGA and hybrids functionals and the def2TZVP basis for DH functionals as suggested in the original paper. Compared to Thiel set, the RLex80-EX7-0 includes also transitions with a sizable intramolecular Charge Transfer character (CT) such as that of the molecule **74** (Figure 1), a push-pull chromophore, or of the molecule **75**.

Overall the same trends already observed for the Thiel set can be noted (table 2). If global hybrids (B3LYP and PBE0) still represent the best cost to accuracy compromise, double hybrids, and particularly B2PLYP, are extremely well performing with total MAD ranging from 0.11 eV (B2PLYP) to 0.19 and 0.21 eV for PBE-QIDH and PBE0-DH, respectively. Of note all three DH functionals perform very well for molecules **74** and **75**, that are those presenting transitions of partial CT character. For molecule **74** the effect of the inclusion of the perturbative correction is particularly large, as can be seen comparing the MAD computed for the PBE-QIH (1.01 eV) and PBE-QIDH (0.49 eV).

Indeed, in such a case the inclusion of a larger percentage of HF exchange in the PBE-QIH it is not sufficient to recover the correct transition energy. Of note PBE0 is providing the smallest error and B3LYP is also showing an error of only 0.14 eV.

Nonetheless if both B3LYP and PBE0 provide very accurate intramolecular CT excitation energies in the case of molecule **74** and **75**, it is well known that these global hybrid functionals fail to reproduce through space CT excitations.

To test the performance of DH functionals in the prediction of through-space CT excitations, the set of molecules recently proposed by Baer and collaborators⁴² was considered in the case of the PBE family of functionals (PBE, PBE0, LC-PBE and PBE-QIDH). This set contains a number of dimers composed by an aromatic molecule (benzene, toluene, o-xylene, naphthalene and substituted anthracene) acting as a donor, and tetracyanoethylene (TCNE) acting as an acceptor as shown below in figure 3:

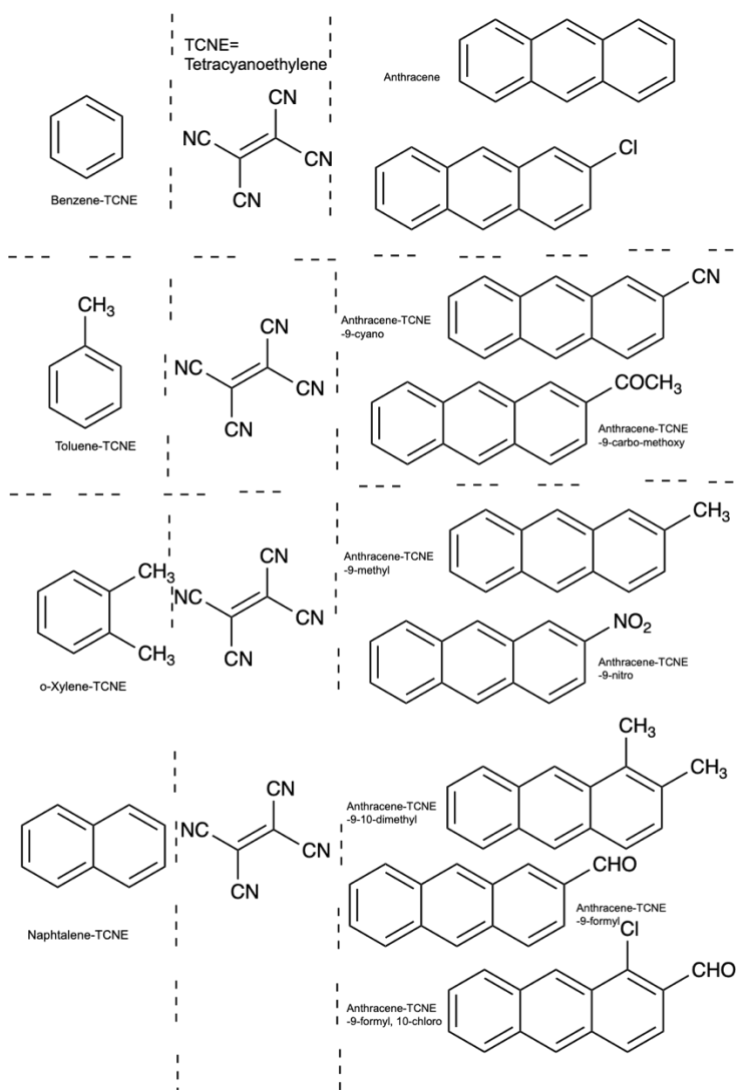


Figure 3. Benchmark set of molecules considered from Stein, T.; Kronik, L.; Baer, J. *Am. Chem. Soc.* 2009, 131, 2818–2820.

For these molecules accurate experimental data both in the gas phase and/or in solution can be found in literature^{71,72}. Of note we consider here only the effect of the functional on excitation energies, the geometry of each dimer being kept fixed at the B3LYP-optimized one as in the original paper of Baer⁴².

First, the results obtained for the Ar-TCNE dimers (Ar=benzene, toluene, o-xylene and naphthalene) will be considered since for these systems experimental data both in the gas-phase and in methylene chloride solution are available⁷¹.

As reported in Table 3, for all dimers the first transition corresponds, as expected, to an HOMO-LUMO excitation, the HOMO being centered on the aryl donor and the LUMO on the TCNE acceptor. Analogously, for all systems also the second transition (of HOMO-1 to LUMO character) corresponds to an intramolecular $\pi_{\text{Ar}}-\pi^*_{\text{TCNE}}$ CT excitation. These two transitions are generally non-degenerate their difference in transition energies increasing with the size of the aromatic systems up to a value of 0.8 eV in the case of the naphthalene. This trend is general roughly independently of the functional considered and of the presence or absence of the solvent. Starting from the third electronic transition, different functionals provide different ordering of the electronic transitions, pure functional predicting essentially a CT excitation of $n_{\text{Ar}}-\pi^*_{\text{TCNE}}$ (Figure 4) character while global, range-separated and double hybrids are predicting a local (and intense) $\pi_{\text{TCNE}}-\pi^*_{\text{TCNE}}$ excitation. In the case of the naphthalene-TCNE system all functionals predict a third intermolecular CT excitation of $\pi_{\text{Ar}}-\pi^*_{\text{TCNE}}$ character.

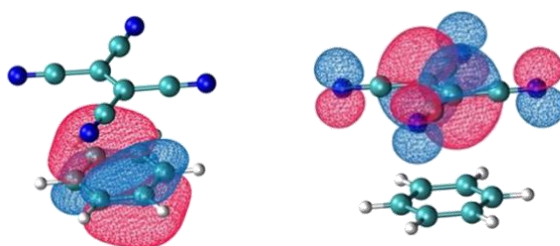


Figure 4. $\pi_{\text{Benzene}}-\pi^*_{\text{TCNE}}$ Charge Transfer excitation.

In order to evaluate the error in computed transition energies, since the reference data are experimental, two different MADs have been reported in Table 3.

Gas phase													
TCNE-	PBE		PBE0		LC-PBE		PBE-QIH ^a		PBEQID ^a		ωB97X-D		exp ^b
	E	<i>f</i>	E	<i>f</i>	E	<i>f</i>	E	<i>f</i>	E	E	<i>f</i>	E	
Benzene													
ES-I	1.42	0.00	2.13	0.00	4.16	0.00	3.55	0.00	3.09	3.03	0.00	3.59	
ES-II	1.55	0.03	2.21	0.03	4.17	0.03	3.59	0.03	3.12	3.07	0.03		
ES-III	3.27	0.00	4.38	0.29	4.85	0.34	5.04	0.46	5.08	4.52	0.31		
Toluene													
ES-I	1.37	0.04	1.94	0.03	3.81	0.03	3.28	0.04	2.78	1.92	0.07	3.36	
ES-II	1.43	0.00	2.10	0.00	4.07	0.00	3.49	0.00	3.00	2.10	0.00		
ES-III	3.17	0.00	4.37	0.00	4.85	0.32	5.04	0.44	5.08	3.92	0.00		
Xylene													
ES-I	1.06	0.00	1.68	0.01	3.55	0.01	3.02	0.01	2.51	2.50	0.01	3.15	
ES-II	1.47	0.05	2.01	0.04	3.85	0.03	3.33	0.04	2.80	2.79	0.03		
ES-III	3.10	0.00	4.26	0.00	4.84	0.31	5.02	0.43	5.06	4.50	0.29		
Naphtalene													
ES-I	0.36	0.00	1.07	0.00	3.17	0.00	2.48	0.00	2.02	0.75	0.00	2.60	
ES-II	1.07	0.00	1.83	0.00	3.93	0.00	3.27	0.00	2.78	1.66	0.00		
ES-III	2.03	0.01	2.99	0.00	4.78	0.00	4.79	0.01	4.02	2.95	0.01		
MAD_r	1.99		1.37		0.76 ₅		0.23		0.39 ₅		0.67		
MAD_{1st}	2.12		3.16		0.50		0.09		0.57 ₅		1.12		
Solvent													
TCNE-	PBE		PBE0		LC-PBE		PBE-QIH ^a		PBE-QIDH ^a		ωB97X-D		exp ^b
	E	<i>f</i>	E	<i>f</i>	E	<i>f</i>	E	<i>f</i>	E	E	<i>f</i>	E	
Benzene													
ES-I	1.42	0.00	2.13	0.00	4.11	0.00	3.53	0.00	3.07	3.00	0.00	3.22	
ES-II	1.56	0.04	2.20	0.04	4.12	0.04	3.55	0.05	3.09	3.03	0.04		
ES-III	3.22	0.00	4.27	0.37	4.75	0.43	4.90	0.56	4.93	4.41	0.40		
Toluene													
ES-I	1.40	0.06	1.95	0.05	3.76	0.05	3.25	0.06	2.75	2.72	0.05	3.05	
ES-II	1.45	0.00	2.11	0.00	4.04	0.00	3.48	0.00	3.00	2.93	0.00		
ES-III	3.14	0.0000	4.26	0.35	4.74	0.42	4.90	0.55	4.93	4.41	0.38		
Xylene													
ES-I	1.19	0.01	1.77	0.02	3.56	0.03	3.07	0.03	2.55	2.54	0.03	2.89	
ES-II	1.50	0.06	2.03	0.05	3.84	0.03	3.33	0.04	2.81	2.78	0.03		
ES-III	3.11	0.00	4.22	0.22	4.73	0.41	4.89	0.53	4.91	4.39	0.37		

Naphthalene												
ES-I	1.22	0.10	1.54	0.09	3.18	0.07	2.63	0.09	2.12	2.22	0.07	2.26
ES-II	1.60	0.00	2.13	0.00	3.95	0.00	3.38	0.0	2.86	2.92	0.00	
ES-III	2.56	0.01	3.25	0.01	4.71	0.26	4.84	0.16	4.59	4.22	0.01	
MAD_f	1.43		0.92		0.80		0.34		0.16	1.02		
MAD_{1st}	1.55		1.01		0.80		0.27		0.23	0.24		

Table 3. Computed and experimental excitation energies (eV) for Ar-TCNE systems. For the sake of clarity, only the three lowest electronic transitions are reported. In bold transitions that have been considered to compute the MAD_f. Highlighted in yellow intramolecular $\pi_{Ar}-\pi^*_{TCNE}$ CT transitions; in green intramolecular $n_{Ar}-\pi^*_{TCNE}$ CT transitions; in pink local $\pi_{TCNE}-\pi^*_{TCNE}$ excitations and in grey local $\pi_{Ar}-\pi^*_{Ar}$ excitations. ^{a)} Within the Tamm-Dancoff approximation. ^{b)} from reference 72.

The first (MAD_f) considering always the first CT excitation with the largest oscillator strength and the second one (MAD_{1st}) considering always the first computed transition independently of the associated intensity. The transition energies considered in the first case are reported in bold face in Table 3. Of note the computed oscillator strengths are, in agreement with the experimental data, relatively small and –using the basis set here considered, i.e. cc-pVDZ- not necessarily converged as already noted by Baer et al.⁴² Nonetheless the use of the larger aug-cc-pVDZ does not significantly change the general trend here reported (see SI for corresponding data). Independently of the criteria used to compute the MAD, both in the gas phase and in solution, the smallest errors are obtained using the PBE-QIDH functional while extremely large errors are computed at the GGA (PBE) or global hybrid (PBE0) level. DHs are better performing also with respect to range-separated hybrids (LC-PBE). Of note the agreement with the experimental data increases in going from the gas-phase to solution data. This is due essentially to error cancellation since transition energies are basically underestimated at all levels of theory as it is the effect of the solvent, which is experimentally also red-shifting the transition energies. As consequence the underestimation of solvent effect compensates the underestimation in computed transition energies allowing to afford extremely low values for the computed MAD in solution in the case of PBE-QIDH (0.16-0.23 eV).

Overall from the analysis of our data we can conclude that DHs represent a good alternative to adjusted range separated hybrids for the treatment of intramolecular charge transfer excitations provided that the double correction is correctly included. Indeed excitation energies of 3.8 eV, 3.4 eV, 3.0 eV and 2.7 eV were reported for Aryl-TCNE (Aryl = benzene, toluene, o-xylene, naphthalene, respectively) by Baer and collaborators⁴² using the BNL functional and of 3.9 eV, by Truhlar and collaborators, using the revM11 functional in the case of the benzene-TCNE system.⁷³

To further confirm these findings, the set of substituted anthracene-TCNE dimers (Table 4, Figure 5) by Baer was also considered. In this case experimental data are only available in solution⁷².

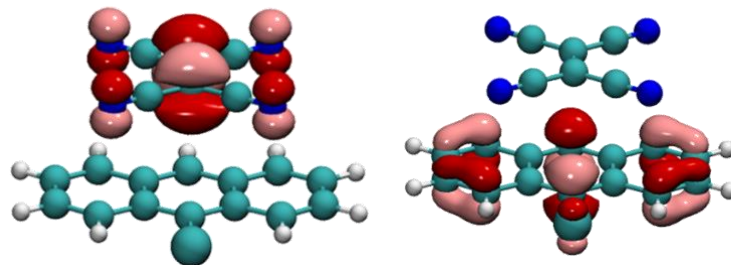


Figure 5. π Anthracene- π^* TCNE Charge Transfer excitation

<i>Substituent</i>	Solvent							exp. ^c
	PBE	PBE0	LCPBE	PBEQIH	PBEQIDH	ω B97D	BN ^d	
<i>none</i>	1.38	1.47	2.47	2.09	1.58	1.77	1.82	1.73
<i>9-cyano</i>	0.65	1.02	3.12	2.42	1.90	2.11	2.03	2.01
<i>9-chloro</i>	1.16	1.27	2.56	2.08	1.58	1.73	1.82	1.74
<i>9-carbomethoxy</i>	1.06	1.22	2.66	2.15	1.64	1.77	1.84	1.84
<i>9-methyl</i>	1.26	1.34	2.31	1.93	1.42	1.62	1.71	1.55
<i>9-nitro</i>	0.92	1.43	2.68	2.50	1.98	2.1	2.12	2.03
<i>9,10-dimethyl</i>	1.52	1.59	2.24	2.03	1.53	1.73	1.77	1.44
<i>9-formyl</i>	0.85	1.26	2.72	2.20	1.7	1.84	1.95	1.9
<i>9-formyl 10-chloro</i>	0.83	1.25	2.83	2.30	1.79	1.91	1.96	1.96
MAD	0.63	0.49	0.81_s	0.39_s	0.14	0.09	0.09	

Table 4. Computed and experimental excitation energies (in eV) for a series of substituted anthracene-TCNE systems. ^{a)} Within the Tamm-Dancoff approximation; ^{b)} Obtained from the solution data reported in reference 42 subtracting 0.32eV (see text for explanation). ^{c)} From reference 73. ^{d)} From reference 42.

Contrary to Baer previous work⁴² but analogously to what reported in Table 3, transition energies were thus directly computed in solution using a polarizable continuum model. Of note BNL energies in solution taken from Baer work are instead estimated subtracting 0.32 eV from gas phase computed data, the 0.32 eV shift being estimated as an average experimental gas-phase to solvent shift⁵⁸ on the basis also of a previous theoretical work⁷⁴.

The general trend observed are, as expected, in line with those of the previously discussed Ar-TCNE systems with a large/slight underestimation of transition energies provided by the GGA/global hybrid functional (PBE/PBE0) and an overestimation of transition energy provided by the range-separated LC-PBE. The results obtained with the PBE-QIDH functional

are indeed in very good agreement with the experimental data in solution but generally all red-shifted with the prediction obtained at BNL level of theory in the gas-phase (see Table 4). These data are consistent with the previously pointed out error compensation between the underestimation of gas to solvent shift and transition energies.

Overall when considering the overall performance of the PBE-QIDH, this functional not only shows a very small MAD with respect to solution data (0.14 eV), comparable to that of the BNL functional (0.09 eV), but, more relevantly is able to correctly recover the ordering of computed energies as a function of the substituent with the only exception of the inversion between the 9-methyl and 9, 10 dimethyl substituent. Furthermore, it should be underlined that, contrary to adjusted range separated functionals, in double hybrids no parameter is tuned on a specific class of compounds to reproduce its excited state properties making them more appealing for a general use.

2.5 Conclusions

The results show how a Double Hybrids DFAs can be an effective tool to predict excited states energies of molecular compounds of relatively large size. Indeed, the algorithm described and implemented is characterized by the same computational cost scaling as that of the ground state algorithm employed for MP2 and double hybrid DFAs, although a linear increase in cost is observed as a function of the number of states considered. From the point of view of the performance we showed that the use of double hybrids allows for a better description of through space charge-transfer excitations which are well known to be very problematic to be described with commonly used functionals, such as global hybrids.

In particular, our results show, beside the robustness of the implementation, that double hybrids enable to obtain results comparable to that of adjusted range separated functionals, with the relevant difference that for DHs no parameter is tuned on a specific class of compounds to reproduce its excited state properties thus making them more appealing for a general use.

References

- 1) Ernzerhof, M. *Chem. Phys. Lett.*, **1996**, 263, 499.
- 2) Grimme, S. *J. Chem. Phys.*, **2006**, 124, 034108.
- 3) Peverati, R.; Head-Gordon, M. *J. Chem. Phys.*, **2013**, 139, 024110.
- 4) Barone, V.; Orlandini, L.; Adamo, C. *Chem. Phys. Lett.*, **1994**, 231, 295.
- 5) Stephens, P. J.; Devlin, F. J.; Chabalowski, C. F.; Frisch, M. J. *J. Phys. Chem.*, **1994**, 98, 11623.
- 6) Adamo, C.; Barone, V. *J. Chem. Phys.*, **1999**, 110, 6158.
- 7) Ernzerhof, M.; Scuseria, G. E. *J. Chem. Phys.*, **1999**, 110, 5029.
- 8) Sharkas, K.; Toulouse, J.; Savin, A. *J. Chem. Phys.*, **2011**, 134, 064113.
- 9) Toulouse, J.; Sharkas, K.; Brémond, E.; Adamo, C. *J. Chem. Phys.*, **2011**, 135, 101102.
- 10) Souvi, S. M. O.; Sharkas, K.; Toulouse, J. *J. Chem. Phys.*, **2014**, 140, 084107.
- 11) Fromager, E. *J. Chem. Phys.*, **2011**, 135, 244106.
- 12) Brémond, E.; Adamo, C. *J. Chem. Phys.*, **2011**, 135, 024106.
- 13) Bousquet, D.; Brémond, E.; Sancho-García, J. C. ; Ciofini, I.; Adamo, C. *J. Chem. Theory Comput.*, **2013**, 9, 3444.
- 14) Brémond, É.; Sancho-García, J.C.; Pérez-Jiménez, A.J.; Adamo, C. *J. Chem. Phys.*, **2014**, 141, 031101.
- 15) Mardirossian, N.; Head-Gordon M. *Mol. Phys.*, **2017**, 119, 2315-2372.
- 16) Cohen, A.J.; Mori-Sánchez, P.; Yang, W. *Chem. Rev.*, **2012**, 112, 289–320
- 17) Zhao, Y.; Truhlar, D. G. *Acc. Chem. Res.*, **2008**, 41, 157-167.
- 18) Görling, A.; Levy, M. *Phys Rev B*, **1993**, 47, 13105–13113.
- 19) Görling, A.; Levy, M. *Phys Rev A*, **1994**, 50, 196–204.
- 20) Grimme, S. *J. Chem. Phys.*, **2006**, 124, 034108.
- 21) Zhao, Y.; Lynch, B. J.; Truhlar, D. G. *J. Phys. Chem. A*, **2004**, 108, 4786-4791.
- 22) Goerigk, L.; Grimme, S. *Comput. Mol. Sci.*, **2014**, 4, 576-600.

- 23) Sancho-García, J. C.; Adamo, C. *Phys. Chem. Chem. Phys.*, **2013**, *15*, 14581-14594.
- 24) Toulouse, J.; Sharkas, K.; Brémond, E.; Adamo, C. *J. Chem. Phys.*, **2011**, *135*, 101102.
- 25) Brémond, E. ; Sancho-García, J. C.; Pérez-Jiménez, Á. J.; Adamo, C. *J. Chem. Phys.*, **2014**, *141*, 031101-031104.
- 26) Brémond, É.; Adamo, C. *J. Chem. Phys.*, **2011**, *135*, 024106.
- 27) Goerigk, L.; Grimme, S. *Phys. Chem. Chem. Phys.*, **2011**, *13*, 6670-6688
- 28) Schwabe, T.; Grimme, S. *Phys. Chem. Chem. Phys.*, **2006**, *8*, 4398-4401
- 29) Grimme, S.; Neese, F. *J. Chem. Phys.*, **2007**, *127*, 154116.
- 30) Head-Gordon, M.; Rico, R.J.; Oumi, M.; Lee, T.J. *Chem. Phys. Lett.*, **1994**, *219*, 21-29.
- 31) Goerigk, L.; Moellmann, J.; Grimme, S. *Phys. Chem. Chem. Phys.*, **2009**, *11*, 4611–4620.
- 32) Goerigk, L.; Grimme, S. *J. Chem. Phys.* **2010**, *132*, 184103.
- 33) Di Meo, F.; Trouillas, P.; Adamo, C.; Sancho-García, J.C. *J. Chem. Phys.* **2013**, *139*, 164104.
- 34) Brémond, E.; Savarese, M.; Pérez-Jiménez, A.J.; Sancho-García, J.C.; Adamo, C. *J. Chem. Theory Comput.*, **2017**, *13*, 5539–5551.
- 35) Grimme, S. *J. Chem. Phys.*, **2003**, *118*, 9095-9102.
- 36) Kozuch, S.; Martin, J.M.L. *Phys. Chem. Chem. Phys.*, **2011**, *13*, 20104–20107,
- 37) Schwabe, T.; Goerigk, L. *J. Chem. Theory Comput.*, **2017**, *13*, 4307–4323.
- 38) Dreuw, A.; Head-Gordon, M. *J. Am. Chem. Soc.*, **2004**, *126*, 4007-4016.
- 39) Magyar, R.J.; Tretiak, S. *J. Chem. Theory Comput*, **2007**, *3*, 976-987.
- 40) Autschbach, J. *Chem.Phys.Chem.*, **2009**, *10*, 1757-1760.
- 41) Maitra, N.T. *J. Phys. Condens. Matter*, **2017**, *29*, 423001.
- 42) Stein, T.; Kronik, L.; Baer, R. *J. Am. Chem. Soc.*, **2009**, *131*, 2818–2820.
- 43) Jacquemin, D.; Mennucci, B.; Adamo, C. *Phys. Chem. Chem. Phys.*, **2011**, *13*, 16987–16998.
- 44) Szabo, A.; Ostlund, N.S. *Modern Quantum Chemistry: Introduction to Advanced Electronic Structure Theory*, Dover Publications, **1996**, New York.

- 45) Foresman, J.B.; Head-Gordon, M.; Pople, J.A.; Frisch, M.J. *J. Phys. Chem.*, **1992**, *96*, 135-149.
- 46) Rhee, Y. M., Head-Gordon, M. *J. Phys. Chem. A*, **2007**, *111*, 5314-5326.
- 47) Feyereisen, M.; Fitzgerald, G.; Komornicki, A. *Chem. Phys. Lett.*, **1993**, *208*, 359-363.
- 48) Neese, F. *WIREs Comput Mol Sci*, **2018**, *8*, e1327.
- 49) Shao, Y.; Gan, Z.; Epifanovsky, E.; Gilbert, A. T. B.; Wormit, M.; Kussmann, J.; Lange, A. W.; Behn, A.; Deng, J.; Feng, X.; Ghosh, D.; Goldey, M.; Horn, P. R.; Jacobson, L. D.; Kaliman, I.; Khaliullin, R. Z.; Kus, T.; Landau, A.; Liu, J.; Proynov, E. I.; Rhee, Y. M.; Richard, R. M.; Rohrdanz, M. A.; Steele, R. P.; Sundstrom, E. J.; Woodcock, H. L., III; Zimmerman, P. M.; Zuev, D.; Albrecht, B.; Alguires, E.; Austin, B.; Beran, G. J. O.; Bernard, Y. A.; Berquist, E.; Brandhorst, K.; Bravaya, K. B.; Brown, S. T.; Casanova, D.; Chang, C.-M.; Chen, Y.; Chien, S. H.; Closser, K. D.; Crittenden, D. L.; Diedenhofen, M.; DiStasio, R. A., Jr.; Do, H.; Dutoi, A. D.; Edgar, R. G.; Fatehi, S.; Fusti-Molnar, L.; Ghysels, A.; Golubeva-Zadorozhnaya, A.; Gomes, J.; Hanson-Heine, M. W. D.; Harbach, P. H. P.; Hauser, A. W.; Hohenstein, E. G.; Holden, Z. C.; Jagau, T.-C.; Ji, H.; Kaduk, B.; Khistyayev, K.; Kim, J.; Kim, J.; King, R. A.; Klunzinger, P.; Kosenkov, D.; Kowalczyk, T.; Krauter, C. M.; Laog, K. U.; Laurent, A.; Lawler, K. V.; Levchenko, S. V.; Lin, C. Y.; Liu, F.; Livshits, E.; Lochan, R. C.; Luenser, A.; Manohar, P.; Manzer, S. F.; Mao, S.-P.; Mardirossian, N.; Marenich, A. V.; Maurer, S. A.; Mayhall, N. J.; Oana, C. M.; Olivares-Amaya, R.; O'Neill, D. P.; Parkhill, J. A.; Perrine, T. M.; Peverati, R.; Pieniazek, P. A.; Prociuk, A.; Rehn, D. R.; Rosta, E.; Russ, N. J.; Sergueev, N.; Sharada, S. M.; Sharma, S.; Small, D. W.; Sodt, A.; Stein, T.; Stuck, D.; Su, Y.-C.; Thom, A. J. W.; Tsuchimochi, T.; Vogt, L.; Vydrov, O.; Wang, T.; Watson, M. A.; Wenzel, J.; White, A.; Williams, C. F.; Vanovschi, V.; Yeganeh, S.; Yost, S. R.; You, Z.-Q.; Zhang, I. Y.; Zhang, X.; Zhou, Y.; Brooks, B. R.; Chan, G. K. L.; Chipman, D. M.; Cramer, C. J.; Goddard, W. A., III; Gordon, M. S.; Hehre, W. J.; Klamt, A.; Schaefer, H. F., III; Schmidt, M. W.; Sherrill, C. D.; Truhlar, D. G.; Warshel, A.; Xu, X.; Aspuru-Guzik, A.; Baer, R.; Bell, A. T.; Besley, N. A.; Chai, J.-D.; Dreuw, A.; Dunietz, B. D.; Furlani, T. R.; Gwaltney, S. R.; Hsu, C.-P.; Jung, Y.; Kong, J.; Lambrecht, D. S.; Liang, W. Z.; Ochsenfeld, C.; Rassolov, V. A.; Slipchenko, L. V.; Subotnik, J. E.; van Voorhis, T.; Herbert, J. M.; Krylov, A. I.; Gill, P. M. W.; Head-Gordon, M. *Mol. Phys.*, **2015**, *113*, 184-215.
- 50) Frisch, M. J.; Trucks, G. W.; Schlegel, H. B.; Scuseria, G. E.; Robb, M. A.; Cheeseman, J. R.; Scalmani, G.; Barone, V.; Petersson, G. A.; Nakatsuji, H.; Li, X.; Caricato, M.; Marenich, A. V.; Bloino, J.; Janesko, B. G.; Gomperts, R.; Mennucci, B.; Hratchian, H. P.; Ortiz, J. V.; Izmaylov, A. F.; Sonnenberg, J. L.; Williams-Young, D.; Ding, F.; Lipparini, F.; Egidi, F.; Goings, J.; Peng, B.; Petrone, A.; Henderson, T.; Ranasinghe, D.; Zakrzewski, V. G.; Gao, J.; Rega, N.; Zheng, G.; Liang, W.; Hada, M.; Ehara, M.; Toyota, K.; Fukuda, R.; Hasegawa, J.; Ishida, M.; Nakajima, T.; Honda, Y.; Kitao, O.; Nakai, H.; Vreven, T.; Throssell, K.; Montgomery, J. A., Jr.; Peralta, J. E.; Ogliaro, F.; Bearpark, M. J.; Heyd, J. J.; Brothers, E. N.; Kudin, K. N.; Staroverov, V. N.; Keith, T. A.; Kobayashi, R.; Normand, J.; Raghavachari, K.; Rendell, A. P.; Burant, J. C.; Iyengar, S. S.; Tomasi, J.; Cossi, M.; Millam, J. M.; Klene, M.; Adamo, C.; Cammi, R.; Ochterski, J. W.; Martin, R. L.; Morokuma, K.; Farkas, O.; Foresman, J. B.; Fox, D. J. *Gaussian Development Version, Revision J.1*, Gaussian, Inc., **2018**, Wallingford CT.

- 51) Frisch, M.J.; Head-Gordon, M.; Pople, J.A. *Chem. Phys. Lett.*, **1990**, *166*, 281-289.
- 52) Frisch, M.J.; Head-Gordon, M.; Pople, J.A. *Chem. Phys. Lett.*, **1990**, *166*, 275-280.
- 53) Møller, C.; Plesset, M.S. *Phys. Rev.*, **1934**, *46*, 618–622.
- 54) Ditchfield, R.; Hehre, W.J.; Pople, J.A. *J. Chem. Phys.*, **1971**, *54*, 724-728.
- 55) Hehre, W.J.; Ditchfield, R.; Pople, J.A. *J. Chem. Phys.*, **1972**, *56*, 2257-2261.
- 56) Schreiber, M.; Silva-Junior, M.R.; Sauer, S.P.A.; Thiel, W. *J. Chem. Phys.* **2008**, *128*, 134110.
- 57) Jacquemin, D.; Duchemin, I.; Blase, X. *J. Chem. Theory Comput.*, **2015**, *11*, 5340–5359.
- 58) Becke, A. D. *J. Chem. Phys.*, **1993**, *98*, 5648-5652.
- 59) Dunning Jr., T.H. *J. Chem. Phys.*, **1989**; *90*, 1007-1023.
- 60) Becke, A. D. *Phys. Rev. A*, **1998**, *38*, 3098-3100.
- 61) Lee, C. T.; Yang, W. T.; Parr, R. G. *Phys. Rev. B*, **1988**, *37*, 785-789.
- 62) Stephens, P. J.; Devlin, F. J.; Chabalowski, C. F. N.; Frisch, M. J. *J. Phys. Chem.*, **1994**, *98*, 11623-11627.
- 63) Yanai, T.; Tew, D. P.; Handy, N. C. *Chem. Phys. Lett.*, **2004**, *393*, 51-57.
- 64) Perdew, J. P.; Burke, K.; Ernzerhof, M. *Phys. Rev. Lett.*, **1996**, *77*, 3865-3868
- 65) Adamo, C.; Barone, V. *J. Chem. Phys.*, **1999**, *110*, 6158-6170.
- 66) Ernzerhof, M.; Scuseria, G. E. *J. Chem. Phys.*, **1999**, *110*, 5029-5036.
- 67) Iikura, H.; Tsuneda, T.; Yanai, T.; Hirao, K. *J. Chem. Phys.*, **2001**, *115*, 3540-3544.
- 68) Schäfer, A.; Huber, C.; Ahlrichs, R. *J. Chem. Phys.*, **1994**, *100*, 5829-5835.
- 69) Weigend, F.; Ahlrichs, R. *Phys. Chem. Chem. Phys.*, **2005**, *7*, 3514-3305.
- 70) Barone, V.; Cossi, M. *J. Phys. Chem. A*, **1998**, *102*, 1995-2001.
- 71) Hanazaki, I. *J. Phys. Chem.*, **1972**, *76*, 1982-1989.
- 72) Masnovi, J.M.; Seddon, E.A.; Kochi, J.K. *Can. J. Chem.* **1984**, *62*, 2552-2559.
- 73) Verma, P.; Wang, Y.; Ghosh, S.; He, X.; Truhlar, D.G. *J. Phys. Chem. A*, **2019**, *123*, 2966-2990.
- 74) Liao, M.-S.; Lu, Y.; Parker, V.D.; Scheiner, S. *J. Phys. Chem. A*, **2003**, *107*, 8939-8948.

A global view of excited states using *global transition contributions* grids: the triphenylene molecule as test case

3.1 Introduction

Density Functional Theory (DFT)¹ and Time Dependent DFT (TD-DFT)² can nowadays undoubtedly be considered as the most spread quantum chemical methods to describe ground and excited states of molecular systems within the chemists' community. Their advantage relies essentially in on a good accuracy over cost ratio while their main drawback is related to their intrinsically approximate nature, due to the necessity of using an approximate form of the - unknown and exact- universal functional. Nonetheless, their recent wide application to the description of different systems/properties, and to the increasing number of studies of comparison with "exact" quantum chemical approaches (most often post-HF in the case of chemically relevant systems), helped also to clearly point out the main failures of DFT and TD-DFT or, at least, to trace the origin of their inaccuracy.

Focusing on electronic excited states, many papers have pointed out the intrinsic deficiencies of TD-DFT when used in conjunction with exchange correlation functionals not possessing the correct asymptotic behavior (such as all LDAs, GGAs and global hybrids not possessing a large –ideally 100%- of HF exchange) in describing electronic excitations with marked Charge Transfer (CT) character. In particular, all these functionals are unable to correctly describe the dependence of the electronic excitation energy with respect to the variation of the CT distance (that is the hole electron separation produced upon excitation) leading to the prediction of the presence of un-physically and low energy electronic states of CT character commonly referred to as 'ghost states'.

One of the ways that has been proposed in literature to cure this erratic behavior is to use functionals treating the electron-electron exchange for large interelectronic distances (that is at long range) as in HF³ while describing electron-electron exchange at short interelectronic distances (that is at short range) at GGA⁴ level. This type of functionals –called range separated hybrids or Long Range Corrected functionals⁵ is thus, by construction, free of the presence of ghost states.

Nonetheless, the question may arise on how to define the short to long range separation that is how to define when the electron-electron interaction may better be treated at HF or GGA level and if, given a GGA form, the parameter defining this range separation is unique and system independent or not. For most of current range separated hybrids, the range separation parameter is fixed, (e.g. CAM-B3LYP⁶ or LC-PBE⁵) and these functionals, though being free of an erroneous prediction of the presence of CT ghost states are known to sizably overestimate electronic transition energies thus predicting spectra normally shifted to higher energies.

Recent work of Baer and collaborators⁷ proposed a smart and efficient way to define the range separation parameter in order to provide extremely accurate CT energies leading to the formulation of the so-called tuned range separated functionals. If the results obtained with such an approach are definitely good in this case, the range separation parameter is indeed system dependent, questioning about their efficient use in the case of instance of the study of compounds of very different nature or even worst if aiming at describing reactions occurring at the excited state.

In this scenario it has to be underlined that global hybrid functionals with low to medium percentage of HF exchange (i.e. below 30% such as for instance the popular B3LYP⁸, PBE0⁹) normally produce very good results for valence excitations possessing local or limited CT character. Of note the same class of functionals are also extremely well performing in the modeling of reactivity at the ground and, though validated to a minor extent, also at the excited state. It's thus very tempting to use them and it would be interesting to be able to define – clearly and on the fly- their range of validity and accuracy. In this context it is important to try to establish connections between the pictures provided by the different classes of functionals for the description of vertical excited states comparing to only the excitation energies but also, and possibly in a condensed way of representation, their character and nature. While comparing energetics provided by different methods (also with experiment) is rather straightforward, comparing the nature (or the character) of the electronic excited states or transition obtained with different functionals is a more delicate task. Within the TD-DFT formalism an excited state is described as (the sum of) one electron excitation(s) from occupied to virtual orbitals, thus its analysis requires inspection of all orbitals involved. This task may be simplified by the use of Natural Transition Orbitals (NTO)¹⁰ allowing to obtain a more compact view of the hole-electron excitation. Analogously, descriptors quantifying the hole-electron separation may also help since condensate in a scalar or vectorial quantity the distance between the hole and the electron and thus allow to define the local or non-local (thus CT) character of a transition though losing all information about the actual molecular orbitals involved.

In this work we apply a condensed way of analysis of the electronic transition comparing the behavior of different functionals in the description of the excited state based on a 2D interlinked graphical representation of their energetic and nature, inspired by the so called *Transition Contribution Map* (TCM) analysis¹¹. This analysis will be referred to as *Global Transition Contribution Grid* (G_TCG) analysis.

We have applied this type of analysis to molecular system belonging to the family of polycyclic aromatic hydrocarbons (PAH) family –such as those depicted (Figure 1) - which are known to be problematically described at the excited state by local exchange correlation functionals¹².

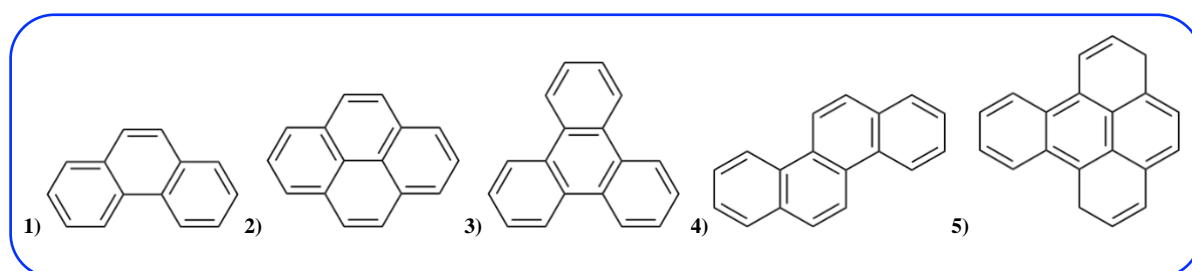


Figure 1. phenanthrene (1), pyrene (2), triphenylene (3), chrysene (4), benzo[e]pyrene (5).

Within this thesis we will detailed and discuss only data concerning the triphenylene molecule. Indeed, these molecules show two low lying excited states both of π - π^* type commonly denoted as 1L_a and 1L_b : the first possessing transition density nodes at the atoms and the second at the bond midpoints. As a function of the increase in size of the systems (number of the aromatic rings), the 1L_a state (also referred to as “ionic state”) is strongly underestimated by local and global hybrids functionals while the 1L_b state (also referred to as “covalent state”) seems to be systematically overestimated by all functionals. On this basis, it was argued that the 1L_a possesses a ‘CT type character’ while the 1L_b state was considered as a locally excited state.

Due to the fact that a large difference between functionals can be found in the energetics predicted for one of these two transitions while the all provide almost equivalent results for the energetic of the other, we selected this family of molecules as an ideal test to check if our graphical representation is able to spot difference in nature and energetics.

3.2 Computational Details

All the calculations were performed with a version G16 of the Gaussian development code¹³. Ground state structural optimization was performed, in the gas phase, using the B3LYP⁹ functional and the 6-31G(d)^{14,15} basis set.

Vertical singlet excited states were computed at the TD-DFT level using the following exchange-correlation functionals: BLYP^{16,17}, B3LYP⁸, CAM-B3LYP⁶, PBE¹⁸, PBE0⁹, LC-PBE⁵. The Dunning's correlation consistent triple zeta basis set, cc-pVTZ basis set¹⁹, was used for all vertical excited states calculations.

The transition contribution map (TCM) and global transition contribution grid (G_TCG) analysis

The *transition contribution map* (TCM) analysis is a way to represent the computed excited states in terms of one sum of one-electron excitations and in particular in terms of contributing hole-electron pairs. This analysis –firstly proposed by Hakkinen²⁰ and collaborators and later on applied by other groups²¹- is indeed interesting in the case of excited states and transitions displaying contribution of several electron-hole pairs that makes difficult to have a simple view of the hole-electron pairs contributing to each vertical excitation. The TCM analysis relies on the fact that each excited state can be defined as sum of one electron excitations and, inversely to standard analysis based on global transition density analysis, allows to easily identify the contribution of each hole-electron pair to the transition.

In a more formal way three axes are defined in TCM : i) the x axis that reports the eigenvalue energy of the occupied KS orbital (that can be considered the energy of the hole state); this is referred to as ϵ_{occ} ; ii) the y axis that reports the eigenvalues of the unoccupied KS orbitals (that can be considered the energy of the electron state); this is referred to as ϵ_{unocc} ; and iii) the z axis which corresponds to a quantity to which a defined hole-electron pair can contribute. In the original TCM analysis this z-axis was associated to squared magnitude of the coefficient $[c_{i\alpha}^\omega]^2$ describing the contribution of each i - α hole-electron pair to an electronic transition of frequency ω . The individual transitions are broadened by gaussian functions for visualization purposes using smoothing parameter $\Delta\epsilon$ (of the order of 0.1 eV in previous publications) leading to the general formula:

$$TCM(\epsilon_{occ}, \epsilon_{unocc}) = \sum_i^{occ} \sum_\alpha^{unocc} [c_{i\alpha}^\omega]^2 e^{\left[-\left(\frac{\epsilon_{occ}-\epsilon_i}{\Delta\epsilon}\right)^2 - \left(\frac{\epsilon_{occ}-\epsilon_\alpha}{\Delta\epsilon}\right)^2\right]} \quad 3.1$$

In literature, other choices for the axes of the TCM can be found such as partial density of states or a spatial projection.

In the present work, we are interest in using the TCM idea to graphically spot difference between functionals in predicting energy and nature of several excited states.

Therefore, the following modifications to the original TCM analysis we introduced:

- 1) Instead of considering the energies of the occupied and unoccupied orbitals we considered a regular grid identifying each occupied and unoccupied orbital by its orbital number. Of course, in this case no broadening is applied.
- 2) Instead of considering a different grid for each electronic transition we sum up over all computed excited states so that the corresponding global TCM so obtain is actually depicting the contribution of each hole-electron pair to all the transition

These modification leads to what we will call *Global Transition Contribution Grids* (G_TCG). In this grid for each occupied/unoccupied orbital pairs a z-value is defined as it follows:

$$G_TCG(i, \alpha) = \sum_{A=1}^{Nstates} [c_{i\alpha}^A]^2 \quad 3.2$$

where $Nstates$ indicates the total number of excited states that have been computed while i and α runs over all occupied and unoccupied orbitals number. In the present case the first 20 excited states will be considered for each functional

For purpose of analysis other Global Transition Contribution Grids have been plotted including a weighting of global quantities related to the electronic transition such as oscillator strengths (f , equ. (3)), excitation energies (EA, equ. 4) or charge transfer character quantified by the charge transfer distance (D_{CT} eq. 5). In the last two cases the z-axis is in eV and Å, respectively.

$$G_TCG_f(i, \alpha) = \sum_{A=1}^{Nstates} f_A [c_{i\alpha}^A]^2 \quad 3.3$$

$$G_TCG_E(i, \alpha) = \sum_{A=1}^{Nstates} E_A [\delta_{i\alpha}^A] \quad \delta_{i\alpha}^A = 1 \text{ if } c_{i\alpha}^A > 0 \text{ otherwise } \delta_{i\alpha}^A = 0 \quad 3.4$$

$$G_TCG_D(i, \alpha) = \sum_{A=1}^{Nstates} D_{CT} [\delta_{i\alpha}^A] \quad \delta_{i\alpha}^A = 1 \text{ if } c_{i\alpha}^A > 0 \text{ otherwise } \delta_{i\alpha}^A = 0 \quad 3.5$$

3.3 Results and Discussion

For the sake of clarity, we will first discuss the trends observed in the G_{TCG} plots for two different families of exchange correlation functionals, namely the non-parametrized PBE family and the BLYP derived one. For each family a GGA (PBE and BLYP, respectively), a global hybrid (PBE0 and B3LYP) and a range separated hybrid (LC-PBE and CAM-B3LYP) have been considered. Of note, both global hybrid considered contains a similar percentage of HF exchange and are normally claimed to provide a very similar description of the excited states and to be subject to the same pathological behavior (i.e. the prediction of ghost state for long range, though space charge transfer) while the two range separated functionals have a slightly different asymptotic behavior, only LC-PBE recovering 100% HF type exchange at long distance.

In Figure 2 the computed G_{TCG} for the two families. In appendix B all corresponding molecular orbitals iso-density are reported. Of note if orbital energies spreading varies depending the functional considered, the MO ordering is the same meaning that all functionals predict the same ordering of the molecular orbitals thus making possible a direct comparison of the maps.

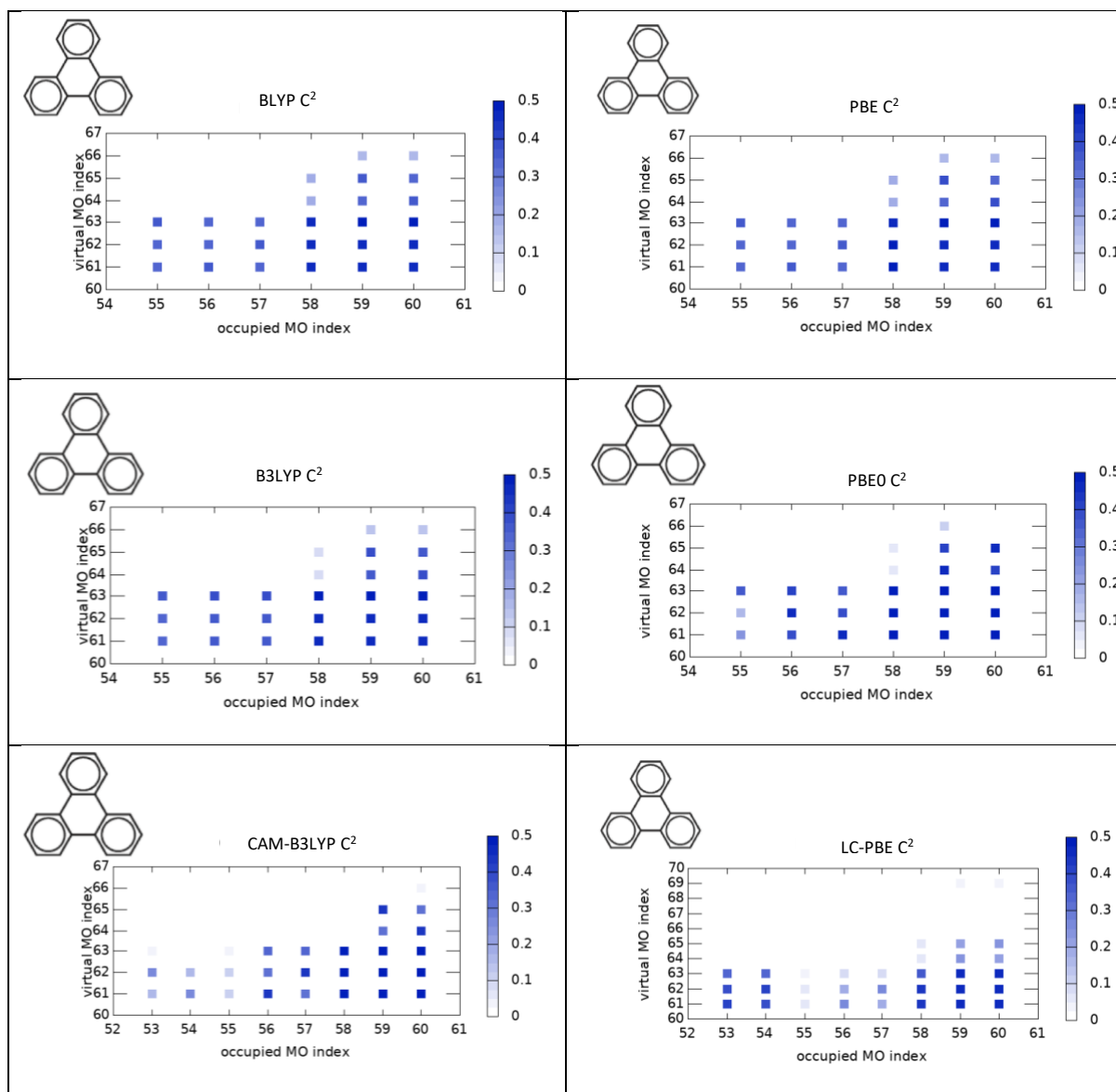


Figure 2. Computed G_{TCG} for the BLYP and PBE families ($HOMO=60$; $LUMO=61$). To facilitate comparison, the axis z color scale is the same for all functionals.

Not surprisingly, overall the computed transitions (which are the first lowest 20) are mostly involving molecular orbitals close to the HOMO-LUMO ones (in particular HOMO to HOMO-2 ie 60 to 58 for the holes and LUMO to LUMO+2 ie 61 to 63 for the electrons).

It is clear that no qualitative and quantitative difference can be found comparing the two patterns computed using GGA or global hybrid of the two families. In particular, one can note that the PBE and BLYP pattern are practically identical both qualitatively and quantitatively and that the same hold for the PBE0 and B3LYP one, the only difference in this latter case being a slight contribution of the H->L+5 (60->66) hole-particle pair to the excited state that cannot be highlighted for the PBE0 pattern.

On the other hand, a more important difference can be found when comparing the patterns computed at CAM-B3LYP and at LC-PBE level, this latter showing larger contribution of the hole-electron pairs involving deeper MO (ex. HOMO-6 and HOMO-7 ie MO 53 and 54) to LUMO up to LUMO-3 (ie MO 61 to 63) while at CAM-B3LYP level it is observed a more sizable contribution of hole-electron pairs stemming from HOMO-2 to HOMO-4 to LUMO/LUMO+2.

More generally comparing GGA to global or range separated hybrids within each family one can note that the contributions of higher lying unoccupied molecular orbitals to the computed transitions progressively vanish and that seem somehow connected to the percentage of HF exchange (for instance this type of contributions are minimal in the case of LC-PBE).

Nonetheless it is worth to recall that the analysis performed up to now takes into account all computed transition independently of their oscillator strength that is independently of the fact that the corresponding excited states will contribute to the observed spectra (bright transitions $f > 0$) or not (dark transition $f = 0$ or small).

To analyze the possible difference in the nature of the transitions actually contributing to the computed absorption spectra, in Figure 3 are reported the plots corresponding to G_TCG_f , where each of the hole-particle pairs is weighted for the oscillator strength of the transition to which it is contributing. In these maps the brighter the electronic transitions (that is the larger is f) the higher will be the weight of the hole-electron pair. These charts will be discussed together with the plots corresponding to the G_TCG_E , reported in Figure 4, where each of the hole-particle pairs is weighted for the energy of the transition to which it is contributing.

The general patterns discussed previously for the un-weighted hole-electron pairs clearly still holds and are even more clearly showing up. Comparing with the G_TCG maps shows that may on the inner to high energy unoccupied orbitals hole-electron pairs actually mainly contribute to dark transitions since the corresponding spots practically disappear in the G_TCG_f maps independently on the functional. On the other hand, all hybrid functionals (global or range separated) show a more important contribution stemming from the HOMO/HOMO-1 to LUMO+1 pairs while the HOMO-2 to LUMO/MUMO+1 hole-electrons pair seems to be contributing to bright transitions for all functionals but CAM-B3LYP. Nonetheless, the analysis of the G_TCG_f maps still does not allow to draw definitive conclusions on the difference between the difference functionals since, for instance a given hole-electron pair may have a relevant contribution to the G_TCG_f map either because it is strongly contributing to few –or even only to one- bright electronic excitation or because it is contributing to many but less intense transitions.

To have an idea, it is thus worth to analyze the G_TCG_E maps reported in Figure 5. In all cases it seems that these pairs are actually contributing to more than one transition since they show a sizable to high value in the corresponding G_TCG_E plots. Furthermore, all GGAs and global hybrid functionals display a relatively similar pattern while range separated hybrids are characterized by small but numerous contributions to electronic excitations also by inner molecular orbitals and higher lying unoccupied MOs as more clearly shown by the plots, reported in Figure 5 where the G_TCG_E grids are weighted by the $[c_{i\alpha}^A]^2$ coefficients.

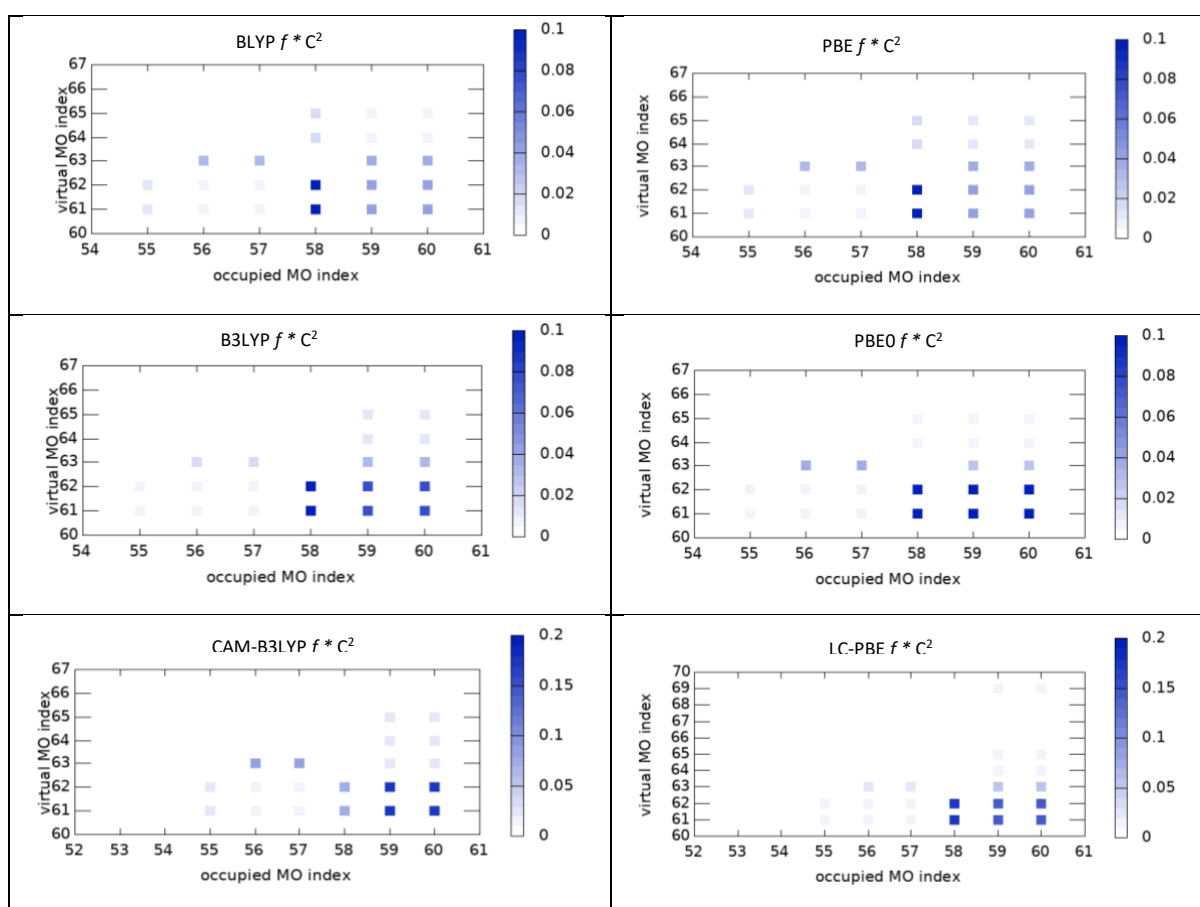


Figure 3. Computed G_TCG_f for the BLYP and PBE families (HOMO=60; LUMO=61). To facilitate comparison, the z axis color scale is the same for all functionals.

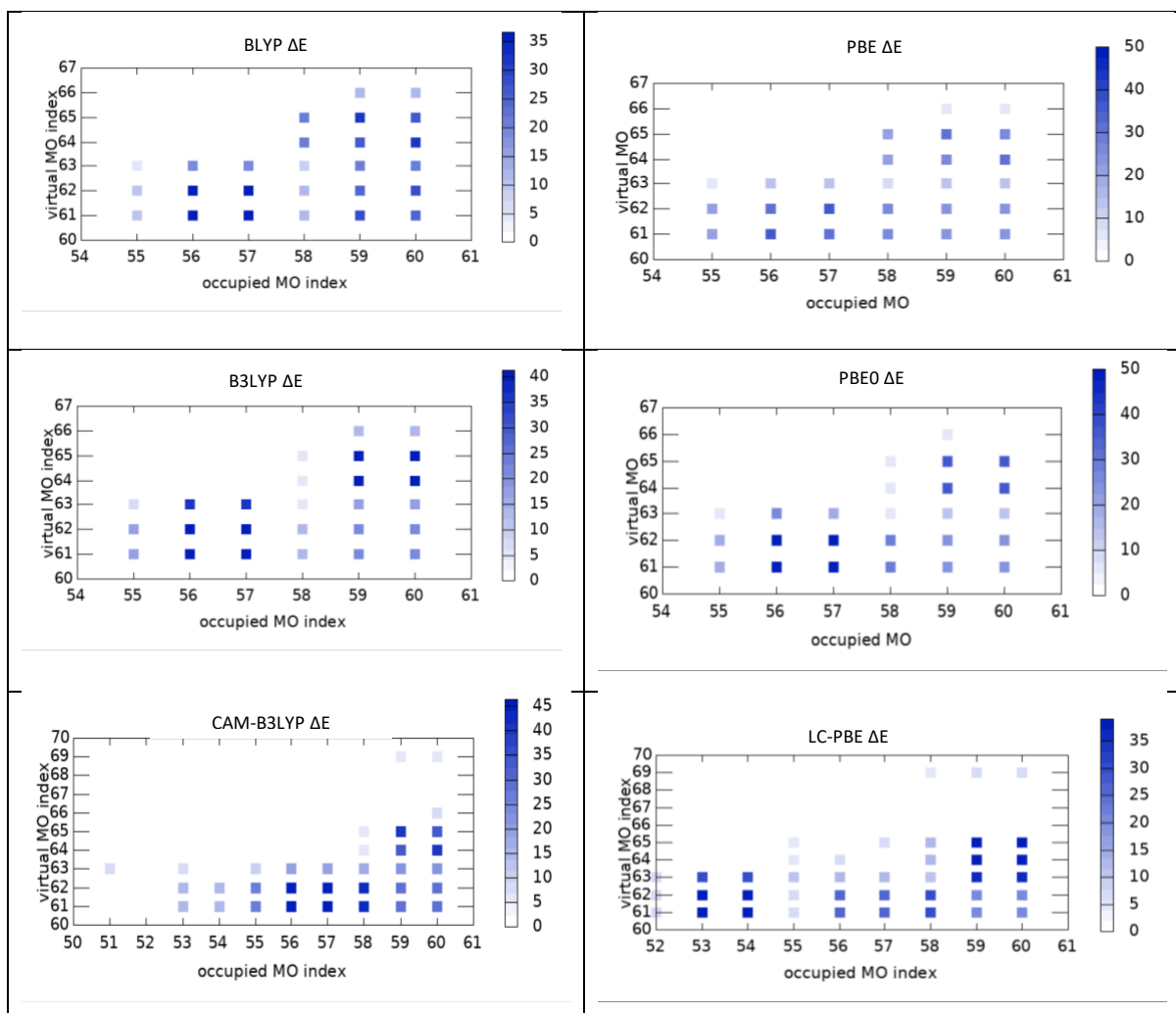


Figure 4. Computed G_{TCG_E} for the BLYP and PBE families (HOMO=60; LUMO=61). Please note that the z axis color scale is not the same for all functionals.

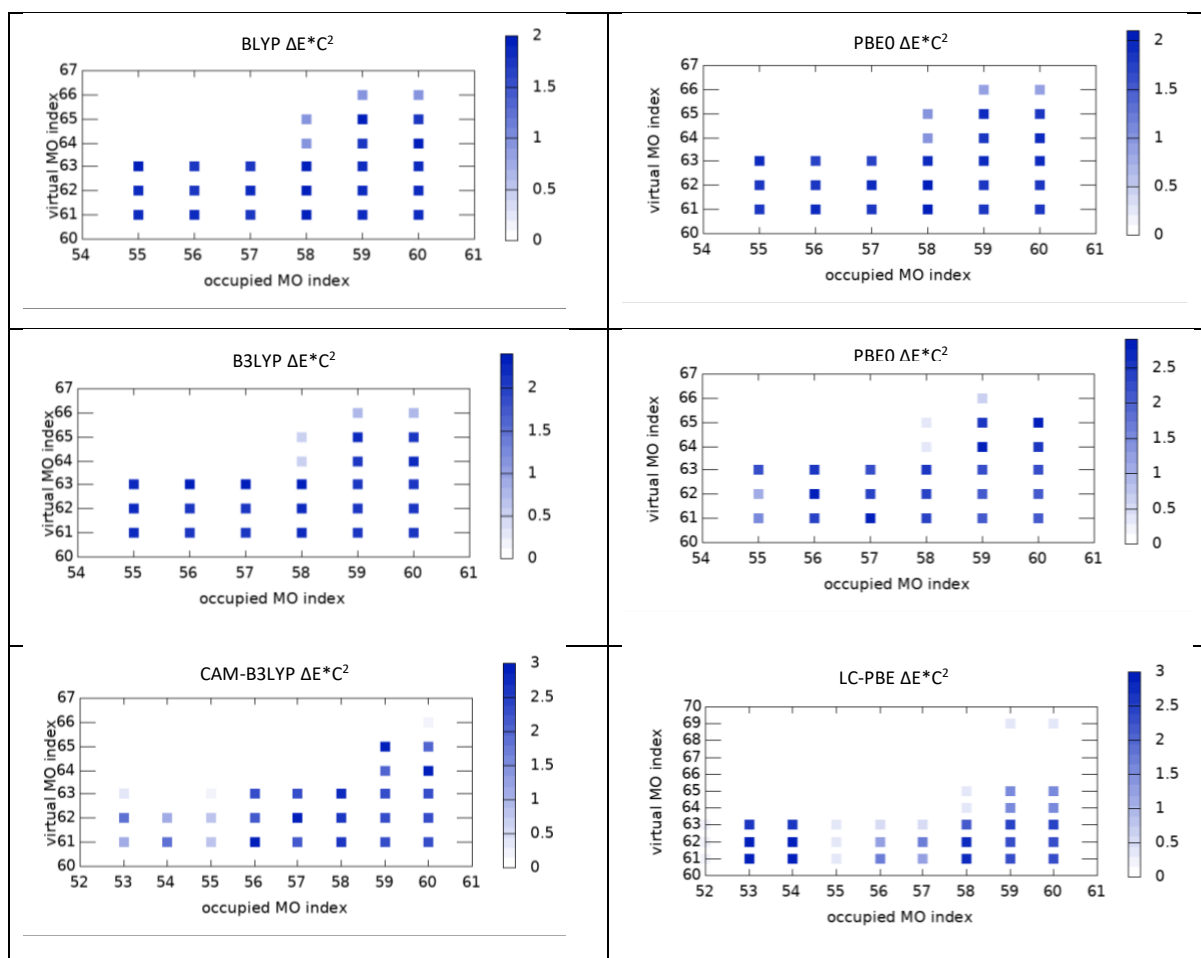


Figure 5. Computed G_{TCG_E} scaled for the $[c_{i\alpha}^A]^2$ factor ^(2*) for the BLYP and PBE families (HOMO=60; LUMO=61). To facilitate comparison, the z axis color scale is the same for all functionals.

Finally, in order to see if some global insights can be drawn on the nature of the computed excited states (local or non-local nature) we decided to plot the computed G_{TCG_D} values, that are now plotted in Figure 6.

^(2*) In the case of this scaled G_{TCG_E} maps the following formula has been used : $G_{TCG_f}(i, \alpha) = \sum_{A=1}^{Nstates} E_A [c_{i\alpha}^A]^2$

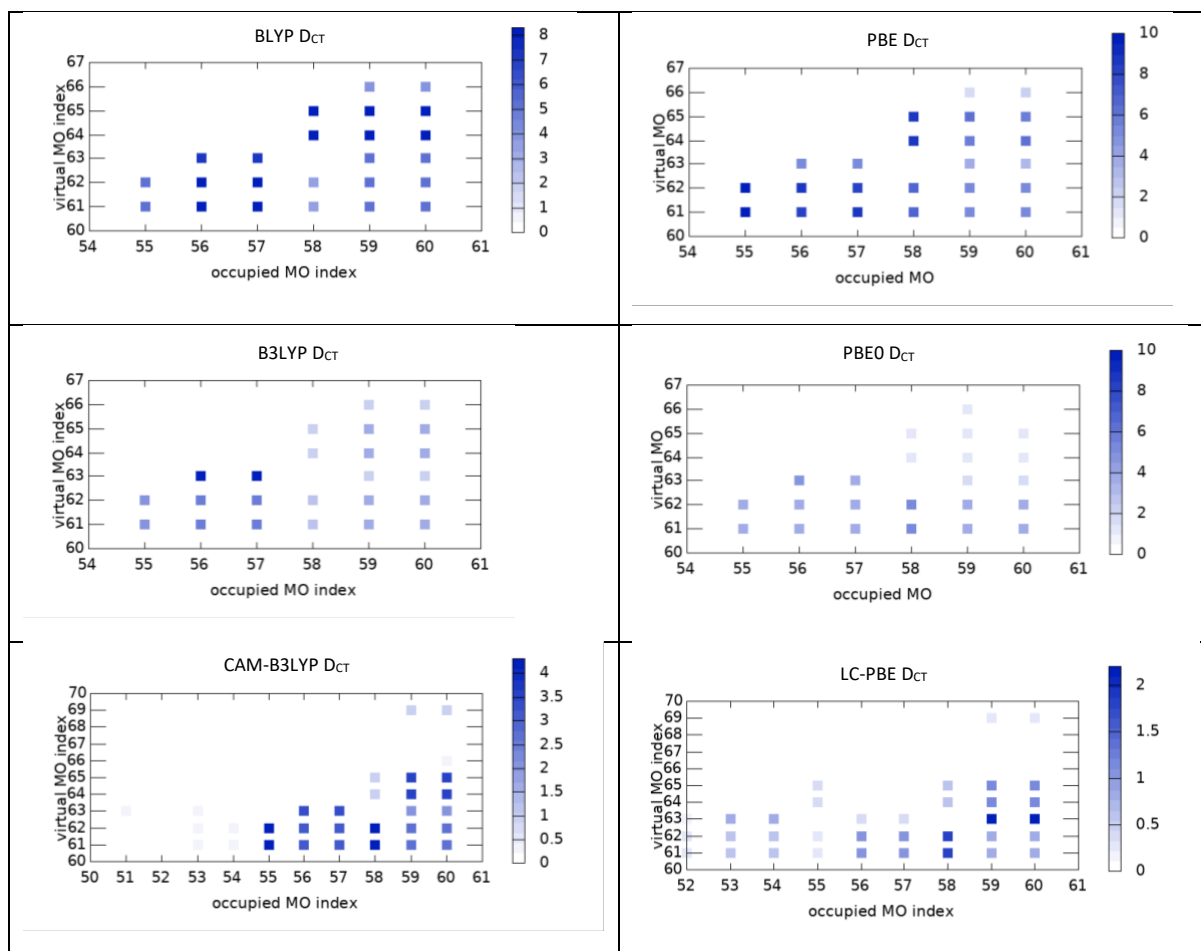


Figure 6. Computed G_{TCG_D} for the BLYP and PBE families (HOMO=60; LUMO=61). To facilitate comparison, the z-axis color scale is the same for all functionals.

Interestingly, the plots obtained for the different functionals show sizable differences. In particular one can note that if GGA and global hybrids independently on the family show very similar trends and values, both range separated hybrids show a different global behavior and more importantly an overall more local value as can be deduced from the fact that the z-axis scale is reduced by a factor of 2.

3.4 Conclusions and Perspectives

From the analysis of the different global grids derived from the Transition Composition Maps here proposed in the case of the triphenylene molecule the following conclusions and perspectives can be drawn:

- G_TCG can be used to qualitatively spot difference in the behavior of the different functionals not only in energetics but also in the nature of the computed transition in a condensed and qualitative way
- Analysis of the transition contributing to the computed spectra can be performed by the analysis of the G_TCG_f maps
- When aiming at comparing grids computed with different functionals this analysis nonetheless requires previous comparison of the molecular orbitals involved which may reveal tedious
- Global maps here as reported have been drawn for a given –fixed- number of excited states which results in a different span of the computed absorption energies. An alternative choice could be to constructing global grids not at fixed number of excited states but summing up to all excited state within a given spectral window of interest
- Analogously here all contributions to the excitations have been considered. A –large- threshold on the contributing $[c_{i\alpha}^A]^2$ factors may simplify the pattern and allow a better qualitative interpretation of the spectra
- A different type of analysis could be provided focusing exclusively on contribution of specific occupied -i- unoccupied – α - orbital pairs
- More generally we believe that this global grid-based analysis could help in the analysis of systems possessing a complex electronic structures and dense molecular orbitals manifold close to the frontier orbitals such as for instance nanoparticles or large π -conjugated systems

Work is currently in progress to analyze the results obtained for the complete set of PAHs depicted in Figure 1.

References

- 1) Hohenberg, P. Kohn W.; *Phys. Rev.*, **1964**, 136B864–B871.
- 2) Runge, E.; Gross, E. K. U. *Phys. Rev. Lett.*, **1984**, 52 (12): 997–1000.
- 3) Hartree, D. R. *Math. Proc. Camb. Philos. Soc.*, **1928**, 24 (1): 111.
- 4) Perdew, J.P.; Burke, K.; Ernzerhof, M. *Phys. Rev.Lett.* **1997** vol 78 1396.
- 5) Song, J-W.; Hirose, T.; Tsuneda, T.; Hirao, K. *J. Chem. Phys.*, **2007**, 126, 154105.
- 6) Perdew, J. P.; Burke, K.; Ernzerhof, M. *Phys. Rev. Lett.* **1996**, 77, 3865-3868.
- 7) Stein, T.; Kronik, L.; Baer, R. *J. Am. Chem. Soc.*, **2009**, 131, 2818–2820.
- 8) Becke, D. *J. Chem.Phys.*, **1993**, 98, 5648–5652.
- 9) Adamo, C.; Barone, V. *The Journal of Chemical Physics.* **1999**, 110 (13): 6158–6170.
- 10) R. L. Martin, *J. Chem. Phys.*, 2003, 10.1063/1.1558471.
- 11) Malola, S.; Lehtovaara, L.; Enkovaara, J.; Hakkinen, H. *ACS Nano*, **2013**, 7, 10263–10270.
- 12) Richard, R. M.; Herbert, J.M. *J. Chem. Theory Comput.*, **2011**, 7, 1296–1306.
- 14) Frisch, M. J.; Trucks, G. W.; Schlegel, H. B.; Scuseria, G. E.; Robb, M. A.; Cheeseman, J. R.; Scalmani, G.; Barone, V.; Petersson, G. A.; Nakatsuji, H.; Li, X.; Caricato, M.; Marenich, A. V.; Bloino, J.; Janesko, B. G.; Gomperts, R.; Mennucci, B.; Hratchian, H. P.; Ortiz, J. V.; Izmaylov, A. F.; Sonnenberg, J. L.; Williams-Young, D.; Ding, F.; Lipparini, F.; Egidi, F.; Goings, J.; Peng, B.; Petrone, A.; Henderson, T.; Ranasinghe, D.; Zakrzewski, V. G.; Gao, J.; Rega, N.; Zheng, G.; Liang, W.; Hada, M.; Ehara, M.; Toyota, K.; Fukuda, R.; Hasegawa, J.; Ishida, M.; Nakajima, T.; Honda, Y.; Kitao, O.; Nakai, H.; Vreven, T.; Throssell, K.; Montgomery, J. A., Jr.; Peralta, J. E.; Ogliaro, F.; Bearpark, M. J.; Heyd, J. J.; Brothers, E. N.; Kudin, K. N.; Staroverov, V. N.; Keith, T. A.; Kobayashi, R.; Normand, J.; Raghavachari, K.; Rendell, A. P.; Burant, J. C.; Iyengar, S. S.; Tomasi, J.; Cossi, M.; Millam, J. M.; Klene, M.; Adamo, C.; Cammi, R.; Ochterski, J. W.; Martin, R. L.; Morokuma, K.; Farkas, O.; Foresman,

J. B.; Fox, D. J. *Gaussian Development Version, Revision J.1, Gaussian, Inc.*, **2018**, Wallingford CT.

13) Ditchfield, R.; Hehre, W.J.; Pople, J.A. *J. Chem. Phys.*, **1971**, 54, 724-728.

14) Hehre, W.J.; Ditchfield, R.; Pople, J.A. *J. Chem. Phys.*, **1972**, 56, 2257-2261.

15) Becke, A. D. *Phys. Rev. A* **1998**, 38, 3098-3100.

16) Lee, C. T.; Yang, W. T.; Parr, R. G. *Phys. Rev. B* **1988**, 37, 785-789.

17) Yanai, T.; Tew, D. P.; Handy, N. C. *Chem. Phys. Lett.* 2004, 393, 51-57.

18) Perdew, J. P.; Burke, K.; Ernzerhof, M. *Phys. Rev. Lett.* **1997**, 78, 1396 (E).

19) T. H. Dunning Jr. *J. Chem. Phys.*, **1989**, 90 1007-23.

20) Knoppe, S.; Lehtovaara, L.; Häkkinen, H. *J. Phys. Chem. A*, **2014**, 118, 4214–4221.

21) Fortunelli et al. *J. Phys. Chem. C*, **2016**, 120, 12773.

Amino-Oligo Phenylene Ethynylenes (Amino-OPEs) as biocompatible photosensitizers in PDT: A Theoretical investigation of optical properties

4.1 Introduction

In this chapter, the optical properties of different derivatives of Amino-OPEs, found to be good photosensitizers and thus good candidates for Photodynamic therapy (PDT) have been investigated. The dyes under study differ in their chemical functionalization: they have a common OPE skeleton that is substituted either with electron withdrawing or donating groups. Density functional theory (DFT) and time dependent DFT (TD-DFT) have been applied to disclose their absorption and emission properties as well to understand their peculiar behavior upon protonation. These properties make these molecules suitable candidates for PDT.

Photodynamic therapy (PDT) is a non-invasive therapeutic technique for the treatment of different kind of tumors based on the in-situ production of reactive oxygen species (ROS) that can act as cytotoxic agents. PDT works through the associated action of three key components:

- A Photosensitizer (PS), that is a molecule able to absorb light
- A source of Visible (or near-infrared) light
- Molecular oxygen present in tissues.

The working mechanism of PDT drugs is the following: after the injection of a PS agent and its subsequent accumulation in the target tissues, the PS is activated by irradiation with light of appropriate wavelength to give a photosensitization of the endogenous oxygen (photoreaction of type II) or the production of free radicals from the surrounding molecules (photoreaction of type I). Both mechanisms will be detail later in this chapter. In both cases cytotoxic species are generated, which will determine the destruction of the cancer cells. The main advantage of PDT with respect to other cancer treatments relies on its non-

invasive nature allowing can selectively annihilate altered cells by selective irradiation and thus activation of the drugs without undesirable side effects.

If recent research in PDT has been essentially focused on the development of more specific and powerful PSs (see later), the idea of using light in medical procedure (that is phototherapy) is indeed a rather old medical approach.

Indeed, the history of phototherapy dates back to around 2000 B.C. For instance, it was explored in China to cure smallpox and was also called heliotherapy in ancient Greece. Nonetheless, the discovery of phototherapy as a scientific method has been attributed to Niels Rydberg Finsen (Nobel Prize in Physiology or Medicine in 1903). Examining the effects caused by various kinds of radiation on animals, he realized that the red light possessed the best therapeutic effect, in particular, to cure smallpox. He became famous for the development of a phototherapeutic method to cure lupus vulgaris by ‘filtered’ sunlight (light from a carbon arc appropriately fitted to reduce IR intensity). Some researchers, however, believe that the real ‘father’ of phototherapy is Antonino Sciascia¹, who invented the system ‘photocautery’ (got the patent in 1894) by selective concentration of light with a specific wavelength. The invention was applied to the treatment of several diseases, and he introduced phototherapy as a scientific method for the first time in the XIII Ophthalmologic Congress of Palermo in 1892².

Since then, several milestones have been achieved. Raab³ reported a photodynamic reaction for the first time in 1900. He studied the toxicity of several dyes, drugs exposed to light with Herman von Tappeiner⁴, who introduced the term ‘photodynamic action’ in 1904. He carried out a series of photodynamic experiments not only to reveal that topical application of eosin, in combination with sunlight exposure, can cure skin carcinoma, but also to study more sophisticated techniques of irradiating different kinds of sensitizers with two light sources, i.e. sunlight and arc lamp. Although this kind of PDT seemed to be very promising, the selectivity of the chromophore for the tumor tissue could not be proven. The missing point was established by Lipson *et al.*^{5,6} in 1960 when they developed a Hematoporphyrin derivative, HpD, that represents the basis of modern PS for PDT. Lipson and co-workers showed selective localization of HpD in the tumor tissue, hence it was considered a good diagnostic agent for cancer detection due to their fluorescent properties. Afterwards, several studies proved the cytotoxic action of HpD as a PS. For instance, one decade after the characterization of HpD, Diamond *et al.*⁷ reported its use in the photodegradation of glioma cells implanted in rats, and in 1978, Dougherty

and co-workers⁸ clinically tested PDT in subcutaneous malignant tumours using HpD as a PS. HpD led to the rapid development of PDT, and the first PDT agent was approved for clinical use by Canadian authorities in 1993.

The therapeutic success of PDT relies on the advantage that a non-invasive technique can selectively annihilate altered cells without incurring further risks. The recent increasing interest in PDT involves shifting focus onto the development of more specific and powerful sensitizers.

As previously mentioned, PDT works through the integration of three key components (PSs, visible or near infrared region light, and molecular oxygen in tissues) and its procedure can be summarized in four steps:

- I. Injection of PSs into the bodies
- II. Concentration of PSs at the tumor sites
- III. Activation of the PSs by visible light with suitable wavelength to generate reactive oxygen species (ROS) cytotoxic species
- IV. Selective destruction of cancer cells

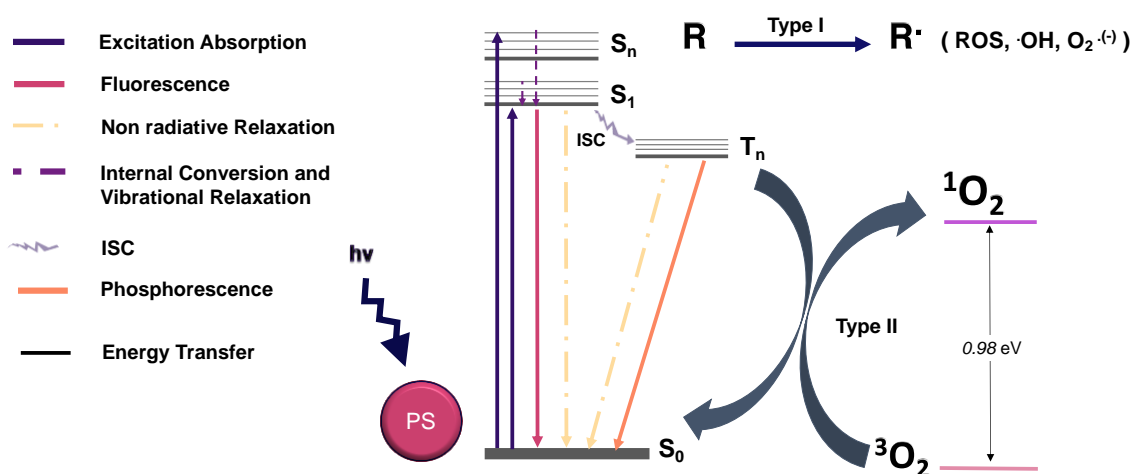


Figure 1. Schematic Jablonski's diagram showing the two photodynamic pathways for the different types of chemical reactions⁹.

In the PS activation process by light (Figure 1), the PS will typically be excited from the electronic ground state S_0 (usually closed-shell ground state: characterized by a spin multiplicity of 1, called a singlet, S) to a singlet electronically excited state (here S_1). Normal lifetime of a singlet excited state (of the ns order) will be too short to allow interaction with surrounding molecules. Energy releasing allowing relax from the S_1 excited state to the S_0

ground state will thus take place either through a radiative process, i.e. fluorescence, or non-radiative process and eventually occurring after an inter-system crossing (ISC) to the triplet excited state (here T₁).

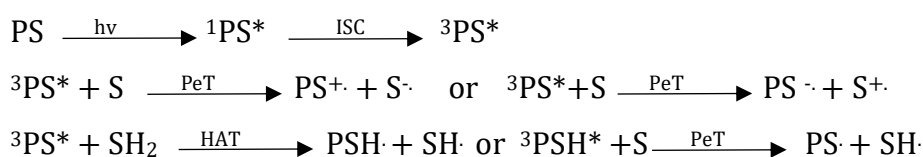
This transition is actually spin-forbidden by the selection rules but may be allowed by spin-orbit coupling. Further deactivation from the T₁ state can be caused either by internal conversion or by a radiative phenomenon (i.e. phosphorescence).

In order to reach the S₀ ground state from the T₁ one, a second spin forbidden process must occur. Since the transition probability and the lifetime of excited states are inversely correlated, the lifetime of T₁ is usually longer than that of S₁. The longer lifetime of the T₁ state is sufficient to allow energy or electron transfer to the surrounding molecules to generate cytotoxic species. Therefore, recent development of PDT target, together an efficient absorption of light –and thus population of the singlet state also the efficient formation of triplet states.

Generation of cytotoxic species (radicals) can take place through two different photochemical processes:

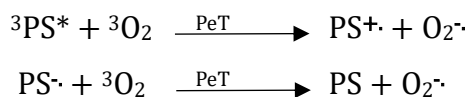
- Photochemical reactions of type I
- Photochemical reactions of type II

The ratio between type I and type II photoreactions occurring in biological media depends on the type of PS and the local dioxygen concentration. Photochemical reactions of type I produce free radicals through the interaction between the PS in the excited state (usually T₁) and surrounding molecules (e.g. lipids as biological molecules and molecular oxygen). The free radicals can be generated in different ways, for example via photoelectron transfer (PeT) or hydrogen atom abstraction (HAT) as shown in the following reaction schemes:



Scheme 1. Reaction schemes for the generation of free radicals via PeT or HAT.

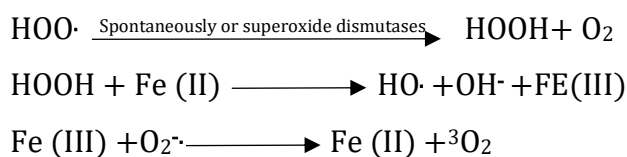
The excited or radical PS reacts with the molecular oxygen present in the tissues to generate superoxide, O₂^{•-}, as shown in Scheme 2 below:



Scheme 2. Generation of superoxide.

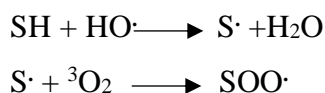
The pH in cancer cells is usually less than 7.0 (acidic condition), therefore the superoxide can be protonated to produce hydroperoxyl radical as shown in Scheme 3.

The generation of hydroperoxyl radicals is not enough to ensure cell death due to the lower reactivity of these radicals. The last two processes are known as Fenton reactions, where ferrous iron (Fe^{2+}) or other transition metal ions present in the system reacts with the hydrogen peroxide to produce hydroxyl radical and ferric iron (Fe^{3+}). The Fe^{3+} is reduced to Fe^{2+} by superoxide. Thus, iron can work as a good catalyst even in trace amounts.



Scheme 3. Generation of reactive oxygen species.

The free radical generated in the photochemical reaction mentioned above will propagate sequential free radical reactions in the dark and generate highly reactive species as shown in Scheme 4. Therefore, exposing the cells to oxidative environments causes damage and ultimately leads to cell death.



Scheme 4. Sequential reaction scheme mediated by free radicals.

In the photochemical reaction of type II, the excited state of the PS (usually ${}^3\text{PS}^*$) returns to the ground state via energy transfer to the triplet dioxygen, generating singlet oxygen (Scheme 5). The singlet oxygen is the major reactive oxygen species and reacts readily with various biomolecules such as cholesterol, amino acid derivatives, nucleobases, and unsaturated lipids.

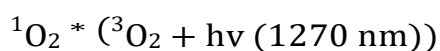


Scheme 5. Generation of singlet oxygen.

In order to produce singlet oxygen, the energy gap between S_0 and T_1 of the PS must be larger than the energy gap required to generate excited oxygen (${}^1\Delta_g$), i.e. 0.98 eV^{10} .

The tests allowing distinguishing if a PS acts through a photoreaction mechanism of type II are based on the detection of singlet oxygen which can be measured in different ways:

- Detecting the singlet oxygen by its near-infrared luminescence at 1270 nm¹¹ in the reaction mixture. The luminescence of singlet oxygen gives rise to two weak emissions:



Indeed, detection of the second emission is complicated due to the luminescence of substrate molecules.

- Chemical trapping of singlet oxygen, which causes a decrease in reaction rate. The generated singlet oxygen species can indeed be quenched by 9,10-diphenylanthracene in the lowest excited singlet or triplet states, followed by the measure of its quantum yield for photo-peroxidation¹².
- Reaction of singlet oxygen with cholesterol, in which 5 α -hydroperoxide is formed as a main product.

On the other hand, tests to detect the photoreaction of type I are based on the detection of free radicals as follows:

- Reaction with cholesterol, in which a mixture of 7 α , and 7 β , hydroperoxides is formed;
- Addition of an antioxidant such as α -tocopherol to quench the autoxidation chain.

In principle, both photoreaction types can contribute to the final therapeutic process. The ratio of their contributions depends on the characteristic of the administered PS, e.g. the affinity for the substrates, and concentration of dioxygen in the target tissue.

Required components for PDT

The electromagnetic spectrum can be divided into various regions, as shown in Figure 2.

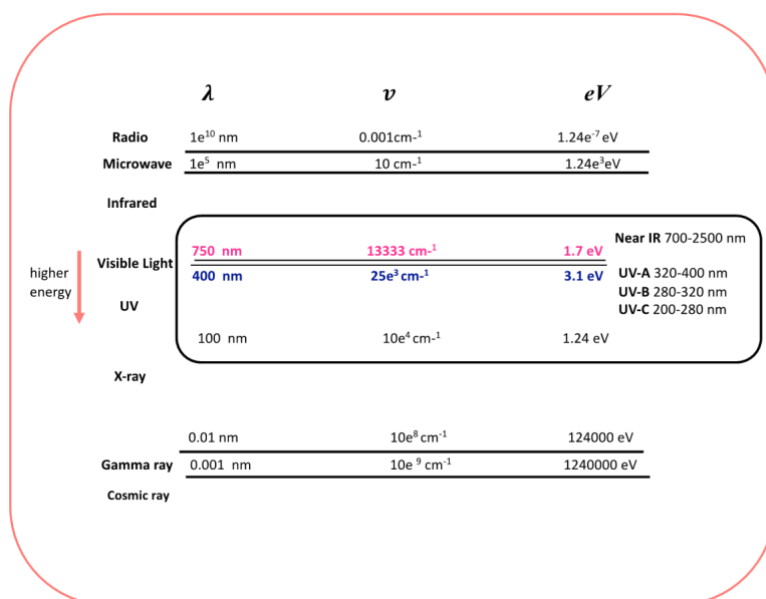


Figure 2. Classification of the electromagnetic spectrum.

The black box emphasizes the UV region which is important for the photo-biological processes.

The visible light occupies a narrow range (from 400 to 750 nm) of the electromagnetic spectrum (Figure 2). The UV region is divided into three parts, UV-A, UV-B and UV-C, and this plays a very important role in photobiological processes. A wavelength shorter than 300 nm (UV-B and UV-C) can damage the skin due to the absorption of radiation by specific nucleobases of DNA and specific α -amino acids. The light sources that were and are currently used in PDT are summarized below:

-Sunlight: Sunlight is neither convenient nor reliable enough to use routinely for the phototherapeutic purposes.

-Incandescent lamp: Incandescent lamps were the first light source used in PDT. This source is composed of one metal filament (e.g. the common light bulb) in vacuum inside a glass bulb, the filament being heated by an electric current. This kind of light source was employed in the treatments of basal cell carcinoma, with δ -aminolevulinic acid as the precursor for PSs.

-Arc lamp^a: The mercury arc lamp is widely used in the organic photochemistry and can be applied for photomedicine. These lamps can work by using different pressure loaded on mercury: low-pressure (10^{-3} mmHg), medium-pressure (1 atm) and high, pressure (100

atm). Only one line of emission at 253.7 nm (UV-C region) is obtained at low-pressure and is used as germicidal lamps.

Medium pressure ensures a greater number of emission lines and the principal lines are found at 366 and 546 nm. If the radiation is filtered with a Wood's glass, the emission in the UVB region can be used to observe the fluorescence from the porphyrins or other pigments. The high-pressure working mode gives a continuum emission with a very short lifetime and needs a cooling system. The arc lamp with xenon or xenon/mercury gives more intense and economic light source under a pressure of 20 atm, and they do not need to be cooled.

-Light-emitting Diodes (LEDs): LEDs are devices based on semiconductors, which are able to emit non-coherent radiation with low-power. The wavelength can be modulated by changing the semiconductor. A useful advantage for PDT is the small size of these devices that assures the adaptability to the patient's diseased area.

-Lasers: Lasers (light amplification by stimulated emission of radiation) are the most used devices among the radiation source instruments and are based on the stimulated emission of one excited state.

The emitted radiation will be intense, coherent, and monochromatic. Among the different types of lasers in PDT, that based on organic pigments are the most suitable. For example, the rhodamine 6G gives fluorescence in the range between 570 and 620 nm, and the dye laser is tunable over this region as a function of the PS used in PDT. Lasers allow for the control of several light parameters such as intensity, wavelength, direction, duration of pulse (flash), polarization and phase. The various outcomes of an interaction between electromagnetic radiation and a biological tissue¹³ are shown in Figure 3. The light can be absorbed by chromophores, reflected or scattered, or further transmitted.

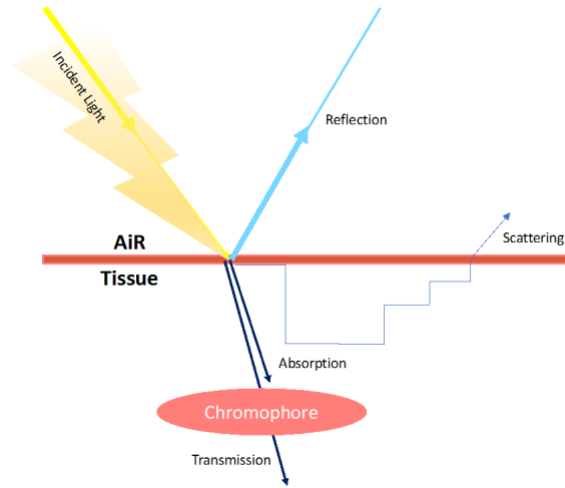


Figure 3. The phenomena that can occur in the interaction between light and biological tissue.

These phenomena take place to different extents depending on the optical properties of the tissue and the light (e.g. energy of the radiation, light exposure time, attenuation coefficient). The scattering phenomenon occurs inside the skin, and more precisely in the stratum corneum (the outmost layer of skin composed of dead keratinocytes, keratin, melanin, lipid), where different structures have different indices of refraction.

Absorption occurs due to the presence of endogenous chromophores (e.g. melanin, hemoglobin and their derivatives), therefore, it depends essentially on the skin type¹⁴. Melanin and hemoglobin strongly absorb at shorter wavelengths (~600 nm).

Svaasand¹⁵, Wilson et al.¹⁶ and Bolin et al.¹⁷ demonstrated that radiation with wavelength of 800 nm can cross the epidermal layer and effectively reach the subcutaneous tissue (around 3.5 mm in depth). The use of wavelengths less than 800 nm increases the scattering phenomenon that is inversely proportional to the light wavelength¹⁸.

Another important factor, attenuation coefficient, α (cm^{-1}), denotes the gradual intensity decay of an electromagnetic radiation through a tissue. According to the diffusion theory, it is possible to describe the attenuation of radiation using experimental data. The variation of the radiation flux (Ψ) into media, is defined by the following equation:

$$\psi = \psi_0 \frac{e^{-\alpha r}}{r}$$

where r is the distance from the radiation source. The radiation flux decreases exponentially with distance r , and small variation in the attenuation constant α leads to a large variation in the flux depending on the tissue depth. Thus, it is better to use PSs that

absorb around 800 nm to maximize the depth of the PDT treatment in various tissues. The penetration depth, δ (cm), is the reverse of α , and refers to the depth at which the radiation is attenuated to $1/e$ ($\sim 37\%$) ($e=2.72$, called Euler's number).

A general scheme of the human skin structure is shown in Figure 4. The epidermis, from 0.0 to ~ 0.1 mm in depth, is composed primarily of keratinocytes and melanocytes. The latter is responsible for regenerating skin surfaces and producing melanin.

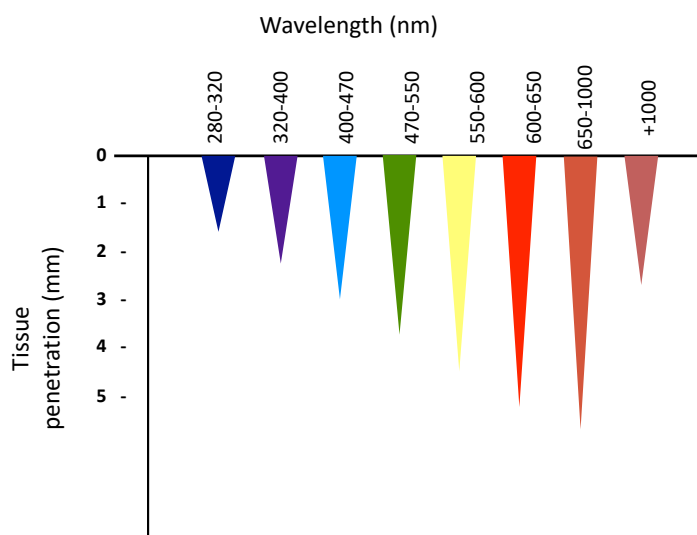


Figure 4. Schematic representation of the human skin structure, and dependency of the penetration depth on light wavelength. (image taken from "Upconverting nanoparticles for the near infrared photoactivation of transition metal complexes: new opportunities and challenges in medicinal inorganic photochemistry").

The dermis layer, from ~ 0.1 to ~ 2.0 mm, contains connective tissues, fat, supportive tissues, blood and lymph vessels, sebaceous glands and sweat glands (these last three components mainly regulate body temperature). The subcutaneous tissue (or hypodermis) lies below the dermis at a depth of more than 4.0 mm and consists primarily of adipocytes. Figure 4 shows the dependency of the penetration depth into the human skin on light wavelength. A radiation ranging from 600 to 700 nm penetrates 50-200% more than that ranging between 400 and 500 nm. The therapeutic window for PDT includes wavelength from 600 to 850 nm. The water molecules contained in the tissues absorb radiation with a wavelength over 850 nm and generate heat. Furthermore, administration of PSs with high molar attenuation coefficient in tissues containing high concentrations of endogenous chromophores attenuate the radiation penetration¹⁹.

Amino-OPEs: a new class of third generation photosensitizers?

Due to their selectivity towards tumor tissue in PDT, porphyrins and porphyrin-related macrocycles are at the forefront of PDT²⁰. Several compounds belonging to a first generation of PSs, such as the hematoporphyrin derivative HpD (Photofrin)^{21,22}, are already in clinical use or in clinical trials to treat cancer patients and are approved by the Food and Drug Administration (FDA) for the palliative treatment of obstructive lung and esophageal cancers. A second generation of PSs, with improved pharmacokinetics and reduced skin photosensitivity²³ is represented by compounds known as hydroporphyrins, chlorins and texaphyrin²⁴.

We can define the class of PSs studied in this chapter as a possible third generation of photosensitizers. This class of PSs is based on amphiphilic skeletons, bearing lipophilic and hydrophilic moieties, and they are in continuous development due to their biological applications. Hence, the third generation of PSs as mentioned above is called Amino-OPE^{25,26,27}; this group of molecules are luminescent linear oligomers with extended conjugated aromatic and ethynylene moieties. These compounds, in combination with UVA light, have been checked on two tumor cell lines stability, on the basis of singlet oxygen production, biocompatibility, easy cell-internalization. They have shown very good response even at low concentration, making them promising PS for application in PDT. The presence of hydrophobic (aryl conjugated fragments) and hydrophilic (glucose) moieties in these structures was expected to facilitate cellular membrane permeation. Terminal glucose molecules favor the advanced glycolytic process of tumor carbohydrate metabolism (Warburg effect)²⁸.

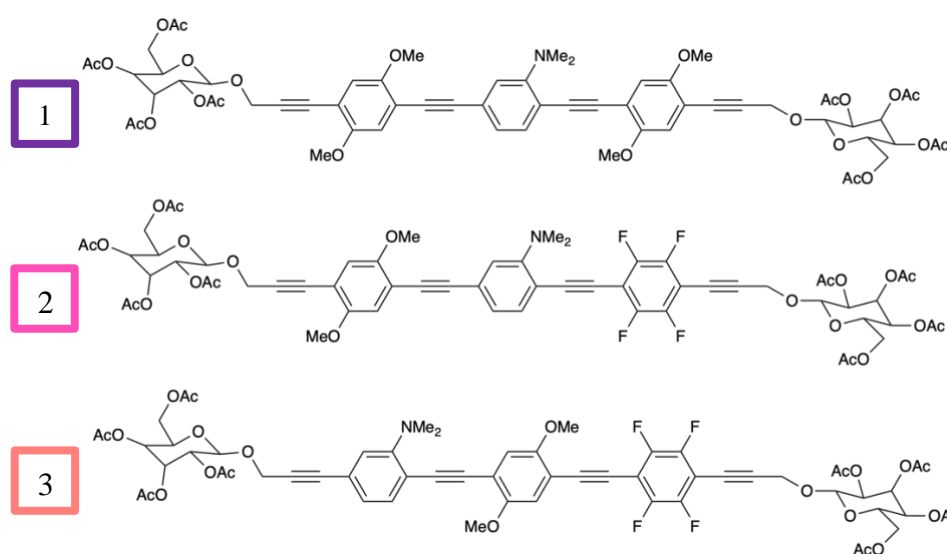


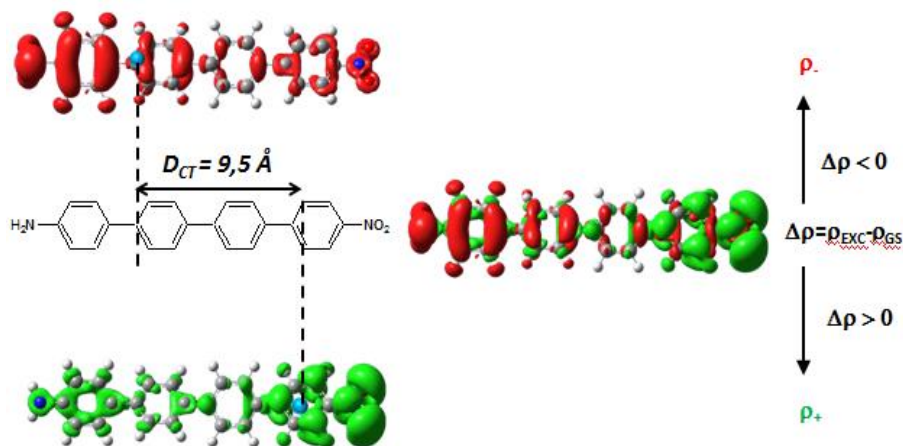
Figure 5. Representation of the structures of the Amino OPE family.

In this chapter we will focus on the analysis of the absorption and emission properties of a family of functionalized Amino – Oligo Phenylene Ethynylene (OPE) molecules depicted: **1**, **2** and **3** as shown in the figure above (Figure 5). The aim is to understand how the presence of electron-donor and electron-acceptor groups affects their optical properties. To go further, the influence of the relative positions of the different groups (here -OMe, -NMe₂ and -F groups) will also be taken into account and discussed. One can also notice that in all cases the molecules are substituted with glucose moieties to favor the glycotyc process. Here we will analyze the impact of these terminal groups on optical properties. To conduct the computational studies, we relied on the density functional theory (DFT) approach and its time-dependent version, TD-DFT. As this project is the fruit of a direct collaboration with an experimental team from the University of Messina (Professor Fausto Puntoriero) the results obtained will be compared to the experimental ones.

4.2 Computational Details

All the calculations were performed with a development version of G16 software²⁹. Model systems where the sugar terminal group substituted by an H capping atom were considered. The structural optimization was carried out using the global hybrid XC functional PBE0 in conjunction with 6-311G(d) basis set. An implicit solvation model (CPCM³⁰) was considered to mimic the effect of the solvent (CH₂Cl₂, dichloromethane) used experimentally. For the optical properties, two XC functionals were considered: PBE0 and the range separated CAM-B3LYP³¹ in conjunction with the 6-311+G(d) basis set. Each time, 20 states were computed during the TD-DFT calculations. In order to simulate the absorption spectra a convolution of the computed vertical transition was done using gaussian function with half width at half height of 0.333 eV.

Also, in order to better describe the excited state evolution even far from the Franck Condon region, density based index the so called D_{CT} ³², was used. That index measures (i.e. quantify) the global density redistribution upon excitation with the specific aim of defining the charge transfer character associated to a given electron excitation.



Scheme 6. Schematic representation of the D_{CT} index.

Simply speaking, and as schematically illustrated in Scheme 6, this index just measures the distance of the barycenters of density distributions describing the regions where the density is enhanced (ρ_+) or depleted (ρ_-) upon excitation.

The computed associated centroids of charges, on the other hand, give a flavor of the localized or delocalized character of this density redistribution. Therefore, the D_{CT} simply translates and quantifies the chemical concept of charge ‘separation length’ produced at the excited state. In the case of molecule **1** additional calculations were performed using the ONIOM model^{33,34} as detailed below.

Validation of the model

The presence and relative position of electron withdrawing/donating groups is expected to be the most relevant parameter influencing the spectroscopic features of these conjugated dyes. In particular, two different systems have been synthesized with the aim of highlighting the influence of the relative distance of the electron-donating $-NMe_2$ and $-OMe$ aromatic rings from the electron-accepting fluorinated termination, that are **2**, bearing a central dimethyl-amino aromatic ring, and **3**, bearing a central dimethoxy aromatic ring (Figure 3). One can notice that **2** and **3** derives from **1**. As previously mentioned, the molecules consist of an amphiphilic skeleton with terminal protected sugars. These groups are expected to have no effect on the electronic structure of the OPE core but they may alter the geometrical structure of it. To study their structural influence of the optical properties of the core we verified how much the presence of sugars influenced the absorption properties of it using **1** as case study. To this end, we performed a preliminary study using a two layers QM/QM’ ONIOM model^{33,34}. For the layer considered at “high” level of theory (the QM part) we considered PBE0 for the optimization and vertical excitation with the 3-21G and 6-311+G(d) basis set respectively, while the low level layer is treated using the semi-empirical method AM1. The high level QM layer consists of the OPE core while the sugar moieties are considered at QM’ level (Figure 6).

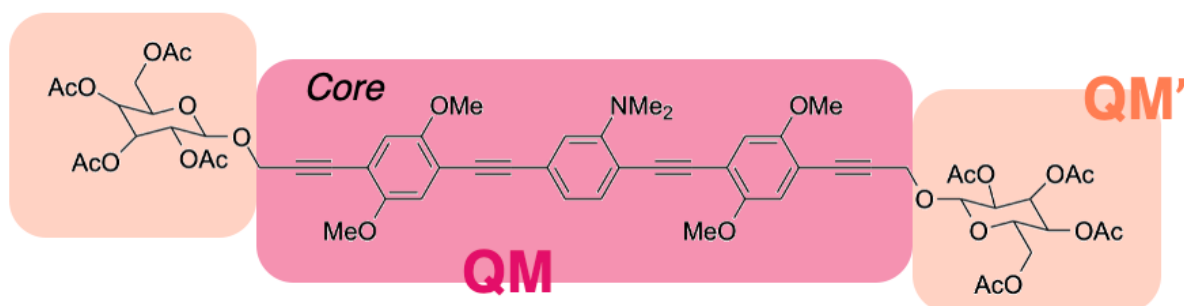


Figure 6. High Level (Core) and low level (sugars) in Oniom model.

We first optimized the structure within the ONIOM QM/QM' approach. We compared the results obtained for vertical excited states at the ONIOM QM/QM' level with that obtained for the OPE core (the model compound) performed at the QM level as described in the computational detail part (that is to say structural optimization at the PBE0/6-311G(d) level and vertical excitation at the PBE0/6-311+G(d) one).

It appears that the computed absorption properties within the two different approaches (QM/QM' or QM) with or without sugars are similar.

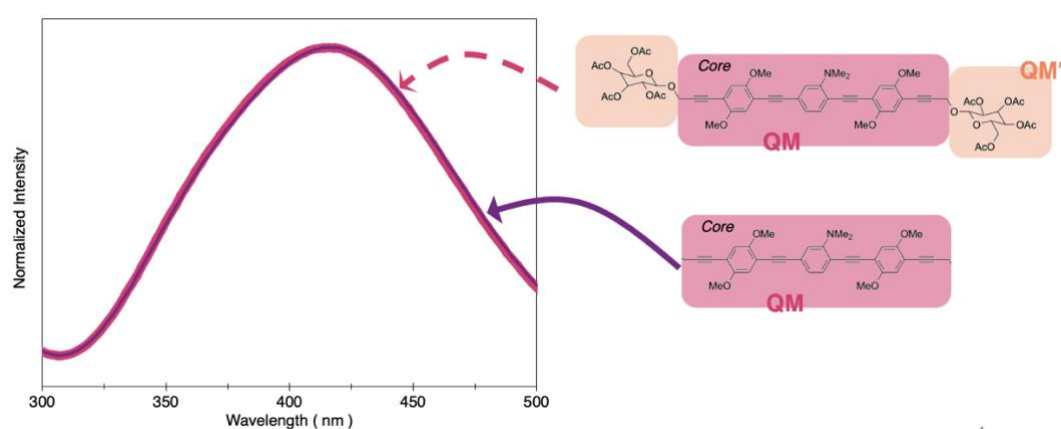


Figure 7. Absorption spectra of **I**, with and without sugars.

The maximum absorption being $\lambda_{max} = 428$ nm within the ONIOM QM/QM' approach and 428 nm for the QM approach on the model compound (Figure 7). We thus concluded that, if the sugar can be important for the metabolism of the compounds they have very low structural impact on the core and thus negligible effect on the calculation of the optical properties of the OPE core. Therefore, for the rest of the study, all molecules will be considered without their sugar terminal groups.

4.3 Results and Discussion

Ground state: structural features

In Table 1, selected optimized geometrical parameters obtained for the three molecules in their ground state geometries are reported. Looking at the triple C-C bond distances, one can say that there is no variation upon substitution of the OPE core. This distance is almost always equal to 1.21 Å for the three triple C-C bond of the three molecules. This distance is characteristic of a triple bond.

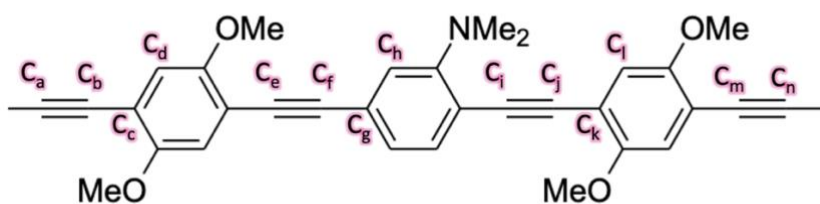


Figure 8. Representation of the structure of the OPE family CORE. The atom denomination along with the definition of important dihedrals are also provided.

	1		2		3	
	S ₀	S ₁	S ₀	S ₁	S ₀	S ₁
Bond						
C _a - C _b	1.21	1.20	1.21	1.21	1.21	1.21
C _e - C _f	1.21	1.22	1.21	1.21	1.21	1.23
C _i - C _j	1.21	1.23	1.21	1.23	1.21	1.22
C _m - C _n	1.21	1.20	1.21	1.20	1.21	1.20
Dihedral						
C _a -C _b -C _c - C _d	5	-8	6	-6	152	168
C _e -C _f -C _g - C _h	-4	151	11	177	-1	-2
C _i -C _j -C _k - C _l	13	8	43	13	-23	-18

Table 1. Selected geometrical parameters calculated for molecules 1,2,3 in the ground and excited states. The intramolecular parameters are given on Figure 8. Distances are in Angstroms and dihedral angles in degrees.

Then, we identified three dihedrals that accounted for the flatness of the molecules. It appears that **1** is almost planar with dihedrals ranging from -4° to 13° . Nevertheless, for **2** and **3** there is a loss of planarity. There is a tilt for the third ring fluorinated of **2** ($C_i-C_j-C_h$ - C_l is equal to 43°) and for the first and the third ring of **3**, the dihedrals being equal to 152° and -23° respectively. This difference in planarity may have an impact on the optical properties.

Ground state : absorption properties

Absorption properties of molecules **1**, **2**, **3** were computed following the protocol presented above. All the results, along with the experimental data, are gathered in Table 2 and in Figure 16. The performance of the PBE0 and CAM-B3LYP functionals were evaluated by comparison with the available experimental data.

	PBE0						CAM-B3LYP			
	Transition	$\lambda_{\text{abs}}(\text{nm})$	f(a.u.)	MO	Character	DCT	$\lambda_{\text{abs}}(\text{nm})$	f(a.u.)	Character	DCT
1	S ₁	428	2.04	H → L	LE/ICT	1.64	377	2.40	LE	0.70
	S ₂	370	0.93	H-1 → L	LE/ICT	2.34	322	0.65	LE/ICT	1.82
2	S ₁	442	1.47	H → L	LE/ICT	2.15	394	2.19	LE/ICT	1.41
	S ₂	386	1.17	H-1 → L	LE/ICT	4.68	331	0.91	ICT	2.23
3	S ₁	457	1.94	H → L	LE/ICT	6.93	400	2.46	ICT	2.94
	S ₂	382	0.59	H-1 → L	LE/ICT	6.11	327	0.24	ICT	2.17

Table 2. Maximum computed absorption wavelength (nm) together with the computed maximum oscillator strength values for the ES, and DCT for the three molecules with CAM-B3LYP and PBE0 functionals.

For the three molecules, the most intense transition, that is the one with the largest oscillator strength, always corresponds to an $S_0 \rightarrow S_1$ excitation which involved an excitation from the Highest Occupied Molecular Orbital (HOMO) and Lowest Unoccupied Molecular Orbital (LUMO) (see Figure 9 for the representation of the HOMO and LUMO orbitals of the three molecules). As clear from Figure 7 this transition corresponds to a $\pi \rightarrow \pi^*$ excitation.

Indeed, a slight charge transfer (CT) is observed for **1** and **2**. This CT character is more pronounced for **3**.

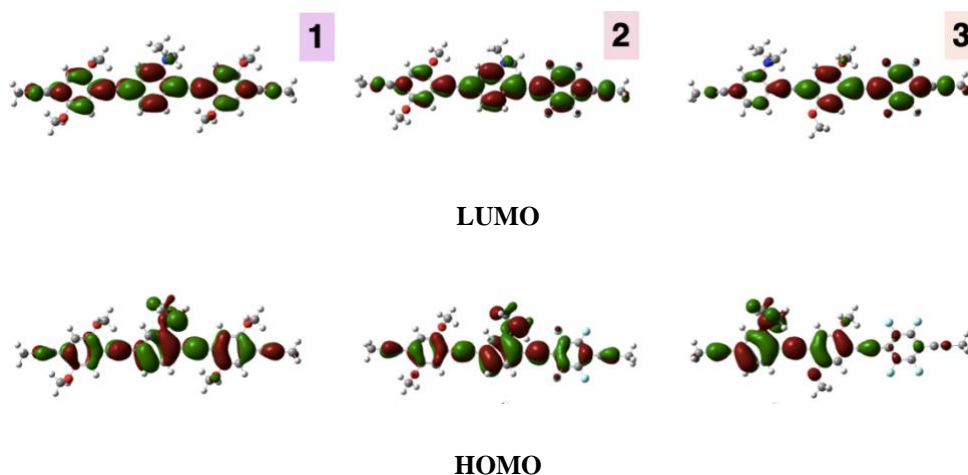


Figure 9. Molecular Orbitals (MO) of **1**, **2**, **3** calculated at the CPCM(CH₂Cl₂)-CAM-B3LYP level (isodensity = 0.025 au).

This more pronounced CT character can be explained by the fact that the donor (-NMe₂) and acceptor (-F) groups are far from each other in the **3**. This qualitative observation can be quantified and confirmed by the computed associated D_{CT} indexes, reported in Table 2. In figure 9 the hole electron separation is also graphically depicted as a green dot. We recall that the D_{CT} index measures the “length” of the charge transfer, the distance between the barycenters of “positive” (where there is a gain of electronic density) and “negative” (where there is a loss of electronic density) densities. The computed D_{CT} for **1** is small due to the symmetric nature of the compound but is also relatively small for **2** (1.20 Å). The one of **3** is on the other hand sizably large (2.94 Å). From the analysis of the HOMOs and the LUMOs it is quite evident that the larger CT character obtained for **3** is related to the larger distance between the donor (-NMe₂) and the acceptors. Indeed, while the LUMOs are strongly delocalized over the molecule the HOMO is more localized onto the donor -NMe₂ group leading to the aimed push-pull effect. Nonetheless this improved CT character has only a minor effect on the computed (and observed) transition energies.

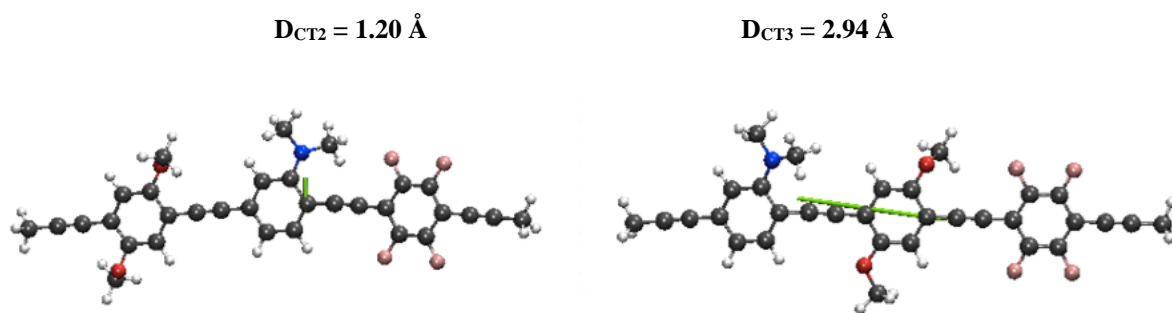


Figure 10. D_{CT} index of **2** and **35**(green arrow, indicating the direction of the density) respectively calculated at the CPCM(CH_2Cl_2)-CAM-B3LYP level.

If we now compare the simulated and experimental spectra (reported in Figure 11 and whose absorption maxima are reported for sake of clarity in Table 3) it is possible to observe that, for the absorption, CAM-B3LYP has better performance than PBE0. If we consider the difference in energy between the experimental maximum absorption wavelength and the calculated one ($\Delta E_{(calc-exp)}$, in eV) for example, for **1**, ΔE is equal to 0.29 eV when PBE0 is used while it is only 0.10 eV when CAM-B3LYP is considered. Similar conclusions can be drawn for **2** (**3**) with ΔE equal to 0.55 eV (0.48 eV) and 0.20 eV (0.10 eV) for PBE0 and CAM-B3LYP respectively. For this reason, CAM-B3LYP will be used for the study of the emission properties. PBE0 is indeed more strongly underestimating the energies of all these transitions which indeed possess a CT character.

MM	Exp	PBE0			CAM-B3LYP		
		λ_{max} (nm)	ΔE /eV	DCT(\AA)	λ_{max} (nm)	ΔE /eV	DCT(\AA)
1	389	428	+0.29	1.64	377	-0.10	0.7
2	370	442	+0.55	2.15	394	+0.20	1.41
3	388	457	+0.48	6.94	400	+0.10	2.94

Table 3. Maximum computed and experimental absorption wavelength (nm) together with the difference between computed and experimental maxima ΔE (eV) for the three molecules with CAM-B3LYP and PBE0 functionals

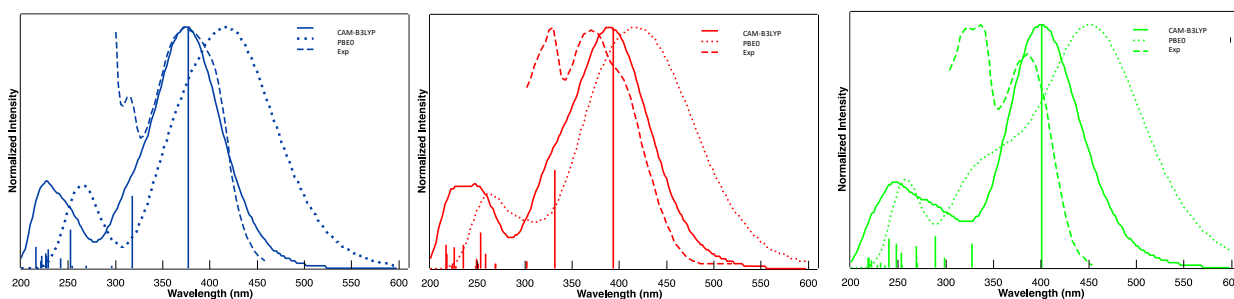


Figure 11. Absorption spectrum of molecule **1**(blue), **2**(red) and **3**(green) compared with PBE0(small dash lines) and CAM-B3LYP (solid lines) functional along with the experimental data (dash lines).

Excited state: structural features and emission energies

Emission was considered to occur by the first singlet excited state in agreement with the Kasha rule³⁵ and with the high oscillator strength of this state for all molecule considered. The key structural parameters we analyzed for the ground state were also gathered for the optimized first excited state and reported in Table 1. There is no modification of the length of the triple C-C bond upon excitation, the average length being 1.20 Å. Concerning the dihedrals, it appears that upon excitation there is a loss of planarity for **1** ($C_e-C_f-C_g-C_h=151^\circ$ while it was -4 for the ground state). On the contrary, for **2** and **3**, there is a global gain of planarity ($C_e-C_f-C_g-C_h=177^\circ$ (ES) and 11° (GS); $C_e-C_f-C_g-C_h=-2^\circ$ (ES) -1° (GS) respectively for **2** and **3**). The computed emission values are reported in Table 4. The computed emission energies at CAMB3LYP level (460, 468 and 492 nm, for **1**, **2** and **3** respectively) should be compared with the experimental values of 472, 501 and 541 nm. This leads to energy differences (ΔE in Table 4) between the computed and the experimental absorption value of 0.07, 0.17 and 0.23 eV, respectively, showing a good agreement between our calculations and the experience. Indeed, though a quantitative agreement is reached only for **1**, calculations are able to predict the qualitative trends in emission and related Stokes shifts. In Figure 12 experimental emission spectra of **1**, **2** and **3** are reported and compared with the computed ones.

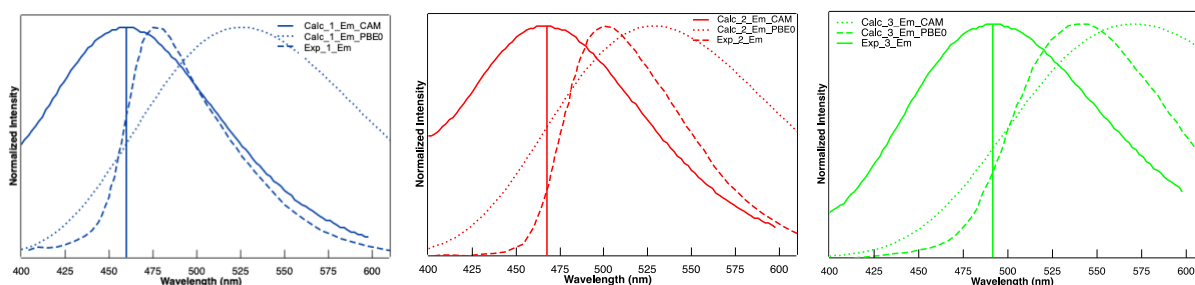


Figure 12. Emission spectrum of molecule 1(blue), 2(red) and 3(green) calculated with PBE0 (small dash lines) and CAMB3LYP (solid lines) functionals along with experimental data (dash lines).

More in detail, while the absorption spectra resulted quite similar for the three species, red-shifted emission maxima, with respect to the **1** ($\lambda_{em}=460$ nm), are observed for both the fluorinated **2** and **3** ($\lambda_{em}=468$ nm and $\lambda_{em}=492$ nm, respectively). The computational trend is the same as the experimental one ($\lambda_{em}=472$ nm, $\lambda_{em}=501$ and $\lambda_{em}=541$ nm respectively for **1**, **2** and **3**), we are thus able to reproduce the red shift observed when moving for **1** to **3**. As already discussed for absorption, our data indicate that the introduction of the fluoroaryl moiety, in the presence of electron-donating groups here NMe_2 , influences the energy gap between HOMO and LUMO in the ground state, creating a push-pull system.

This effect is more pronounced in **3** (~70 nm shift from experimental data and ~30 nm shift from computational data in emission in comparison with **1**), where the dimethyl-amino aromatic unit is farther from the fluorinated one, and thus a larger CT distance.

The values of the D_{CT} of **1** and **2** shows LE, and with respect to absorption, in the emissions there is an increase for molecule **1** of 0.07 Å, while for **2** the D_{CT} decreases very little. For **3** the D_{CT} increases by 0.40 Å and its values indicate that in both processes there is an intramolecular charge transfer (2.94 Å and 3.44 Å for absorption and emission respectively).

MM	Absorption					Emission				
	λ_{max} nm	f	$\lambda_{max,exp}$ nm	ΔE eV	$D_{CT}(\text{Å})$	λ_{em} nm	f	$\lambda_{em,exp}$ nm	ΔE eV	$D_{CT}(\text{Å})$
Neutral										
1	377	2.4094	389	-0.10	0.70	460	2.0596	472	-0.07	1.14
2	394	2.1937	370	+0.20	1.41	468	1.8813	501	-0.17	1.10
3	400	2.4633	388	-0.10	2.94	492	2.3651	541	-0.23	3.44
Protonated										
1+	392	2.9180	378	+0.12	0.70	458	2.9980	462	-0.02	0.82
2+	391	2.7986	392	-0.01	3.73	463	2.8465	513	-0.26	3.69
3+	385	2.7580	402	-0.21	0.10	451	2.7795	446	+0.03	0.22

Table 4. Maximum absorption wavelength (nm), oscillator strength, ΔE (eV) for the three molecules in neutral and acid conditions.

Protonated species: structures and optical properties

Due to the presence in all molecules of a -NMe₂ group that can be protonated depending on the pH conditions, it is interesting to test if absorption and emission properties can be change upon its degree of protonation, thus making these molecules suitable as pH probes for qualitative intracellular pH measurements.

On the basis of our calculations on neutral compounds, since the -NMe₂ group is involved as primary donor in all relevant transitions it can be expected that its protonation can significantly alter the absorption wavelength for these compounds. This effect should be amplified for the molecule(s) for which the HOMO is more strongly localized on the -NMe₂ moiety. The protonated -NMe₂ and thus charged molecules have been finally optimized at the ground state. These protonated molecules will thus be called **1⁺**, **2⁺** and **3⁺**.

	1 ⁺		2 ⁺		3 ⁺	
	S ₀	S ₁	S ₀	S ₁	S ₀	S ₁
Bond						
C _a - C _b	1.21	1.20	1.21	1.20	1.21	1.20
C _e - C _f	1.21	1.23	1.21	1.23	1.21	1.23
C _i - C _j	1.21	1.23	1.21	1.22	1.21	1.22
C _m - C _n	1.21	1.20	1.21	1.20	1.21	1.20
Dihedral						
C _a -C _b -C _c - C _d	10	-12	12	-13	-177	-171
C _e -C _f -C _g - C _h	-50	-134	-33	-129	174	39
C _i -C _j -C _h - C _l	-179	66	-4	-5	-16	-1

Table 5. Selected geometrical parameters calculated for molecules 1⁺,2⁺,3⁺ in the ground and excited states. The intramolecular parameters are given on Figure 8. Distances are in Angstroms and dihedral angles in degrees.

From the structural point of view (table 5) protonation of the methyl amino group at the ground state does not significantly alter the OPE core, even if differences for the dihedral angles were detected with respect to the non-protonated molecules at the GS. Molecules 1^+ and 2^+ contrary to their corresponding neutral analyzed show a lower degree of planarity while molecule 3^+ is rather planar at GS.

The corresponding computed –and experimental absorption spectra in CH_2Cl_2 , are reported in Figure 13.

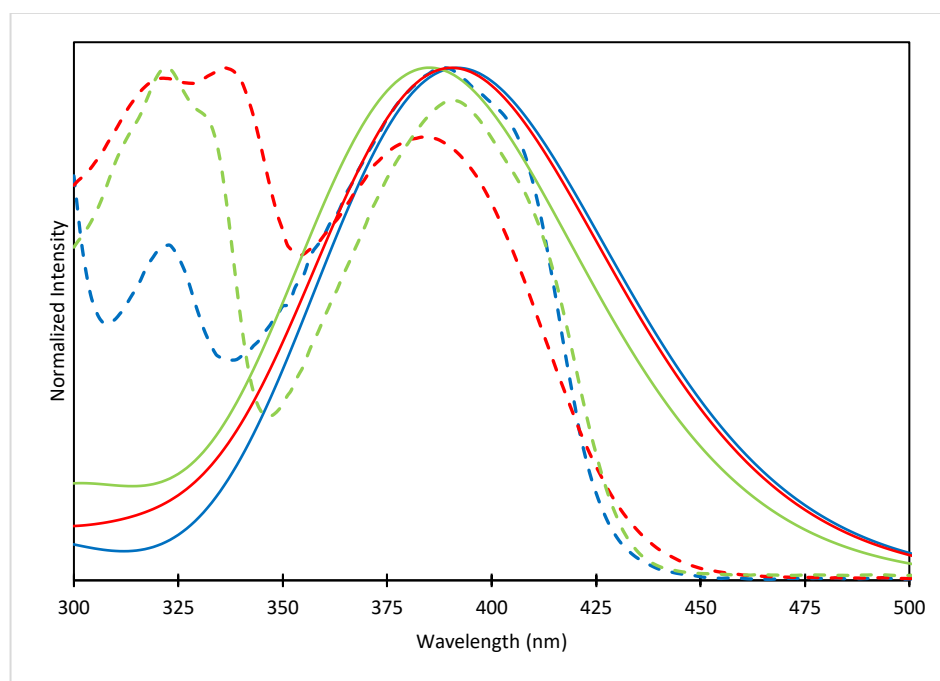


Figure 13. Absorption spectrum of molecule 1^+ (blue line), 2^+ (red line) and 3^+ (green line) calculated CAM-B3LYP (solid lines) functionals along with experimental data (dash lines).

Here dashed lines correspond to the experimental spectra after the addition and mixing of an excess of an aqueous solution of trifluoroacetic acid (TFA) expected to lead to protonated species. From the experimental spectra of the three species, one can notice that 1^+ experience a small blue shift (on 0.09 eV) while 2^+ and 3^+ experience a red shift (of 0.19 and 0.11 eV, respectively) when going from the neutral to the protonated species. These shifts are not quantitatively or qualitatively reproduced by our calculations which predicted a red shift of 0.13 eV for 1^+ and a blue shift of 0.02 and 0.12 eV for 2^+ and 3^+ , respectively. Indeed, even if the absolute errors on the λ_{max} are all below 0.2 eV, the errors have opposite sign for neutral and charged species thus leading to a wrong qualitative trend. Nonetheless we have to stress that these differences are of the order of the accuracy expected for the methods applied.

As in the case of the corresponding neutral systems, the most intense transition is the first one and corresponds to an HOMO-LUMO excitation. The corresponding HOMO/LUMO orbitals of 1^+ , 2^+ and 3^+ are depicted in Figure 14.

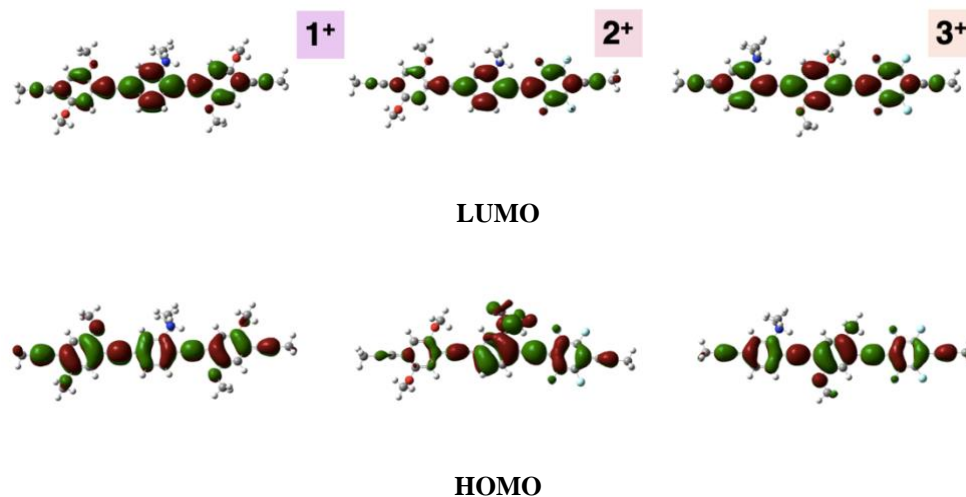


Figure 14. Molecular Orbitals (MO) of 1^+ , 2^+ , 3^+ protonated calculated at the CPCM (CH_2Cl_2)-CAM-B3LYP level (isodensity = 0.025 au).

Comparing the HOMO and LUMO of 1^+ , 2^+ , 3^+ molecules it is clear that the contribution of the donating- NMe_2 groups are reduced for 1^+ and 3^+ and that the orbitals are delocalized along the all π system of the molecules. As a consequence, the ICT is reduced wrt the neutral species except for 2^+ .

From an orbital energy point of view protonation causes a decrease of both the HOMO and LUMO energies gap (Table 6 below) leading to a reduce of the H/L gap for all protonated compounds except for 3^+ for which closer H/L gap is observed with respect 3 . Indeed, in this case the HOMO is strongly stabilized.

MO	1	2	3	1^+	2^+	3^+
LUMO	-1.38	-1.62	-1.65	-1.94	-2.24	-2.08
HOMO	-6.86	-7.01	-6.85	-7.31	-7.47	-7.56
H/L gap	5.48	5.39	5.2	5.37	5.23	5.48

Table 6. HOMO and LUMO energy orbitals for the protonated and neutral compounds (eV) absorption.

For the use of these molecule as pH probes it is necessary to have a sizable shift in optical properties going from neutral to protonated compounds which is not the case in absorption (the maximal shift being experimentally and theoretically predicted below 25 nm).

This situation is not the same when considering emission. Indeed, if shifts between neutral and protonated species are small (below 15 nm) for **1** and **2**, **3** presents a large blue shift with λ_{max} equal to 492 nm for the neutral calculated specie, and λ_{max} equal to 451 nm for the protonated calculated specie (0.23 eV energy difference), making it a potential candidate for application, as graphically depicted in Figure 15.

Indeed, the emission of compound **3** showed a greater shift, if compared with **1** and **2** with respect them corresponding neutral compounds. These results demonstrate that the protonation of the dimethylamino group, which causes substantial changes in its electron-donating properties, together with its relative position with respect to the electron-accepting fluorinated moiety, highly influence the spectroscopic features of our OPE systems (the emission energy increases up to 0.47 in **3**, with respect to **1** which shows a shift of 0.09).

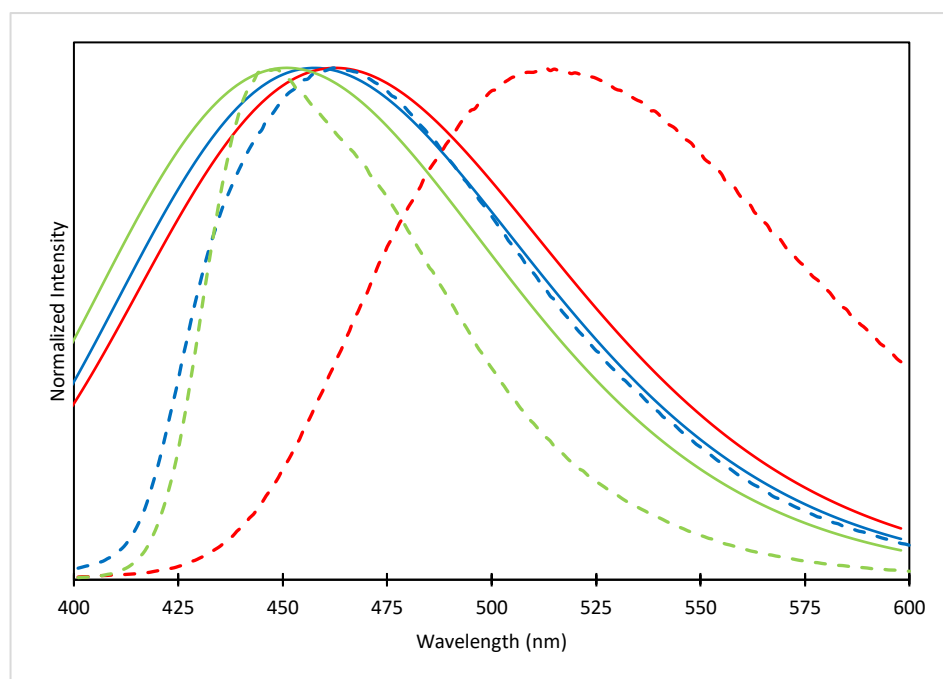


Figure 15. Emission spectra of molecule **1**⁺(blue line), **2**⁺(red line) and **3**⁺ (green line) calculated CAM-B3LYP (solid lines) functional along with experimental data (dash lines).

This trend is particularly clear comparing the emission spectra (exp. and calculated) of one neutral and protonated for each reported in figure 16 and 17.

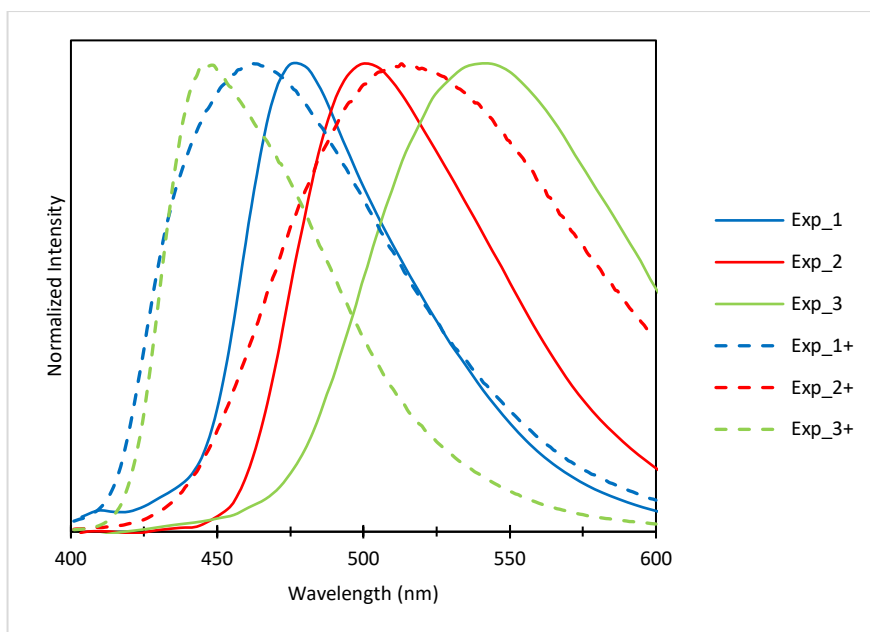


Figure 16. Emission spectra of molecule 1, 2, 3 and 1⁺, 2⁺, 3⁺ from experimental data.

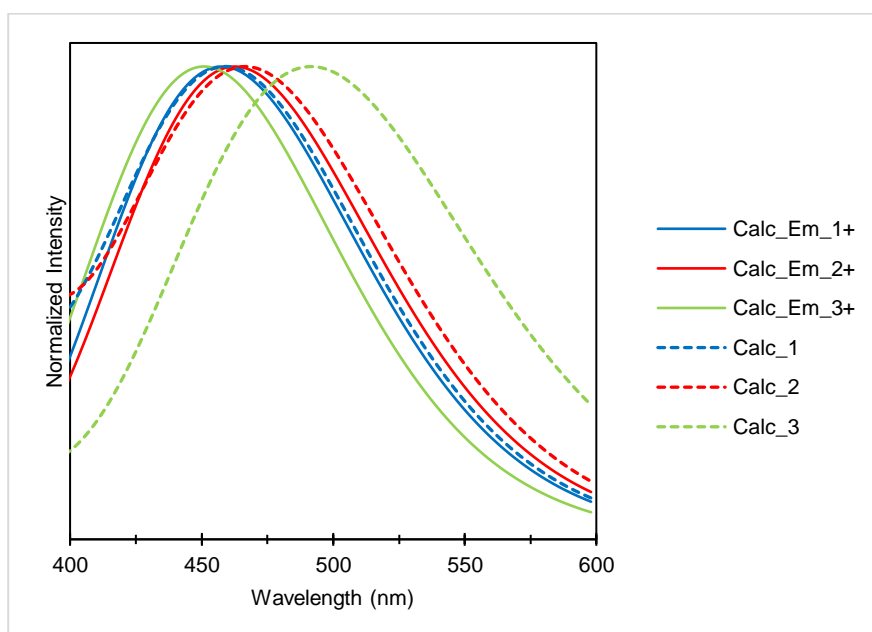


Figure 17. Emission spectra of molecule 1, 2, 3 and 1⁺, 2⁺, 3⁺ calculated with CAM-B3LYP functional.

By analyzing the structural features, one can notice that the ES of 3⁺ shows the greatest deformation when compared to the corresponding GS structure. This deformation consists in a consequent loss of planarity (Ce-Cf-Cg- Ch= 174° and 39° for GS and ES respectively). It induces an increase of the H-L gap and causes the observed blue shift.

4.4 Conclusions and Perspectives

With a combined DFT and TD-DFT study of ground and excited state structural and electronic features of three selected OPE we were able to disclose the effect of substituents on both the absorption and emission properties of these molecular systems and, combined with the study with their mono-protonated forms, to give more understanding of their possible use as pH probes.

Indeed, from a technical point of view by comparison of the computed data with the experimental one, we were able to show that the simple computational protocol used is able to reproduce at least qualitatively the absorption and emission spectra and, though errors in the standard range for hybrids are not surprisingly found, also to correctly predict the observed shifts upon protonation.

Our calculations also allowed to show the important role played by the dimethylamino group as donor in the neutral systems and the consequence that its protonation induces since it causes substantial changes in its electron-donating properties in the positively charged species. Furthermore, the relative position of the dimethylamino donor with respect to the electron-accepting fluorinated moiety, is proven to influence the spectroscopic features of the investigated OPE systems tuning their ICT character.

As possible perspective could be to analyze the full system including deprotected the terminal sugars in order to identify their influence –if any- on the optical properties. Analogously theoretical calculations may help to design new compounds where the relative positions of the –NMe₂ and -OMe groups with respect to the fluorine moieties is optimized on target optical properties (such as absorption, emission, Stokes shift, neutral to protonated change in optical properties).

References

- 1) Olschki, L.S. *Journal of the history of medical and natural sciences*, **1941**, Volume 32, p.107.
- 2) Duke-Elder, S. *Brit. J. Ophthalmol.*, **1928**, *12*, 353–373.
- 3) Raab, O. *Z. Biol.*, **1900**, *39*, 524.
- 4) Tappeiner, H. V. *Dtsch. Arch. Klin. Med.*, **1904**, *80*, 427-487.
- 5) Lipson, R.L. *Master Thesis, University of Minnesota*, **1960**, Minneapolis.
- 6) Lipson, R. L.; Baldes, E. J. *Arch. Dermat.*, **1960**, *82*, 508-516.
- 7) Diamond, I.; Granelli, S. G.; Mcdonagh, A. F.; Nielsen, S. L.; Wilson, C. B.; Jaenicke, R. *Lancet*, **1972**, *2*,1175.
- 8) Dougherty, T.J.; Kaufman, J.E.; Goldfarb, A.; Weishaupt, K.R.; Boyle, D.; Mittleman, A. *Cancer Res.*, **1978**, *38*, 2628–35.
- 9) Lakowicz, J.R. *Principles of fluorescence spectroscopy 2^a ed.*, Springer, **1999**.
- 10) Clark, W.D.K.; Steel, C. *J. Am. Chem. Soc.*, **1971**, *93*, 6347–6355.
- 11) Niedre, M; Patterson, M.; Wilson, B. *Photochem. Photobiol.*, **2002**, *75*, 382-391.
- 12) Drews, W.; Schmidt, R.; Brauer, H.D. *Chem. Phys. Let.*, **1983**, *100*, 466-469.
- 13) Fodor, L.; Elman, M.; Ullmann, Y. *Aesthetic Applications of intense Pulsed Light.*, **2011**, XI, 133 p. 228. ISBN: 978-1-84996-455-5.
- 14) Everett, M.A.; Yeagers, E.; Sayre, R.M. et al. *Photochem. Photobiol.*, **1966**, *5*, 533–542.
- 15) Svaasand, L. O. *Doiron and Gomer editors*, **1984**, New York, 91-114.
- 16) Wilson, B. C.; Jeeves, W. P.; Lowe, D. M.; Adam G. *Prog. Clin. Biol. Res.*, **1984**, *170*, 115-32.

- 17) Bolin, F. P.; Preuss, L. E.; Cain, B. W. *Prog. Clin. Biol. Res.*, **1984**, 170, 211-25.
- 18) Herd, R.M.; Dover, J.S.; Arndt, K.A. *Dermatol. Clin.*, **1997**, 15, 355–372.
- 19) Dougherty, T. J.; Potter, W. R. *Journal of Photochemistry and Photobiology B: Biology.*, **1991**, 8, 233-234.
- 20) Serra, V.V.; Zamarron, A.; Faustino, M.A.F.; Cruz, M.C.I. et al. *Med. Chem.*, **2010**, 8, 6170-6178.
- 21) Agostinis, P. K. Berg, K.A. Cengel, T.H. Foster, A.W. Girotti, et al.; *Cancer. J. Clin.*, **2011**, 61 250-281.
- 22) Yoo, J.O.; Ha, K.S. *Int. Rev. Cell. Mol. Biol.*, **2012**, 295 139-174.
- 23) Wan, M.T.; Lin, J.Y. *Clin. Cosmet. Investig. Dermatol.*, **2014**, 7 145-163.
- 24) Arambula, J.F. et al. *Anticancer Agents Med Chem.*, **2011**, 11(2): 222–232.
- 25) Barattucci, A. et al. *J. Org. Chem.*, **2014**, 79 5113–5120.
- 26) Deni et al. *Eur. J. Med. Chem.*, **2016**, 111-5871.
- 27) A. Mancuso et al. *Chem. Eur. J.*, **2018**, 24 16972 – 16976.
- 28) Heiden, M.; Vander, G.; Cantley, L. C.; Thompson, C. B. *Science*, **2009**, 324 (5930): 1029–1033.
- 29) Frisch, M. J.; Trucks, G. W.; Schlegel, H. B.; Scuseria, G. E.; Robb, M. A.; Cheeseman, J. R.; Scalmani, G.; Barone, V.; Petersson, G. A.; Nakatsuji, H.; Li, X.; Caricato, M.; Marenich, A. V.; Bloino, J.; Janesko, B. G.; Gomperts, R.; Mennucci, B.; Hratchian, H. P.; Ortiz, J. V.; Izmaylov, A. F.; Sonnenberg, J. L.; Williams-Young, D.; Ding, F.; Lipparini, F.; Egidi, F.; Goings, J.; Peng, B.; Petrone, A.; Henderson, T.; Ranasinghe, D.; Zakrzewski, V. G.; Gao, J.; Rega, N.; Zheng, G.; Liang, W.; Hada, M.; Ehara, M.; Toyota, K.; Fukuda, R.; Hasegawa, J.; Ishida, M.; Nakajima, T.; Honda, Y.; Kitao, O.; Nakai, H.; Vreven, T.; Throssell, K.; Montgomery, J. A., Jr.; Peralta, J. E.; Ogliaro, F.; Bearpark, M. J.; Heyd, J. J.; Brothers, E. N.; Kudin, K. N.; Staroverov, V. N.; Keith, T. A.; Kobayashi, R.; Normand, J.; Raghavachari, K.;

Rendell, A. P.; Burant, J. C.; Iyengar, S. S.; Tomasi, J.; Cossi, M.; Millam, J. M.; Klene, M.; Adamo, C.; Cammi, R.; Ochterski, J. W.; Martin, R. L.; Morokuma, K.; Farkas, O.; Foresman, J. B.; Fox, D. J. *Gaussian Development Version, Revision J.1, Gaussian, Inc.*, **2018**, Wallingford CT.

30) Cossi, M; Rega, N et al. *J. Comput. Chem.*, **2003**, 24(6): 669-681.

31) Yanai, T.; Tew, D. P.; Handy, N. C. *Chem. Phys. Lett.*, **2004**, 393, 51-57.

32) Campetella, M. et al.; *Chem. Phys. Lett.*, **2019**, Vol. 714, 16, 81-86.

33) Dapprich, S.; Komaromi, I.; Byun, K.S.; Morokuma, K.; Frisch, M.J. *J. Mol. Struct. THEOCHEM.*, **1999**, 461-462.

34) Svensson, M.; Humbel, S.; Froese, R.D. J.; Matsubara, T.; Sieber, S.; Morokuma, K. *J. Phys. Chem.*, **1996**, 100 (50): 19357.

35) Kasha, M. *Discussions of the Faraday Society*, **1950**, 9: p.14-19.

General conclusions and perspectives

5.1 Outline

The objective of this thesis was to develop computational approaches that allow the design of new single molecule architectures with particular emphasis on exploiting the reversible and light-induced conformational changes in the excited state. To predict qualitatively and, if possible, quantitatively, this type of phenomena it is necessary to describe the potential energy surface (PES) of the excited state or states involved within the Franck-Condon region (i.e. vertical with respect to the ground state) but also away from it. To do this, two fundamental points were considered:

- the use of theoretical methods that allow to describe the energetics of the excited states on all the PES regions with the same accuracy and independently on the chemical nature of the excited states involved (eg. Charge transfer -CT- with respect to Locally Excited - LE-);
- alongside DFT and TD-DFT tools that have made it possible to efficiently sample ES-PES and identify their most relevant regions (i.e. region associated with radiative or non-radiative decay, interconversion between ES ...).

Regarding the first point, the accurate description of the excited state of chemically relevant (i.e. medium-large sized) molecular systems is inherently a difficult problem for quantum approaches. In fact, if nowadays it is possible to find in the literature many works that deal with the definition of accurate and computationally efficient methods for the description of vertical excited states that lead to simulation, the smaller the number of works that deal with the evaluation of the precision of properties structural and energetic of the emitting species in molecular compounds. Furthermore, even less is the amount of work devoted to evaluating their accuracy for the description of the Potential Energy Surfaces (ES-PES) of the excited state outside the Franck Condon region. Indeed, if some relevant works can be found for the description of the shape profiles of the absorption and emission bands, allowing for example the prediction and simulation of the color of molecular systems, in reality these are still dominated by the excited and ground state PES close to their respective minima.

In the last decades, approaches rooted on Time Dependent-Density Functional Theory (TD-DFT) have indeed shown their ability in providing a balanced description of both model and chemically relevant systems, also due to the possible and computationally inexpensive integration of environmental effects (such as solvation or adsorption, encapsulation–) in the case of vertical transition energies. Extensive benchmarks with respect to both experimental and wavefunction (WF) based theoretical calculations enabled also to highlight the deficiencies of TD-DFT rooted methods, mostly related, if one limit to one-electron excitations, to the quality of the underlying DFT exchange correlation functional used. In particular, the erratic description of electronic transitions possessing a relevant through space charge transfer character has been highlighted as one of the most relevant flaws for the description and prediction even of absorption spectra of chemically relevant compounds.

In this general context, the first objective of this thesis, discussed in chapter II, was to carefully define, via extensive benchmark, if latest generation DFT approaches can be successfully integrated in a TD-DFT scheme to improve the current state of the art description of ES in molecular systems. We focused on analyzing the performance of the Double Hybrid Functionals (DHF) for the space description through charge transfer (CT) excitations which are well known to be very problematic to describe with commonly used functionals, such as global hybrids. For this study, two different families of exchange correlation functionals were compared, each containing pure functional, hybrid (global and range-separated) and double hybrid functionals. The results show that excellent performances can be obtained for the description of CT excitations using DH. In particular, these functionals provide results with an accuracy comparable to that of functionals “tuned” range separated functionals, with the relevant difference that for DH no parameter is tuned to a specific class of compounds to reproduce its excited state properties, thus making them more efficient for general use. Furthermore, the described and implemented algorithm is characterized by the same computational cost scaling of the ground state algorithm employed for MP2 and double hybrid DFA. The results show how a double hybrid DFA can be an effective tool for predicting energies of excited states of relatively large molecular compounds.

Nonetheless, DHs are still more expensive than global hybrids and currently less widespread than both global and range-separated hybrid functionals. In Chapter III we thus focus on a graphical and condensed analysis (that we called Global Transition Contribution Grid – G_TCG- analysis) to see if relevant difference both on the nature and on the energetic of the excited states between functional predictions can be easily graphically spotted.

This work, that is currently still undergoing to validate the findings presented for the triphenylene molecule on a larger set of molecular species but it highlights promising aspects together with some limitations of the G_TCG analysis. The most relevant promising aspect is related to the fact that these grids allows to spot the difference between functionals very easily. Nonetheless, the detailed analysis of the differences and their link to the –different- physical nature of the states predicted requires both knowledge and analysis of the involved molecular orbitals pairs, which maybe tedious if the system is complex, and the combined analysis of several grids.

As possible perspectives, beside a more solid validation of these findings, the use of Natural Transition Orbitals and the restriction of a relevant subset of orbital pairs will be firstly tested as ways to provide an efficient tool of global analysis. A quantitative link to other descriptors beside the D_{CT} index is also envisaged.

Finally, in chapter IV as an example of application of TD-DFT to real systems, in collaboration with an experimental group of the University of Messina the optical properties of several Amino-OPE derivatives, photosensitizer candidates for photodynamic therapy (PDT), were investigated. In particular, different chemical functionalization (a common OPE skeleton that is substituted with electron or donor groups) has allowed us to investigate their different response in terms of absorption and emission properties. To do this, density functional theory (DFT) and time-dependent DFT (TD-DFT) were applied to the study of their optical properties, and their peculiar behavior during protonation of the electron donor group was also analyzed. The results showed that the effect of substituents on molecular systems, combined with their protonation, can give an idea of their role as pH-sensitive probes. They also demonstrated good agreement with the trend of the experimental data. Starting from this, a further study could be to deprotect terminal sugars in order to identify their effective role on the optical properties, with the aim of investigating possible applications as a pH sensor. Therefore, the deacetylation of the glucose terminations will be fundamental to study the photophysical properties in aqueous solution. Theoretical calculations will thus help to understand the importance of the relative positions of the -NMe₂ and -OMe groups, with respect to the fluorinated aromatic unit, and support the experimental section.

5.2 Perspectives

More generally, future perspective allowing to show the potential use of the approaches developed in chapter II and III would be to apply them to the study of complex excited states and particularly to the analysis of systems showing non-radiative mechanisms of deactivation of the excited state, which indeed provide a high degree of intrinsic photo-instability. This behaviour is particularly relevant in the case of DNA basis. In recent years, experimental and computational studies have led to the understanding of non-radiative decay mechanisms of isolated DNA bases (adenine, cytosine, guanine, thymine, uracil). For the first three bases, mild absorption spectra were observed for the excited states index of long-lived vibronic states. Subsequently, experimental measurements conducted in solution and in gas phase, confirmed the very short life time of the excitations present in the DNA bases. Computational studies conducted on DNA showed low energy barriers that suggest the presence of conical intersections at low energies. Near conical intersections, the Born-Oppenheimer approach breaks and the coupling between electronic and nuclear motion becomes important, according to the implementation of non-adiabatic processes.

Later, it was understood that the conical intersections linked to specific out-of-plane deformations of the heteroaromatic rings with 6 atoms dominate the radiative deactivation of the lower excited states for adenine, uracil and cytosine. For adenine, it has been shown that conical intersections become accessible to higher excitation energies (about 5eV). Synergistically, these radiation-free decay processes through conical intersections seem to provide the DNA bases with a high degree of photostability over a wide range of UV wavelengths. Regarding thymine, few computational studies have been performed so far. Different teams over the years have obtained vertical excitation energies using both wavefunction methods (CASPT2 and CIS) and time-dependent DFT (TD-DFT). The CIS method was used to determine the minimum energy structure associated to the two lowest energy excited states (i.e. the $1n\pi^*$ and the $1\pi\pi^*$) predicting a non-planar geometries of the aforementioned states, whereas the CASSCF and TD-DFT methods allowed to explore more accurately the potential energy surfaces (PES) of the excited states of Thymine and Uracil. A conical intersection was localized at a CASSCF level of theory between states S_1 and S_0 with an energy barrier of about 0.2 eV. From studies conducted by Perun and collaborators¹, three S_1 - S_0 conical intersections have been identified (that is, three local minima of the hypersurface of the S_1 - S_0 intersection).

The lowest energy intersection, CI1, derives from a crossing of the lowest energy state $1\pi\pi^*$ with the state S_0 . In this general context in order to localize the decay channels readily available for excited states, we made use of the density based index Π^2 :

$$\Pi = \frac{1}{\Delta E \cdot q_{CT} \cdot D_{CT}} \quad 5.1$$

This index (eq. 5.1) formulates the fact that the probability of interconversion between two states will not only depend on an energy law (ΔE which indeed will be explicitly taken into account in the quantitative formulation of the associated new indexes) but also on the *similarity between the density distribution associated to the states that should interconvert*. Typically, in the case of decay from a given excited state, the state (among other states close in energy), possessing most similar pattern of density distribution as that of the latter state of interest, at a given nuclear configuration, will be the most likely to be populated. This index was applied to reveal the non-radiative decay channels from the first excited state to the ground state and its value is not only easy to calculate, but has no additional computational costs if used as a support to quantum methods describing the density of electronic states. Thanks to this descriptor it was possible to identify the 3 conical intersection regions characterized by a very high Π index value.

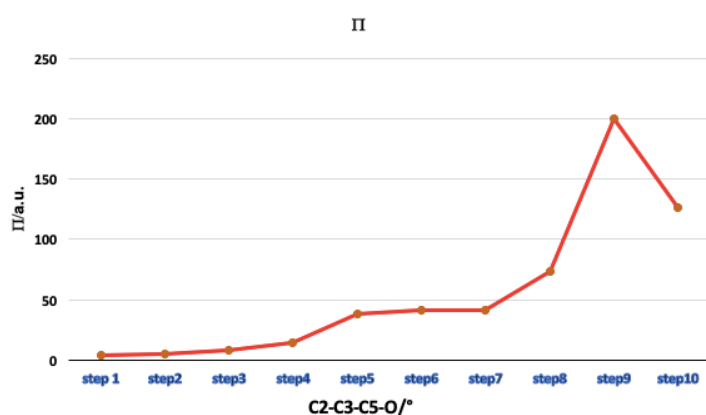


Figure 1. Evolution of the Π index) along the reaction coordinate and dihedral angle representation considered in thymine.

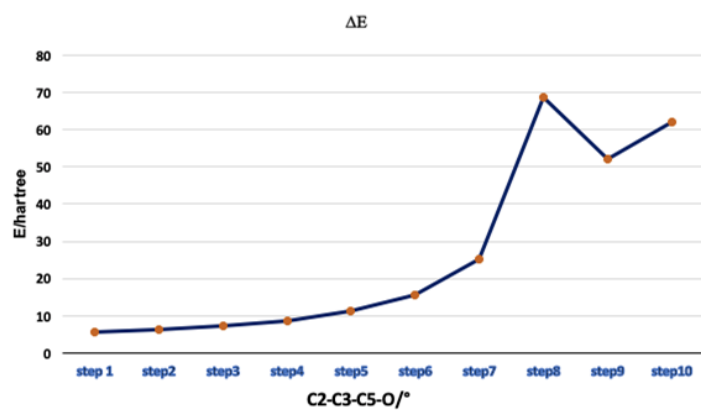


Figure 2. Evolution of the ΔE (Eh) along the reaction coordinate and dihedral angle representation considered in thymine.

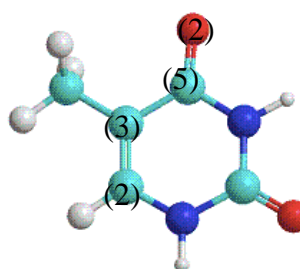
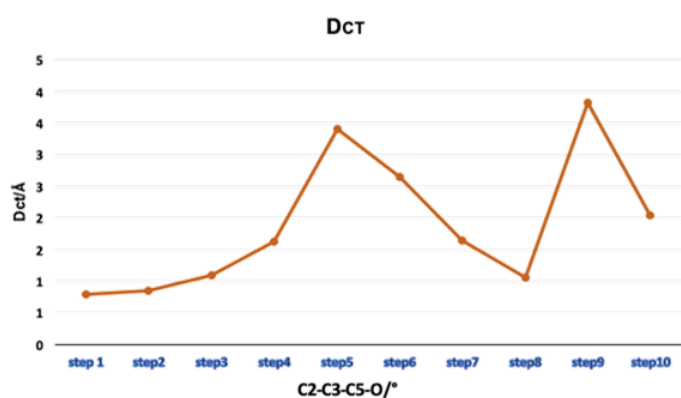


Figure 3. Evolution of the Π index along the reaction coordinate and dihedral angle representation considered in thymine.

For instance, the first conical intersection takes place at step 8 and 9, as clearly highlighted by the change in nature of the two states involved (monitored by the DCT) the energy and Π index evolution as graphically represented in Figure 1, 2 and 3.

The presence of the conical intersection indicates a cross between the electronic states of the considered system.

To verify this cross, the relative molecular orbitals (HOMO \rightarrow LUMO transition) of the steps 8 and 9 involved in the conical intersection are illustrated in Figure 4.

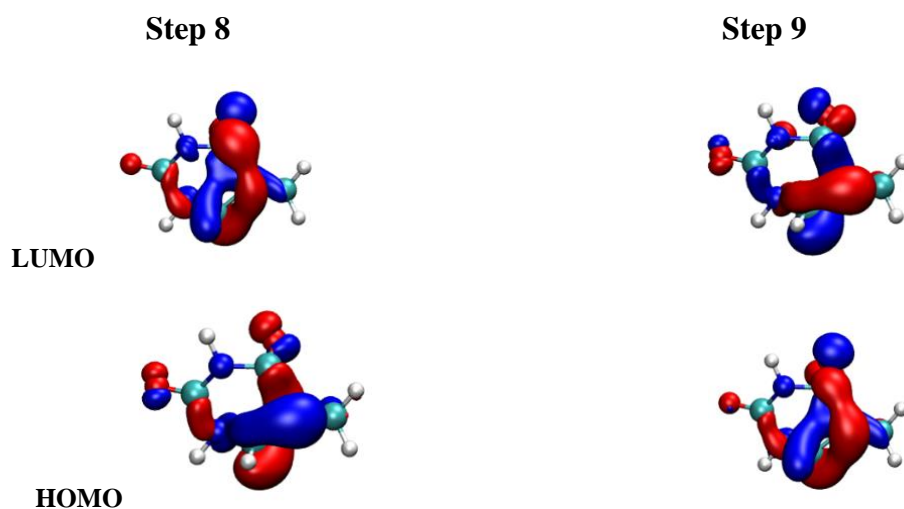


Figure 4. Molecular orbitals, HOMO \rightarrow LUMO transitions, involved in the conical intersection.

The shape of the LUMO orbital in step 8 corresponds to that of HOMO in step 9, confirming the expected conical intersection.

In addition, the structures corresponding to steps 08 and 09 show a clear variation in the angle of carbon-oxygen bond C = O and in that with the methyl group C-CH₃ (Figure 5).

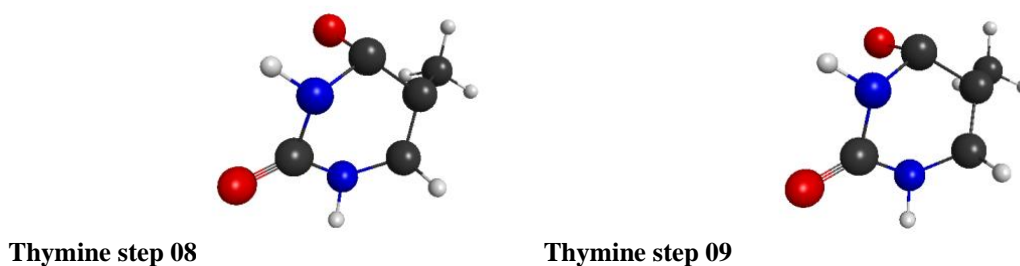


Figure 5. Evolution of Thymine structures in the steps 08 and 09 with variation in the angle of carbon-oxygen bond C = O and in the angle with the methyl group C-CH₃.

Starting from these preliminary studies, it would be appropriate to further investigate the conical intersection of the thymine, adding to the density-based indexes, different exchange and correlation functionals in order to highlight which of these is more performing for this system (or for similar systems), and comparing them with the levels of theory already known in the literature.

References

- 1) Perun, S; Sobolewski, A. L.; *J. Phys. Chem. A*, **2006**, 110, 13238-13244.
- 2) Maschietto, F.; Sanz García, J.; Campetella, M.; Ciofini, I.; *J. Comput. Chem.* **2019**, 40, 650–656.

APPENDICES

Appendix A

Appendix A-1

Table 1. Excitation energies (in eV) computed for molecules belonging to the Thiel set.

^a SA-CASSCF/MS-CASPT2 results using MP2/6-31G* ground-state equilibrium geometries and TZVP basis set. Taken from reference Schreiber, M.; Silva-Junior, M. R.; Sauer, S. P. A. and Thiel, W. *J. Chem. Phys.* **2008**,128, 134110.

(S-trans)-1,3-Butadiene		
	2¹A_g	1¹B_u
BLYP	6.24	5.58
B3LYP	6.82	5.74
CAM- B3LYP	7.44	5.91
B2PLYP	7.14	6.35
PBE	8.08	5.63
PBE0	7.03	5.83
LC-PBE	8.15	6.16
PBE-QIH	8.17	6.46
PBE-QIDH	7.88	6.47
PBE0-DH	7.44	6.41
CASPT2^a	6.62	6.47

e-hexatriene		
	2¹ A_g	1¹ B_u
BLYP	5.03	4.51
B3LYP	5.69	4.69
CAM-B3LYP	6.55	4.9
B2PLYP	6.02	5.24
PBE	5.07	4.54
PBE0	5.90	4.77
LC-PBE	7.31	5.19
PBE-QIH	7.33	5.42
PBE-QIDH	6.57	5.38
PBE0-DH	6.36	5.31
CASPT2^a	5.42	5.31

Ethene	
	1 B_{1u}
BLYP	7.68
B3LYP	7.70
CAM-B3LYP	7.72
B2PLYP	8.18
PBE	7.77
PBE0	7.79
LC-PBE	7.84
PBE-QIH	8.2
PBE-QIDH	8.38
PBE0-DH	8.37
CASPT2^a	8.54

Cyclopropene		
	1¹ B₂	1¹ B₁
BLYP	6.10	6.25
B3LYP	6.31	6.46
CAM-B3LYP	6.42	6.54
B2PLYP	6.89	6.68
PBE	6.12	6.29
PBE0	6.40	6.55
LC-PBE	6.62	6.72
PBE-QIH	6.94	7.03
PBE-QIDH	7.04	6.88
PBE0-DH	6.90	6.77
CASPT2^a	7.06	6.76

Cyclopentadiene			
	2¹A₁	3¹A₁	1¹B₂
BLYP	6.04	7.75	4.88
B3LYP	6.52	8.15	5.02
CAM-B3LYP	6.97	8.47	5.16
B2PLYP	6.70	8.83	5.53
PBE	6.21	7.82	4.95
PBE0	6.69	8.24	5.11
LC-PBE	7.62	8.43	5.42
PBE-QIH	7.74	8.96	5.58
PBE-QIDH	7.11	8.95	5.65
PBE0-DH	7.00	8.90	5.58
CASPT2^a	7.06	6.76	5.51

Norbornadiene				
	1¹A₂	2¹A₂	1¹B₂	2¹B₂
BLYP	4.45	6.55	4.99	6.00
B3LYP	4.79	6.87	5.52	6.88
CAM-B3LYP	5.12	7.15	6.02	7.24
B2PLYP	5.29	7.47	5.95	7.31
PBE	4.48	6.6	5.02	6.2
PBE0	4.91	7.00	5.66	7.02
LC-PBE	5.53	7.92	6.58	7.65
PBE-QIH	5.56	7.73	6.72	7.85
PBE-QIDH	5.52	7.5	6.33	7.59
PBE0-DH	5.35	7.6	6.12	7.55
CASPT2^a	5.34	7.45	6.11	7.32

e-Octatetraene		
	2¹A_g	1¹B_u
BLYP	4.16	3.81
B3LYP	4.84	4.02
CAM-B3LYP	5.78	4.26
B2PLYP	5.19	4.53
PBE	4.19	3.83
PBE0	5.04	4.09
LC-PBE	6.49	4.57
PBE-QIH	6.51	4.74
PBE-QIDH	5.75	4.68
PBE0-DH	5.51	4.60
CASPT2^a	4.64	4.7

Benzene				
	1¹B_{1u}	1¹B_{2u}	1¹E_{1u}	1¹E_{2g}
BLYP	5.95	5.21	6.93	8.22
B3LYP	6.10	5.40	7.07	8.91
CAM-B3LYP	6.21	5.49	7.17	9.52
B2PLYP	6.49	5.34	7.58	9.08
PBE	6.04	5.26	7.58	8.29
PBE0	6.20	5.43	7.16	9.14
LC-PBE	6.37	5.64	7.37	9.50
PBE-QIH	6.41	5.90	8.00	8.84
PBE-QIDH	6.59	5.51	7.72	8.48
PBE0-DH	6.51	5.56	7.76	9.49
CASPT2^a	6.42	5.04	7.13	8.18

Naphtalene				
	2¹A_g	3¹A_g	1¹B_{2u}	2¹B_{2u}
BLYP	5.80	6.16	4.05	5.84
B3LYP	6.18	6.85	4.35	6.12
CAM-B3LYP	6.37	6.47	4.65	6.10
B2PLYP	6.18	7.17	4.78	6.46
PBE	5.86	5.97	4.08	5.88
PBE0	6.01	6.32	4.45	6.23
LC-PBE	6.60	6.85	4.37	6.66
PBE-QIH	6.99	8.41	5.03	7.01
PBE-QIDH	6.45	7.71	4.99	6.67
PBE0-DH	6.47	7.54	4.63	6.67
CASPT2^a	5.87	6.67	4.77	6.33

Furan			
	2¹A₁	3¹A₁	1¹B₂
BLYP	6.32	8.10	6.05
B3LYP	6.70	8.25	6.16
CAM-B3LYP	7.01	8.34	6.23
B2PLYP	6.76	8.85	6.66
PBE	6.40	8.20	6.14
PBE0	6.86	8.36	6.25
LC-PBE	7.51	8.56	6.42
PBE-QIH	7.67	9.13	6.65
PBE-QIDH	7.08	9.00	6.76
PBE0-DH	7.08	9.00	6.70
CASPT2^a	6.50	8.17	6.39

Pyrrole			
	2¹A₁	3¹A₁	1¹B₂
BLYP	6.21	7.80	6.29
B3LYP	6.53	7.96	6.40
CAM-B3LYP	6.78	8.06	6.47
B2PLYP	6.58	8.50	5.89
PBE	6.28	7.88	6.37
PBE0	6.68	8.07	6.50
LC-PBE	7.18	8.29	6.64
PBE-QIH	7.33	8.83	6.65
PBE-QIDH	6.85	8.66	6.42
PBE0-DH	6.86	8.66	6.28
CASPT2^a	6.31	8.17	6.33

Imidazole					
	2¹A'	3¹A'	4¹A'	1¹A''	2¹A''
BLYP	6.26	6.80	8.04	5.86	7.12
B3LYP	6.45	7.04	8.27	6.46	7.45
CAM-B3LYP	6.59	7.22	8.47	6.75	7.74
B2PLYP	6.28	7.16	7.63	6.76	7.98
PBE	6.38	6.88	8.12	5.89	7.06
PBE0	6.57	7.17	8.41	6.62	7.60
LC-PBE	6.84	7.55	8.63	7.06	8.20
PBE-QIH	7.06	7.73	8.81	7.08	7.51
PBE-QIDH	6.83	7.37	8.07	7.02	7.13
PBE0-DH	6.94	7.40	8.13	6.97	7.93
CASPT2^a	6.19	6.93	8.16	6.81	7.90

Pyridine						
	2¹A1	3¹A1	1¹B2	2¹B2	1¹B1	1¹A2
BLYP	6.15	7.22	5.31	7.06	4.38	4.48
B3LYP	6.31	7.32	5.49	7.30	4.80	5.11
CAM-B3LYP	6.43	7.46	5.57	7.42	5.06	5.48
B2PLYP	6.71	7.86	5.00	7.72	5.22	5.44
PBE	6.23	7.28	5.36	7.14	4.36	4.45
PBE0	6.41	7.44	5.58	7.40	4.87	5.23
LC-PBE	6.61	7.67	5.69	7.65	5.29	5.83
PBE-QIH	6.66	8.30	5.66	8.25	6.00	6.57
PBE-QIDH	6.82	8.01	5.26	7.89	5.60	5.65
PBE0-DH	6.74	8.05	5.67	7.94	5.15	5.57
CASPT2^a	6.39	7.46	5.02	7.27	5.17	5.51

Pyrazine								
	1¹B_{1u}	2¹B_{1u}	1¹B_{2u}	2¹B_{2u}	1¹A_u	1¹B_{1g}	1¹B_{2g}	1¹B_{3u}
BLYP	6.36	7.44	5.22	7.61	4.08	5.54	5.08	3.60
B3LYP	6.50	7.68	5.37	7.78	4.69	6.38	5.55	3.96
CAM-B3LYP	6.60	7.82	5.40	7.94	5.04	6.88	5.81	4.19
B2PLYP	6.94	7.95	5.35	7.94	4.80	6.41	5.81	4.17
PBE	6.44	7.52	5.26	7.69	4.03	5.54	5.09	3.56
PBE0	6.60	7.79	5.43	7.91	4.79	6.58	5.66	4.00
LC-PBE	6.77	8.00	5.47	8.22	5.37	7.46	6.05	4.35
PBE-QIH	6.84	8.65	6.11	8.64	5.86	8.46	6.37	4.72
PBE-QIDH	7.05	8.26	5.20	8.27	5.48	7.01	6.09	4.38
PBE0-DH	7.00	8.39	5.13	8.41	5.58	6.96	5.96	4.27
CASPT2^a	6.89	7.79	4.85	7.66	4.70	6.41	5.68	4.12

Pyrimidine						
	2^1A_1	3^1A_1	1^1B_2	2^1B_2	1^1B_1	1^1A_2
BLYP	6.40	7.26	5.55	7.52	3.81	4.03
B3LYP	6.58	7.48	5.74	7.76	4.27	4.60
CAM-B3LYP	6.71	7.61	5.82	7.82	4.55	4.92
B2PLYP	6.98	7.89	5.66	8.12	4.41	4.74
PBE	6.48	7.33	5.59	7.59	3.77	3.99
PBE0	6.68	7.59	5.83	7.80	4.34	4.70
LC-PBE	6.92	7.85	5.94	8.06	4.80	5.23
PBE-QIH	7.00	8.43	6.29	8.69	5.27	5.86
PBE-QIDH	7.10	8.06	5.83	8.31	4.70	5.12
PBE0-DH	7.03	8.12	5.91	8.37	4.62	5.02
CASPT2^a	6.63	7.21	5.24	7.64	4.44	4.12

Pyridazine								
	2^1A_1	3^1A_1	1^1B_{2u}	2^1B_{2u}	1^1A_2	2^1A_2	1^1B_1	2^1B_1
BLYP	5.41	6.64	6.26	7.28	3.54	5.00	3.15	5.44
B3LYP	5.61	7.50	6.43	7.24	4.18	5.44	3.58	6.09
CAM-B3LYP	5.68	7.64	6.55	7.33	4.55	5.73	3.83	6.46
B2PLYP	5.52	8.01	6.85	7.67	4.37	5.57	3.83	6.21
PBE	5.46	7.37	6.34	7.10	3.51	7.58	3.12	6.80
PBE0	5.69	7.62	6.54	7.30	4.30	5.53	3.66	6.22
LC-PBE	5.80	7.88	6.75	7.54	4.89	6.05	4.00	6.82
PBE-QIH	6.13	8.51	6.76	8.17	5.52	6.51	4.48	7.54
PBE-QIDH	5.69	8.18	6.96	7.85	4.83	5.85	4.10	6.64
PBE0-DH	5.77	8.22	6.87	7.88	4.66	5.81	3.97	6.56
CASPT2^a	5.18	7.62	6.31	7.29	4.31	5.77	3.78	6.52

S-triazine							
	2¹A'₁	1¹A'₂	1¹E'	1¹A''₁	1¹A''₂	1¹E''	2¹E''
BLYP	6.81	5.90	7.54	3.85	4.00	4.00	6.65
B3LYP	7.01	6.14	7.79	4.45	4.54	4.54	7.49
CAM-B3LYP	7.17	6.23	7.88	4.75	4.84	4.84	7.88
B2PLYP	7.38	5.97	8.18	4.69	4.67	4.67	7.84
PBE	6.90	5.95	7.62	3.81	3.96	3.96	6.68
PBE0	7.12	6.24	7.89	4.56	4.63	4.63	7.72
LC-PBE	7.43	6.38	8.15	5.04	5.12	5.12	8.22
PBE-QIH	7.49	6.76	8.78	5.61	5.73	5.73	8.78
PBE-QIDH	7.51	6.17	8.37	4.99	5.01	5.01	8.35
PBE0-DH	7.49	6.28	8.18	4.92	4.94	4.94	8.18
CASPT2^a	7.25	5.79	7.50	4.60	4.66	4.70	7.71

s-tetrazine														
	1¹A_u	2¹A_u	1¹B_{1g}	2¹B_{1g}	3¹B_{1g}	1¹B_{2g}	2¹B_{2g}	2¹B_{3g}	1¹B_{1u}	2¹B_{1u}	1¹B_{2u}	2¹B_{2u}	1¹B_{3u}	2¹B_{3u}
BLYP	2.87	4.60	4.10	5.86	6.49	4.77	5.20	8.66	6.75	7.30	5.42	8.03	1.87	5.63
B3LYP	3.51	5.04	4.73	6.64	7.40	5.29	5.99	9.30	6.90	7.48	5.58	8.26	2.24	6.29
CAM-B3LYP	3.87	5.32	5.01	7.05	8.34	5.58	6.49	9.82	7.01	7.57	5.62	8.40	2.46	6.66
B2PLYP	3.64	5.29	5.10	7.09	6.57	5.48	6.01	8.48	7.41	7.78	5.49	8.22	2.45	6.48
PBE	2.82	4.58	4.10	5.84	6.50	4.77	5.20	8.73	6.84	7.37	5.47	8.10	1.82	5.61
PBE0	3.61	5.14	4.86	6.81	7.68	5.40	6.20	9.52	7.01	7.59	5.66	8.36	2.28	6.43
LC-PBE	4.22	5.59	5.18	9.10	5.67	7.21	7.77	10.44	5.86	7.03	7.55	8.68	2.58	7.00
PBE-QIH	4.92	6.03	5.74	6.18	8.08	6.11	8.48	10.36	7.78	7.18	6.03	9.54	3.06	7.78
PBE-QIDH	4.07	5.57	5.43	5.79	6.63	5.63	7.06	7.98	6.92	7.50	5.57	8.45	2.67	6.92
PBE0-DH	3.96	5.67	5.25	5.77	6.81	6.62	8.11	8.46	7.13	8.10	5.46	8.94	2.57	7.39
CASPT2^a	3.51	5.50	4.73	6.45	6.73	5.20	6.06	8.34	6.94	7.42	4.93	8.14	2.29	6.77

Formaldehyde			
	1¹A₂	1¹B₁	2¹A₁
BLYP	3.80	7.21	8.74
B3LYP	3.87	8.89	9.18
CAM-B3LYP	3.85	8.34	9.36
B2PLYP	3.90	9.05	9.71
PBE	3.77	7.33	8.89
PBE0	3.87	8.23	9.35
LC-PBE	3.81	9.08	9.68
PBE-QIH	4.19	10.35	9.85
PBE-QIDH	4.00	9.55	9.93
PBE0-DH	3.97	9.59	9.86
CASPT2^a	3.99	9.14	9.32

Acetone			
	1¹A₂	2¹A₁	1¹B₁
BLYP	4.01	8.2	7.96
B3LYP	4.18	9.04	8.41
CAM-B3LYP	4.24	9.63	8.67
B2PLYP	4.18	9.48	8.7
PBE	4.01	8.31	7.96
PBE0	4.22	9.35	8.51
LC-PBE	4.29	9.95	8.97
PBE-QIH	4.67	11.52	9.64
PBE-QIDH	4.33	10.34	9.25
PBE0-DH	4.32	8.95	8.84
CASPT2^a	4.44	9.31	9.27

<i>p</i> -benzoquinone							
	1¹A_u	1¹B_{1g}	1¹B_{1u}	2¹B_{1u}	1¹B_{3g}	2¹B_{3g}	1¹B_{3u}
BLYP	2.05	1.94	4.47	6.78	3.35	6.08	5.3
B3LYP	2.58	2.44	4.83	7.25	3.73	6.59	5.43
CAM-B3LYP	2.99	2.81	5.18	7.65	4.1	7.07	6.2
B2PLYP	2.63	2.74	5.32	7.37	4.27	6.99	6.1
PBE	2.00	1.87	4.49	6.82	3.37	6.12	4.36
PBE0	2.65	2.48	4.93	7.4	3.84	6.77	5.62
LC-PBE	3.28	3.06	6.00	8.55	5.67	8.18	7.81
PBE-QIH	3.56	3.38	5.96	8.34	4.72	8.37	7.47
PBE-QIDH	3.05	2.9	5.58	7.74	4.57	6.95	6.38
PBE0-DH	3.03	2.9	5.65	7.73	4.55	6.95	6.12
CASPT2^a	2.77	2.76	5.28	7.92	4.26	6.96	5.15

Formamide			
	1¹A''	2¹A'	3¹A'
BLYP	5.44	7.81	9.94
B3LYP	5.55	8.13	10.92
CAM-B3LYP	5.57	8.44	11.17
B2PLYP	5.54	7.28	10.3
PBE	5.45	7.88	10.11
PBE0	5.59	8.22	10.03
LC-PBE	5.58	9.39	10.25
PBE-QIH	6.03	8.45	11.18
PBE-QIDH	5.69	7.78	10.75
PBE0-DH	5.68	7.68	10.25
CASPT2^a	5.63	7.39	10.54

Acetamide			
	1¹A''	2¹A'	3¹A'
BLYP	5.41	6.83	9.39
B3LYP	5.62	7.56	10.23
CAM-B3LYP	5.69	7.88	10.66
B2PLYP	5.61	7.03	10.03
PBE	5.42	6.96	9.41
PBE0	5.68	7.76	9.92
LC-PBE	5.75	8.19	11.22
PBE-QIH	6.24	8.09	10.64
PBE-QIDH	5.80	7.58	10.28
PBE0-DH	5.80	7.52	10.18
CASPT2^a	5.69	7.27	10.09

Propanamide			
	1¹A''	2¹A'	3¹A'
BLYP	5.40	7.24	8.18
B3LYP	5.59	7.76	9.00
CAM-B3LYP	5.67	7.73	8.48
B2PLYP	5.58	7.41	9.56
PBE	5.42	7.33	8.25
PBE0	5.65	8.04	9.15
LC-PBE	5.73	8.73	9.68
PBE-QIH	6.18	8.53	10.31
PBE-QIDH	5.77	7.75	9.94
PBE0-DH	5.76	7.90	9.96
CASPT2^a	5.72	7.2	9.94

Cytosine				
	2 ¹ A'	3 ¹ A'	1 ¹ A''	2 ¹ A''
BLYP	4.17	4.88	3.78	4.46
B3LYP	4.64	5.42	4.76	5.11
CAM-B3LYP	4.98	5.26	5.86	6.03
B2PLYP	4.77	5.56	4.98	5.67
PBE	3.77	4.2	4.48	5.68
PBE0	4.77	5.57	4.92	5.32
LC-PBE	5.29	6.10	5.59	6.42
PBE-QIH	5.7	6.81	6.12	6.61
PBE-QIDH	5.08	5.95	5.37	5.99
PBE0-DH	5.08	5.94	5.28	5.96
CASPT2^a	4.67	5.53	5.12	5.53

Thymine						
	2 ¹ A'	3 ¹ A'	4 ¹ A'	1 ¹ A''	2 ¹ A''	3 ¹ A''
BLYP	4.57	4.78	5.76	4.08	5.3	5.68
B3LYP	5.00	5.97	6.31	4.7	5.8	6.21
CAM-B3LYP	5.26	6.61	6.72	5.04	5.8	6.64
B2PLYP	5.32	6.27	6.4	4.78	6.2	6.48
PBE	4.59	4.78	5.83	4.07	5.32	5.86
PBE0	5.11	6.16	6.46	4.8	6.02	6.5
LC-PBE	5.55	7.16	7.36	5.27	6.58	7.62
PBE-QIH	6.01	7.09	7.33	5.68	7.59	7.78
PBE-QIDH	5.60	6.51	6.96	5.10	6.87	6.76
PBE0-DH	5.54	6.43	6.88	5.03	6.85	6.64
CASPT2^a	5.06	6.15	6.53	4.95	6.38	6.85

Uracil						
	2 ¹ A'	3 ¹ A'	4 ¹ A'	1 ¹ A''	2 ¹ A''	3 ¹ A''
BLYP	4.74	5.18	6.06	3.9691	5.22	5.89
B3LYP	5.19	5.87	6.5	4.62	5.74	6.13
CAM-B3LYP	5.45	6.54	6.91	5.00	6.29	6.86
B2PLYP	5.47	6.07	6.76	4.74	6.074	6.64
PBE	3.95	4.74	5.22	4.76	5.20	5.88
PBE0	5.30	6.06	6.66	4.73	5.94	6.36
LC-PBE	5.27	7.24	7.46	5.24	6.52	8.11
PBE-QIH	6.2	7.65	7.89	5.66	7.02	8.67
PBE-QIDH	5.75	6.69	7.06	5.06	6.44	7.25
PBE0-DH	5.71	6.54	7.07	4.99	6.33	7.15
CASPT2^a	5.23	6.15	6.74	4.91	6.28	6.98

Adenine				
	2 ¹ A'	3 ¹ A'	1 ¹ A''	2 ¹ A''
BLYP	4.96	4.54	4.3	5.04
B3LYP	5.27	5.00	4.97	5.61
CAM-B3LYP	5.47	5.35	5.37	5.98
B2PLYP	5.12	5.53	5.3	5.78
PBE	5.00	4.57	4.28	5.03
PBE0	5.38	5.13	5.01	5.73
LC-PBE	5.73	5.67	5.72	6.33
PBE-QIH	6.31	6.04	5.97	6.81
PBE-QIDH	5.55	5.62	5.53	6.14
PBE0-DH	5.59	5.44	5.51	6.04
CASPT2^a	5.2	5.29	5.19	5.96

Appendix A-2

Table 2. Excitation energies (eV) computed for the molecules belonging to the RLex80-EX7-0.

	PBE type						CC2 ^a
	PBE	PBE0	LC-pbe	PBE-QIH	PBE-QIDH	PBE0-DH	
01mol	4.9	5.38	5.6	5.79	5.41	5.44	5.41
08mol	1.94	2.24	2.68	2.96	2.43	2.5	2.24
33mol	3.03	3.96	4.5	4.73	4.31	4.27	4.06
41mol	3.82	4.15	4.66	4.63	4.64	4.48	4.77
52mol	2.32	2.64	3.15	-	-	-	2.65
74mol	3	3.7	4.58	4.66	4.08	4	3.71
75mol	2.2	2.98	4	-	-	-	3.37

	BLYP type				CC2 ^a
	BLYP	B3LYP	CAM-B3LYP	B2PLYP	
01mol	4.86	5.27	5.43	5.23	5.41
08mol	1.94	2.18	2.44	2.26	2.24
33mol	3.01	3.8	4.21	4.05	4.06
41mol	3.78	4.05	4.34	4.45	4.77
52mol	2.31	2.57	2.86	--	2.65
74mol	2.97	3.55	4.09	3.73	3.71
75mol	2.19	2.82	3.54	--	3.37

^a CC2 data from ref Jacquemin, D.; Duchemin, I.; Blase, X. *J. Chem. Theory Comput.* **2015**, 11, 5340–5359.

Appendix A-3

Table 3. Computed relative and Mean Average Deviations (MAD, in eV) for the molecules of the RLex80-EX7-0 using 6-31+G(d) basis set for GGA and hybrids and the def2TZVP basis for DH functionals. The reference CC2 values are also reported.

	01 Mol	08 Mol	33 Mol	41 Mol	52 Mol	74 Mol	75 Mol	MAD
BLYP	0.55	0.30	1.05	0.99	0.34	0.74	1.18	0.74
B3LYP	0.14	0.06	0.26	0.72	0.08	0.16	0.55	0.28
CAM-B3LYP	0.02	0.20	0.15	0.43	0.21	0.38	0.17	0.22
B2PLYP	0.18	0.02	0.01	0.32	-	0.02	-	0.11
PBE	0.51	0.30	1.03	0.95	0.33	0.71	1.17	0.71
PBE0	0.03	0.00	0.10	0.62	0.01	0.01	0.39	0.17
LC-PBE	-0.19	0.44	0.44	0.11	0.5	0.87	0.63	0.45
PBE-QIH	-0.38	0.72	0.67	0.14	-	0.95	-	0.57
PBE-QIDH	0.00	0.19	0.25	0.13	-	0.37	-	0.19
PBE0-DH	0.03	0.26	0.21	0.29	-	0.29	-	0.22
CC2^a	5.41	2.24	4.06	4.77	2.65	3.71	3.37	

^a CC2 data from ref Jacquemin, D.; Duchemin, I.; Blase, X. *J. Chem. Theory Comput.* **2015**, 11, 5340–5359.

Appendix A-4

Table 4. Computed transition energies (eV) and oscillator strengths for Ar-TCNE systems using the aug-cc-pVDZ basis set in solution/gas phase.

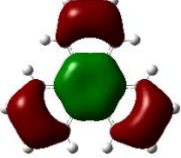
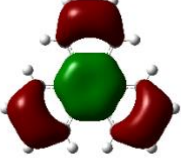
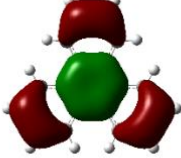


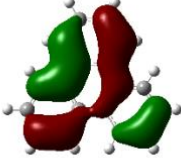
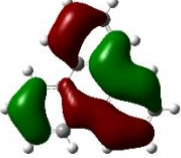
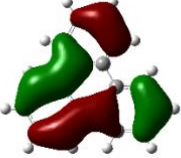
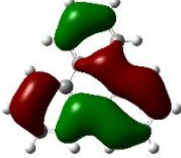

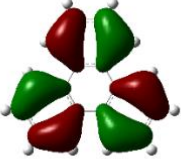
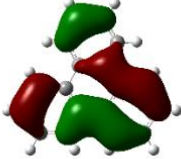
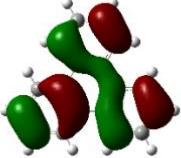
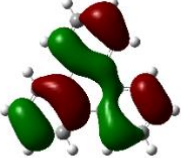
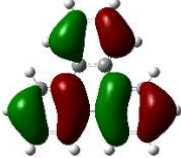
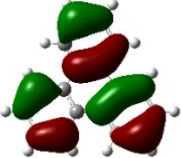
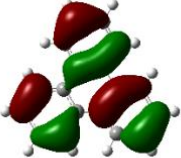
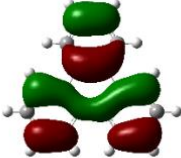
GAS PHASE												
	PBE		PBE0		LC-PBE		PBE-QIH		PBE-QIDH		ωB97X-D EXP ^a	
TCNE-	E(eV)	<i>f</i>	E(eV)	<i>f</i>	E(eV)	<i>f</i>	E(eV)	<i>f</i>	E(eV)	<i>f</i>	E(eV)	<i>f</i>
Benzene												
I	1.35	0.00	2.08	0.00	4.06	0.00	3.52	0.00	3.01		2.98	0.00
II	1.47	0.03	2.15	0.02	4.08	0.03	3.55	0.03	3.03		3.01	0.02 3.59
III	3.16	0.00	4.30	0.29	4.77	0.33	4.95	0.44	4.97		4.43	0.31
Toluene												
I	1.29	0.04	1.88	0.03	3.71	0.03	3.23	0.04	2.69		2.70	0.03
II	1.36	0.00	2.05	0.00	3.98	0.00	3.46	0.00	2.92		2.90	0.00 3.36
III	3.06	0.00	4.29	0.00	4.77	0.32	4.95	0.43	4.97		4.43	0.30
Xylene												
I	1.00	0.00	1.62	0.01	3.46	0.01	2.99	0.01	2.42		2.45	0.01
II	1.40	0.04	1.95	0.04	3.76	0.03	3.30	0.04	2.71		2.74	0.03 3.15
III	3.00	0.00	4.18	0.00	4.75	0.31	4.94	0.42	4.95		4.42	0.29
Naphtalene												
I	0.27	0.00	1.00	0.00	3.05	0.00	2.43	0.00	1.92		2.00	0.00
II	0.98	0.00	1.76	0.00	3.81	0.00	3.22	0.00	2.67		2.77	0.00 2.60
III	1.94	0.00	2.92	0.00	4.71	0.00	4.74	0.01	3.91		4.09	0.00
MAD _{1ST}	2.20		1.53		0.40		0.13		0.67		0.64	
SOLUTION												
	PBE		PBE0		LC-PBE		PBE-QIH		PBE-QIDH		ωB97X-D EXP ^a	
TCNE-	E(eV)	<i>f</i>	E(eV)	<i>f</i>	E(eV)	<i>f</i>	E(eV)	<i>f</i>	E(eV)	<i>f</i>	E(eV)	<i>f</i>
Benzene												
I	1.33	0.00	2.04	0.00	3.98	0.00	3.46	0.00	2.95		2.91	0.00
II	1.46	0.04	2.11	0.04	3.99	0.04	3.50	0.05	2.96		2.93	0.04 3.22
III	3.09	0.00	4.19	0.38	4.66	0.45	4.81	0.56	4.83		4.32	0.41
Toluene												
I	1.32	0.0576	1.87	0.05	3.62	0.05	3.17	0.06	2.63		2.63	0.04
II	1.37	0.0001	2.03	0.00	3.91	0.00	3.40	0.00	2.88		2.84	0.00 3.05
III	3.01	0.0000	4.18	0.36	4.66	0.43	4.81	0.55	4.82		4.32	0.40
Xylene												

I	1.11	0.01	1.70	0.02	3.43	0.0321	3.00	0.03	2.43	2.44	0.03	
II	1.42	0.06	1.95	0.04	3.71	0.03	3.26	0.04	2.70	2.69	0.03	2.89
III	2.99	0.00	4.14	0.14	4.65	0.42	4.80	0.53	4.81	4.31	0.39	
Naphtalene												
I	1.17	0.11	1.46	0.09	3.04	0.07	2.55	0.09	2.00	2.12	0.07	
II	1.52	0.00	2.04	0.00	3.81	0.00	3.30	0.00	2.73	2.82	0.00	2.26
III	2.50	0.01	3.17	0.01	4.62	0.27	4.75	0.20	4.71	4.12	0.01	
MAD_{1ST}	1.62		1.09		0.66		0.19		0.35	0.33		

^a Experimental values taken from reference Hanazaki, I. *J. Phys. Chem.* **1972**, *76*, 1982.

Appendix B

Table 1. Computed molecular orbitals using the different functionals of the BLYP family for the triphenylene molecule.

N	BLYP	B3LYP	CAM-B3LYP
55			
56			
57			
58			
59			
60			

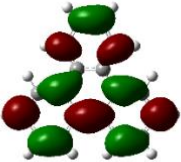
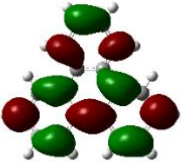
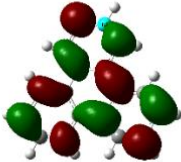
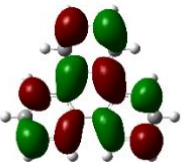
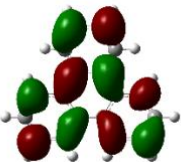
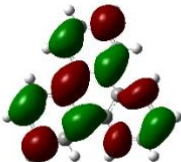
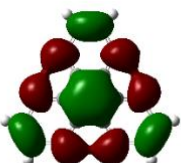
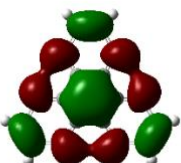
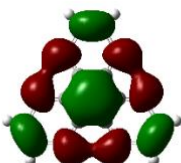
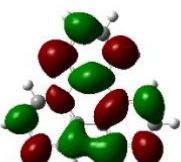
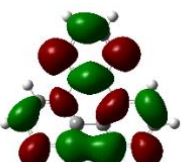
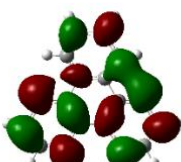
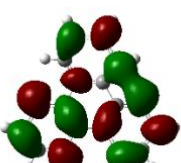
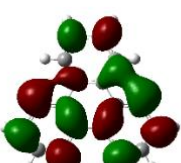
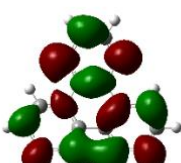
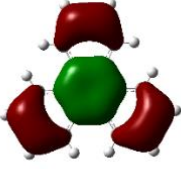
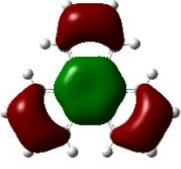
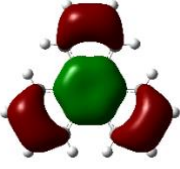
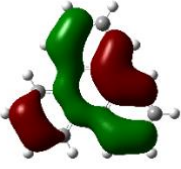
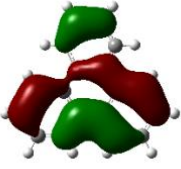
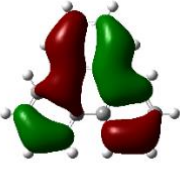
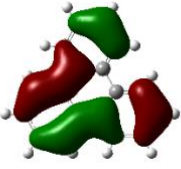
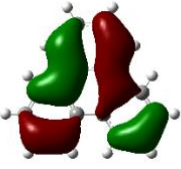
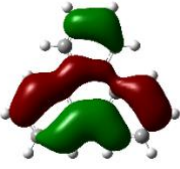
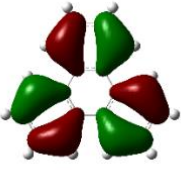
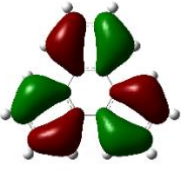

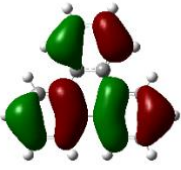
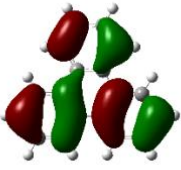

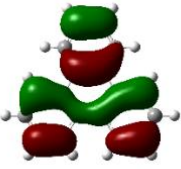
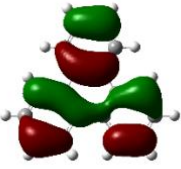
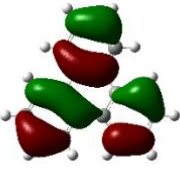
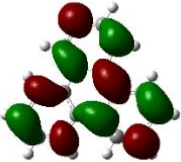
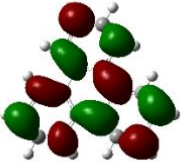
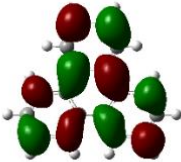
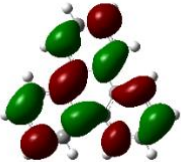
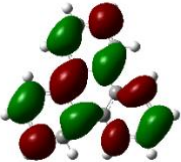
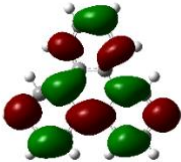
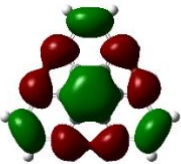
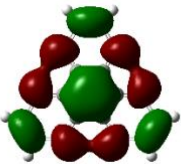
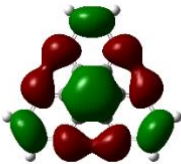
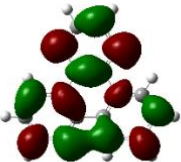
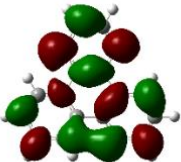
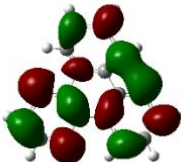
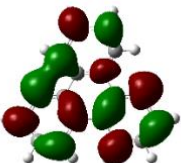
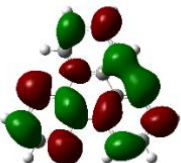
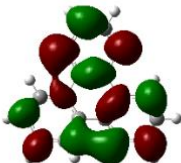
61			
62			
63			
64			
65			

Table 2. Computed molecular orbitals using the different functionals of the PBE family for the triphenylene molecule.

N	PBE	PBE0	LC-PBE
55			
56			
57			
58			
59			
60			

61			
62			
63			
64			
65			

RÉSUMÉ

Le contrôle des propriétés optiques des molécules et des matériaux représente un défi considérable pour les applications de haute technologie. En particulier, la description précise des états excités de systèmes moléculaires chimiquement pertinents est intrinsèquement un problème difficile pour les approches quantiques. Au cours de cette thèse, nous avons testé comment des fonctionnelles d'échange et corrélation de nouvelle génération, telles que les doubles hybrides non paramétrés, peuvent améliorer la description des états excités. Nous avons élaboré une nouvelle façon d'obtenir une description globale des états excités en utilisant une analyse basée sur les Global Transition Contribution Grids. Enfin, la capacité des approches actuelles à décrire les états excités des systèmes moléculaires d'intérêt dans le domaine de la thérapie photodynamique a également été testée.

MOTS CLÉS

États Excités, TD-DFT, Doubles Hybrides, Global Transition Contribution Grids

ABSTRACT

The control of the optical properties of molecules and materials represents a considerable challenge for high-tech applications. In particular, the accurate description of the excited states of chemically relevant molecular systems is intrinsically a difficult problem for quantum approaches. During this thesis, we tested how new generation exchange correlation functionals, such as non-parametrized double hybrids, can ameliorate the description of excited states. We provided a new way to get a global description of the computed excited states using an analysis based on the Global Transition Contribution Grids. Finally, the ability of current approaches in describing the excited states of molecular systems of interest in the domain of Photo Dynamic Therapy was also tested.

KEYWORDS

Excited states; TD-DFT; Double Hybrids; Global Transition Contribution Grids

